PUBLISHER :

Address of Publisher & Editor's Office :

GDAŃSK UNIVERSITY
OF TECHNOLOGY
Faculty
of Ocean Engineering
& Ship Technology

ul. Narutowicza 11/12
80-952 Gdańsk, POLAND
tel.: +48 58 347 13 66
fax : +48 58 341 13 66
e-mail : office.pmr@pg.gda.pl

Account number :
BANK ZACHODNI WBK S.A.
I Oddział w Gdańsku
41 1090 1098 0000 0000 0901 5569

Editorial Staff :
Tadeusz Borzęcki Editor in Chief
e-mail : tadbor@pg.gda.pl
Przemysław Wierzchowski Scientific Editor
e-mail : e.wierzchowski@chello.pl
Jan Michalski Editor for review matters
e-mail : janmi@pg.gda.pl
Aleksander Kniat Editor for international relations
e-mail : olek@pg.gda.pl
Kazimierz Kempa Technical Editor
e-mail : kkempa@pg.gda.pl
Piotr Bzura Managing Editor
e-mail : pbzura@pg.gda.pl
Miłosz Wierzchowski Computer design
e-mail : milosz@froggs.ltd.uk

Domestic price :
single issue : 20 zł

Prices for abroad :
single issue :
- in Europe EURO 15
- overseas US$ 20

ISSN 1233-2585

POLISH MARITIME RESEARCH
in internet
www.bg.pg.gda.pl/pmr/pmr.php

POLISH MARITIME RESEARCH

No S1(63) 2009 Vol 16

CONTENTS

3 ***D. BUTRYMOWICZ, J. GŁUCH, T. HAJDUK, M. TRELA, A. GARDZILEWICZ***
Analysis of fouling thermal resistance of feed-water heaters in steam power plants

9 ***Z. DOMACHOWSKI***
Specificity of automatic control of micro-turbines (steam or gas -driven and expanders) in dispersed generation system of heat and electric power

14 ***A. GARDZILEWICZ, D. OBRZUT, M. SZYMANIAK***
Polish aspects in the modern design solutions of steam turbine flow systems

22 ***J. GŁUCH***
Selected problems of determining an efficient operation standard in contemporary heat-and-flow diagnostics

28 ***P. LAMPART, K. KOSOWSKI, M. PIWOWARSKI, Ł. JĘDRZEJEWSKI***
Design analysis of Tesla micro-turbine operating on a low-boiling medium

34 ***J. MIKIELEWICZ, M. PIWOWARSKI, K. KOSOWSKI***
Design analysis of turbines for co-generating micro-power plant working in accordance with organic Rankine's cycle

39 ***H. PIWOWARSKA, M. PIWOWARSKI***
Evaluation of technical efficiency of heat and electric power generation

45 ***M. PIWOWARSKI***
Optimization of steam cycles with respect to supercritical parameters

52 ***R. PUZYREWSKI, K. ŻOCHOWSKI, P. FLASZYŃSKI***
A method for analysing ram pressure characteristics of impeller pump rotor

58 ***R. STĘPIEŃ, K. KOSOWSKI***
Remarks on aerodynamic forces in seals of turbine stages

64 ***M. TRELA, R. KWIDZIŃSKI, J. GŁUCH, D. BUTRYMOWICZ***
Analysis of application of feed-water injector heaters to steam power plants

71 ***W. WŁODARSKI, K. KOSOWSKI***
On the modelling of aerodynamic force coefficients for over-shroud seals of turbine stages

Editorial

POLISH MARITIME RESEARCH is a scientific journal of worldwide circulation. The journal appears as a quarterly four times a year. The first issue of it was published in September 1994. Its main aim is to present original, innovative scientific ideas and Research & Development achievements in the field of :

Engineering, **Computing & Technology**, **Mechanical Engineering**,

which could find applications in the broad domain of maritime economy. Hence there are published papers which concern methods of the designing, manufacturing and operating processes of such technical objects and devices as : ships, port equipment, ocean engineering units, underwater vehicles and equipment as well as harbour facilities, with accounting for marine environment protection.
The Editors of POLISH MARITIME RESEARCH make also efforts to present problems dealing with education of engineers and scientific and teaching personnel. As a rule, the basic papers are supplemented by information on conferences , important scientific events as well as cooperation in carrying out international scientific research projects.

Scientific Board

Chairman : Prof. **Jerzy Girtler** - Gdańsk University of Technology, Poland
Vice-chairman : Prof. **Antoni Jankowski** - Institute of Aeronautics, Poland
Vice-chairman : Prof. **Mirosław L. Wyszyński** - University of Birmingham, United Kingdom

Dr **Poul Andersen**
Technical University
of Denmark
Denmark

Dr **Mehmet Atlar**
University of Newcastle
United Kingdom

Prof. **Göran Bark**
Chalmers University
of Technology
Sweden

Prof. **Sergey Barsukov**
Army Institute of Odessa
Ukraine

Prof. **Mustafa Bayhan**
Süleyman Demirel University
Turkey

Prof. **Marek Dzida**
Gdańsk University
of Technology
Poland

Prof. **Odd M. Faltinsen**
Norwegian University
of Science and Technology
Norway

Prof. **Patrick V. Farrell**
University of Wisconsin
Madison, WI
USA

Prof. **Wolfgang Fricke**
Technical University
Hamburg-Harburg
Germany

Prof. **Stanisław Gucma**
Maritime University of Szczecin
Poland

Prof. **Antoni Iskra**
Poznań University
of Technology
Poland

Prof. **Jan Kiciński**
Institute of Fluid-Flow Machinery
of PASci
Poland

Prof. **Zygmunt Kitowski**
Naval University
Poland

Prof. **Jan Kulczyk**
Wrocław University of Technology
Poland

Prof. **Nicos Ladommatos**
University College London
United Kingdom

Prof. **Józef Lisowski**
Gdynia Maritime University
Poland

Prof. **Jerzy Matusiak**
Helsinki University
of Technology
Finland

Prof. **Eugen Negrus**
University of Bucharest
Romania

Prof. **Yasuhiko Ohta**
Nagoya Institute of Technology
Japan

Dr **Yoshio Sato**
National Traffic Safety
and Environment Laboratory
Japan

Prof. **Klaus Schier**
University of Applied Sciences
Germany

Prof. **Frederick Stern**
University of Iowa,
IA, USA

Prof. **Józef Szala**
Bydgoszcz University
of Technology and Agriculture
Poland

Prof. **Tadeusz Szelangiewicz**
Technical University
of Szczecin
Poland

Prof. **Witalij Szczagin**
State Technical University
of Kaliningrad
Russia

Prof. **Boris Tikhomirov**
State Marine University
of St. Petersburg
Russia

Prof. **Dracos Vassalos**
University of Glasgow
and Strathclyde
United Kingdom

POLISH MARITIME RESEARCH, Special issue 2009/S1; pp. 3-8

10.2478/v10012-008-0037-1

Analysis of fouling thermal resistance of feed-water heaters in steam power plants

Dariusz Butrymowicz,
Jerzy Głuch,
Tomasz Hajduk,
Marian Trela,
Andrzej Gardzilewicz

Abstract

In this paper a problem is discussed of thermal degradation of shell-and-tube recuperative feed-water heaters due to heat transfer surface fouling. Application (to an example steam cycle of power plant) of DIAGAR software system intended for the analysing of impact of degradation of a particular heat exchanger on whole recuperative system performance, is presented. On the basis of the systematically performed simulative calculations it was concluded that the degradation of feed-water heaters of the lowest extraction pressure results in an additional load imposed on the heaters of higher extraction pressures, moreover it was estimated that the degradation of the heaters due to presence of sediments of the thermal resistance reaching $5*10^{-4}$ m^2*K/W, has resulted in the drop of turbine set efficiency by about 0.3%. Such drop depends on a given configuration of degree of degradation of particular feed-water heaters applied in a considered turbine set.

Keywords: steam power unit, fouling, feedwater heaters

Introduction

Power efficiency improvement of steam power generation systems is today one of the most crucial research problems and concerns both stationary and marine power plants. The problems associated with their operation including thermal degradation of heat power systems resulting from the fouling of their surface, become more and more important.

In this paper is discussed the problem of impact of thermal degradation of heat exchangers working as a low-pressure heat recuperative system on power plant efficiency. An insufficient attention has been paid so far to the problem because it has been assumed that the problem of the fouling sedimented on heat transfer surface and thermal degradation associated with it, would not be very important due to the fact that the working medium of very high purity flows on both sides of such exchangers. As results from the authors' experience which has been gathered so far, the above presented opinion does not comply with real state of the matters, therefore the authors have initiated themselves a systematic research focused on the assessment of degree of thermal degradation of heat exchangers resulting from the fouling of heat transfer surface [1, 2]. In this paper the problem of the assessment of impact of surface fouling of low-pressure feed-water heaters on power plant efficiency, is discussed. The undertaken analysis deals with a supercritical power plant. Such choice is justified by the fact that in the power plant in question number of heaters forming heat recuperative system is the largest.

The below presented analysis is based on calculations which have to be very exact in view of a high precision necessary to determine differences in efficiency of considered cycle configuration variants as well as when various component devices are applied. For the planned scope of the investigations to compare impact of thermal degradation of different feed-water heaters on energy efficiency of a considered cycle, is necessary. For such analysis two quantities are in particular important, namely:

- specific heat consumption defined as the ratio of heat flux delivered to boiler's steam cycle and turbine's internal mechanical power;
- turbine's mechanical power.

The modeled object was thermally calculated and its characteristics were determined. To the calculations DIAGAR software was applied [3,4,5,6]. Some procedures of the program had to be so modernized as to make it possible to calculate the cycles in the range of supercritical steam parameters. Simultaneously, calculation procedures of heat exchangers were so modified as to make it possible to take into account set values of thermal resistance of the fouling sedimented on heat transfer surfaces. Values of thermal resistance were assumed on the basis of the experimental tests on thermal resistance of the fouling accumulated on pipes of one of Polish electric power plants, performed on the authors' original laboratory stand [7,8]. The work was aimed at determination of expected loss of efficiency resulting from fouling sedimented in such heaters. The loss was assessed in relation to the power plant of clean shell-and-tube feed-water heaters.

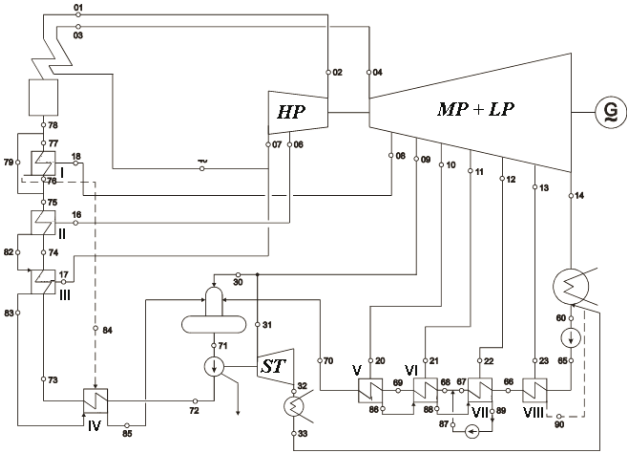

Fig. 1. *Schematic diagram of the analyzed cycle of thermal power plant*

Analyzed system of power plant

In this paper the influence of thermal degradation of low-pressure feed-water heaters on an example thermal cycle of steam power plant, was analyzed. In order to solve the problem to apply a complete model of thermal cycle is necessary; this is however a very complex problem. Therefore it was decided to use a thermal cycle model of steam power plant, which was at disposal of these authors. Results of the analysis can be considered representative in a wide range of operational parameters of steam power plants, both for marine and land applications.

In Fig. 1 schematic diagram of the considered example thermal cycle of 600 MW power, is presented. The remaining heat-and-flow data decisive of operational characteristics of the cycle are given below:

- Live steam pressure: 28.5 MPa
- Live steam temperature: 600 ^{o}C
- Interstage superheating temperature: 620 ^{o}C
- Condensation pressure: 5 kPa
- Degassing pressure: 1.15 MPa

The cycle is intended for co-operation with:

- electric drive of feed-water pump;

as well as

- turbine drive of feed-water pump.

Moreover from the heat-and-flow data the operational characteristics of the thermal cycle's component devices such as: pressure losses, condensate overcooling, ram temperature rise etc, were calculated.

Thermal degradation of heat exchangers

Thermal degradation of heat exchangers is defined as the lowering of exchanger's heat transfer efficiency, which results from operational factors such as: heat transfer surface fouling, inert gas presence, exclusion of a part of heat transfer surface from operation, or other operational causes. In this work special attention has been paid to the degradation caused by heat transfer surface fouling.

Fouling thermal resistance depends on definite operational conditions of heat exchanger. With a view of different chemical composition of water, e.g. in different electric power stations, sediments of a different thickness, structure and chemical compostion can be met. Moreover, even in a given electric power station thickness and structure of sediments can be different as results from observations of state of heat transfer surfaces. Hence any generalization of only once measured values of fouling thermal resistance for all heat exchangers operating in a given electric power station, is very uncertain.

Influence of thermal degradation resulting from the fouling of heat transfer surfaces as well as inert gas presence necessitates one-dimensional model of heat exchangers to be applied. In such model, elaborated by Butrymowicz and Trela [1,2], a change in heat transfer conditions along water flow through exchanger is taken into account. With a view of necessity of taking into account changes of the conditions in particular runs, such model can be considered quasi-two-dimensional. In the model, impact of inert gas content in condensating steam as well as bundle effect are to be taken into account locally. With a view of inert gas presence to take into account local change of the saturation temperature T_{vs} as well as the phase separation surface temperature T_b, is necessary.

In the analyzed model the following balance differential equations have been used for calculations:

$$\dot{m}_w c_{pw} \frac{dT_w}{dA_o} - k(T_w, T_b, T_{to}, \dot{m}_v)\cdot(T_{vs} - T_w) = 0 \tag{1}$$

in which T_w stands for local temperature of water, and the heat transfer coefficient k is given by the following equation:

$$k = \frac{1}{\frac{1}{\alpha_v(T_b, T_{to}, \dot{m}_v)\beta(\dot{m}_v)} + R_a(T_b, \dot{m}_v) + R_{fo} + R_t \frac{D_o}{D_m} + \left(\frac{1}{\alpha_w(T_w)} + R_{fi}\right)\frac{D_o}{D_i}} \tag{2}$$

where the following notation is assumed: α_v and α_w – heat transfer coefficients on the side of condensating steam and cooling water, respectively; T_{to} -pipe outer surface temperature; β -bundle coefficient; T_{vs} -steam saturation temperature; R_{fo}, R_{fi}, R_t -fouling thermal resistance of: outer surface, inner surface and pipe material, respectively; D_o, D_i, D_m -pipe outer, inner and logarithmic mean diameter, respectively; R_a -additional thermal resistance due to inert gas presence. Thermal resistance of inert gas layer can be determined by using Berman relation [10] well experimentally confirmed and often applied to numerical calculations [9].

In the case of the analyzed model the following set of equations is considered:

- the differential equation (1);
- and the following algebraic equations:
  - the equation which combines the heat transfer coefficient on the condensating steam side, α_v, the temperatures T_{to}, T_b, and the steam mass flow rate $\dot{m}_v$ [1,2],
  - the equation which expresses the thermal resistance, R_a, resulting from inert gas presence [2],
  - the energy balance equation for an elementary segment of heat exchanger pipe:

$$d\dot{m}_v \left[h_{fg} + c_{pv}(T_v - T_{vs})\right] = \dot{m}_w c_{pw}\, dT_w \tag{3}$$

  - the equation which combines local steam saturation pressure and air content:

$$p_s = p_v\left(1 + 0.622\frac{\dot{m}_a}{\dot{m}_v}\right)^{-1} \tag{4}$$

where: $\dot{m}_a$ – air flow mass rate; p_v – steam partial pressure; h_{fg} – specific evaporation enthalpy, c_{pv} – specific heat capacity of superheated steam. On the basis of Eq. (4) local value of the steam saturation temperature T_{vs} can be determined provided distribution of the air flow mass rate $\dot{m}_a$ is known. Dependent variables are the following: the water temperature T_w, the steam mass flow rate $\dot{m}_v$, the phase separation surface temperature T_b, the pipe outer surface temperature Tto as well as the steam saturation temperature T_{vs}. All the quantities are local.

In the case of multi-run heat exchangers, heat transfer conditions on the condensating steam side undergo discrete changes, which is covered by the bundle coefficient β. Hence the solving of the set of equations in question is the most convenient if the differential equation (1) is written in the form of a difference equation. In the case of occurrence of the convective cooling of superheated steam (without condensation) the considered set of equations requires to be extended, that is shown in [11].

The one-dimensional model of heat transfer within recuperative heat exchanger is deemed most suitable for diagnostic analysis purposes because it makes it possible to take into account local effects important from the heat transfer point of view, at a relatively low input of numerical calculations.

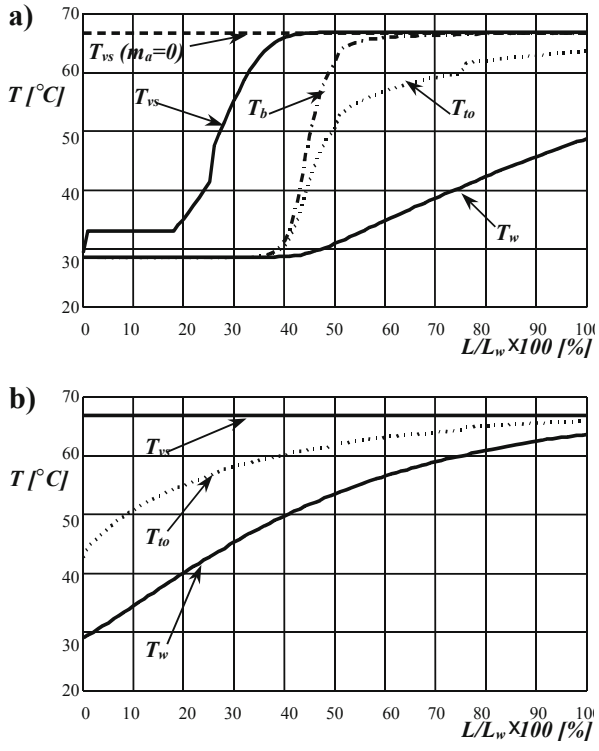

Fig. 2. *Temperature distribution in XN1 heat exchanger along water path, Lw – the total water path length. In calculation it was assumed:* ***a)*** R_f *=1.5 10^{-4} m^{2}K/W; = 1*10^{-3} kg/s;* ***b)*** R_f *= 0;* $\dot{m}_a$ *= 0.*

In Fig. 2 are given example results of calculations of a recuperative heat exchanger absorbing steam from the last extraction of LP turbine of 200 MW steam turbine set, i.e. the feed-water heater VIII. The heat exchangers of the lowest extraction pressure are vertically installed in condenser casings, and their heat transfer surface is made by a bundle of horizontal pipes. The basic geometrical quantities of the example feed-water heater VIII for which heat transfer calculations were performed are the following: – number of pipes: 670; – pipe outer diameter: 19 mm; – pipe inner diameter: 17 mm; – pipe material: brass; – active length: 3.642 m; – active breadth: 0.358 m; – number of vertical pipe rows: 52; – number of water runs: 4; – cross-section area of steam inflow to heat exchanger: 2.548 m×0.200 m; – pipe triangular spacing: 44 mm. For numerical calculations the following operational parameters of the heat exchanger were assumed: – water mass flow rate: 63.74 kg/s; -water inlet temperature: 28.51°C; – steam inlet temperature: 93.06 °C; – steam inlet pressure: 0.271 bar. In the calculations it was assumed – by analogy to power condensers – that the steam mass flow discharged from deaerators is associated with the minimum local condensation temperature higher by 2 ÷ 5 K than the water inlet temperature.

From the point of view of diagnostic assessment of heat exchanger operation its thermal degradation is revealed directly by the increasing of the so called ram temperature rise, i.e. difference between saturation temperature and heated water temperature at outlet from the exchanger.

As results from the presented diagrams, the distribution of the water temperature T_w in the exchanger working in air-presence conditions differs greatly from logarithmic one characteristic for operation of a clean exchanger free from presence of air. The air content in condensating steam, amounting to $\dot{m}_a$ = 1*10^{-3} kg/s which is equivalent to the ratio $(\dot{m}_a/\dot{m}_v)$ = 0.31% assumed for the calculations, results in a significant increase of the ram temperature rise $\delta T_o = T_{vs} - T_{wo}$. For the non-degraded exchanger the increase of the ram temperature rise equal to 3,5 K is obtained, and in the case of a significant degradation due to the heat transfer surface fouling the increase by about 18 K is obtained. On the basis of other analyses [2] it can be stated that the degradation resulting from dirtiness of heat transfer surfaces only causes the increase up to 9.0 K.

Tab. 1. *Design data of low-pressure recuperative heat exchangers*

Name of device	Values of geometrical characteristics of non-degraded recuperative heat exchangers	
	Heat transfer surface area [m2]	Number of pipes in a heater [pieces]
Recuperative heat exchanger VIII	435	704 – horizontal
Recuperative heat exchanger VII	900	3183 – vertical
Recuperative heat exchanger VI	1053	2874 – vertical
Recuperative heat exchanger V	1060	3183 – vertical

By taking into account the available research results on fouling thermal resistance [1,2,7,8,11], for purposes of this work two characteristic values of fouling thermal resistance can be proposed:

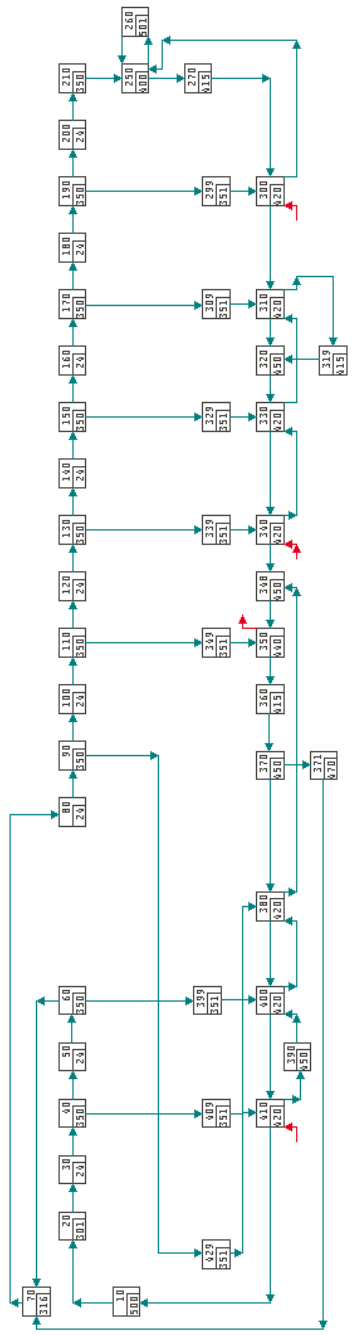

Fig. 3. Numerical scheme of 600 MW steam turbine unit with electrical drive of feed-water pump .
Notation: 10 -boiler; 15 – pipeline with valves; 20 – control stage; 30 – group of HP stages I; 40 -extraction I; 50 -group of HP stages II; 60 -extraction II; 70 – interstage superheater; 80 -group of IP/LP stages I; 90 -extraction III; 100 -group of IP/LP stages II; 110 -extraction IV; 120 -group of IP/LP stages III; 130 -extraction V; 140 - group of IP/LP stages IV; 150 -extraction VI; 160 -group of IP/LP stages V; 170 -extraction VII; 180 -group of IP/LP stages VI; 190 -extraction VIII; 200 -group of IP/LP stages VII; 210 – outlet diffuser TG; 250 – main condenser; 260 – condenser cooling; 270 – main condensate pump; 280 – degasifier steam condenser; 299 – pipeline of extraction VIII; 300 – recuperative heat exchanger VIII; 309 -pipeline of extraction VII; 310 -recuperative heat exchanger VII; 319 - condensate pump; 320 – water distribution; 329 -pipeline of extraction VI; 330 -recuperative heat exchanger VI; 339 -pipeline of extraction V; 340 -recuperative heat exchanger V; 348 – pipline; 349 -pipeline of extraction IV; 350 – odgazowywacz; 360 -pompa zasilająca; 370 - water distribution; 371 – injection of water to interstage superheater; 380 -recuperative heat exchanger III; 399 -pipeline of extraction II; 400 -recuperative heat exchanger II; 409 -pipeline of extraction I; 410 -recuperative heat exchanger I; 429 -pipeline of extraction III; 500 – auxiliary turbine; 505 – auxiliary turbine diffuser; 510 – auxiliary condenser; 520 - auxiliary condenser cooling; 530 – condensate auxiliary pump; 540 -pipeline

- $R_f = 2.5 \cdot 10^{-4} [m^2 \cdot K/W]$ -assumed to be typical for heat exchangers;
- $R_f = 5.0 \cdot 10^{-4} [m^2 \cdot K/W]$ -assumed to be relevant to heat exchangers of an elevated degree of degradation.

In this work the two above mentioned values of thermal resistance were used in assuming various degradation degree configurations of low-pressure recuperative feed-water heaters.

Calculations of the power plant thermal cycle

The presented heat-and-flow calculations of the cycle were performed with the use of DIAGAR software [3,4,5,6]. Each of the considered cycle configuration necessitates the same numerical scheme to be applied. The numerical scheme of the cycle for the electric drive of feed-water pump is presented in Fig. 3.

The estimated values of geometrical characteristics of feed-water heaters were based on the characteristics of the heaters installed in 200 MW power units, namely: the same inner and outer diameter and arrangement of pipes. The characteristic data of the heaters are given in Tab. 1.

The collected results of the calculations are graphically presented in Fig. 4. There are also given the applied configurations of thermal resistance levels of the fouling in LP recuperative system. The results indicate the losses revealed by introducing to the calculations the heat transfer surface fouling of feed-water heaters,

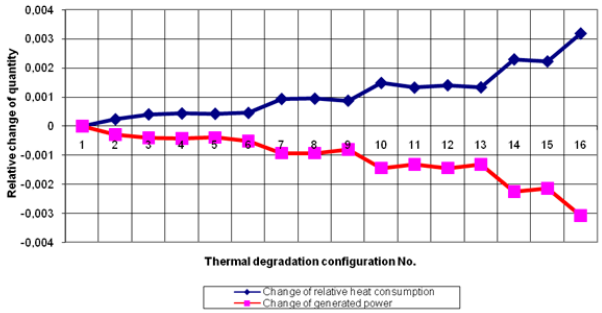

Fig. 4. Changes of operational parameters of 600 MW power unit at various combinations of degree of degradation of low-pressure heat exchangers. Notation: 1 – clean exchangers; 2-moderately degraded heat exchanger VIII; 3 -moderately degraded heat exchanger VII; 4 -moderately degraded heat exchanger VI; 5 -moderately degraded heat exchanger V; 6 – maximum degraded heat exchanger VIII; 7 -maximum degraded heat exchanger VII; 8 -maximum degraded heat exchanger VI; 9 -maximum degraded heat exchanger V; 10 -moderately degraded heat exchangers VIII – V; 11 -maximum degraded heat exchangers: VIII and VII; 12 -maximum degraded heat exchangers: VIII and VI; 13 -maximum degraded heat exchangers: VIII and V; 14 -maximum degraded heat exchangers: VIII, VII and VI; 15 -maximum degraded heat exchangers: VIII, VII and V; 16 -maximum degraded heat exchangers: VIII – V.

***Tab. 2.** Ram temperature rise of low-pressure recuperative heat exchangers*

Name of device	Values of ram temperature rise [K]		
	$R_f = 0$	$R_f = 2.5\ 10^{-4}$ [m^2K/W]	$R_f = 5.0\ 10^{-4}$ [m^2K/W]
Recuperative heat exchanger VIII	1.62	3.55	5.72
Recuperative heat exchanger VII	0.63	3.82	7.88
Recuperative heat exchanger VI	0.73	4.08	7.92

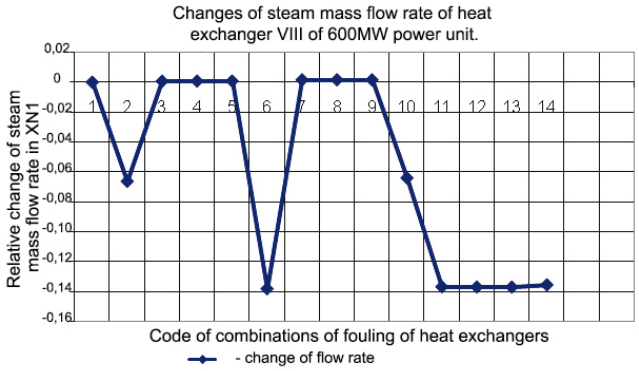

Fig. 5. Changes of steam mass flow rate of heat exchanger VIII at various combinations of degrees of degradation of low-pressure heat exchangers; code of degradation -see Fig. 4

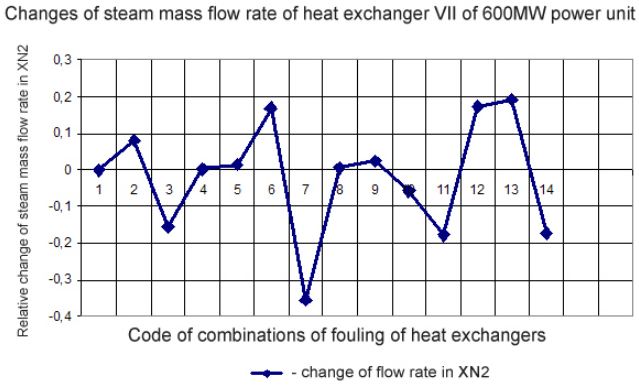

Fig. 6. Changes of steam mass flow rate of heat exchanger VII at various combinations of degrees of degradation of low-pressure heat exchangers; code of degradation -see Fig. 4

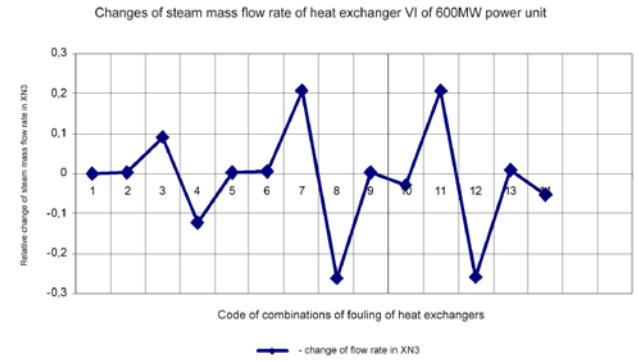

Fig. 7. Changes of steam mass flow rate of heat exchanger VI at various combinations of degrees of degradation of low-pressure heat exchangers; code of degradation -see Fig. 4

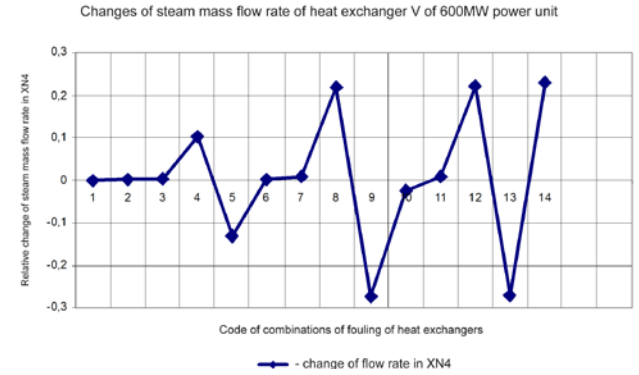

Fig. 8. Changes of steam mass flow rate of heat exchanger VI at various combinations of degrees of degradation of low-pressure heat exchangers; code of degradation -see Fig. 4

expressed in the form of relative changes in turbine-set mechanical power as well as relative changes in specific heat consumption.

As the presented results yield, in the case of the fouling of a single feed-water heater almost the same level of specific heat consumption increase and turbine-set power decrease is obtained for all the feed-water heaters and the typical value of R_{f1} (Case 2, 3, 4 and 5), and for the elevated value of R_{f2} certain diversity of the effects is observed since for the feed-water heater VIII (of the lowest extraction pressure) much lower changes are achieved. However, from the operational point of view the cases are more interesting of different configurations of the fouling of feed-water heaters, having a significant value of the thermal resistance R_{f2} - Case 10 through 13 -where for both the analyzed quantities the same level of changes was obtained. It allows to conclude that in the case of a significant degradation of the feed-water heater of the lowest extraction pressure, degradation of any of the remaining heaters of a higher extraction pressure does not play any important role. The greatest changes are obtained in the case 16 for degradation of three feed-water heaters. The changes in ram temperature rise in particular feed-water heaters are presented in Tab. 2. Along with the increasing of the fouling thermal resistance also the ram temperature rise increases, and in the conditions of the considered geometry especially high values of the ram temperature rise are obtained for feed-water heaters of higher extraction pressures.

In Fig. 5 through 8 the degradation effects in the form of changes in steam mass flow from recuperative extractions to feed-water heaters are presented for various configurations of degradation in the heaters. From the obtained results it can be generally concluded that the fouling of the feed-water heaters of lower extraction pressure values results in the increasing of thermal load imposed on the heaters of higher extraction pressure values because mas flow of steam sucked-in by the heaters then increases. Thermal degradation of a feed-water heater certainly makes that a smaller steam mass flows to it.

Heat transfer surface degradation of feed-water heaters impacts cycle's operational characteristics first of all by increasing the specific heat consumption. The calculation results given in Fig. 4 show that the highest impact on the worsening of cycle's efficiency (i.e. increasing the specific heat consumption) is introduced by the feed-water heater VIII, the first in the row of the recuperative feed-water system. It specially concerns moderate degradation levels, that leads already to necessity of cleaning them. This indicates that special attention should be paid just to cleanless of surface of the feed-water heater. Such conclusion is also confirmed by change in the steam mass flow passing through particular feed-water heaters, which constitutes one of the most important parameters deciding on performace of the exchanger itself.

Summary

In this paper theoretical analysis of impact of thermal degradation of recuperative low-pressure feed-water heaters on change of specific fuel consumption as well as output power of turbine set, has been presented. Degradation of feed-water heaters of the lowest extraction pressure is the most important. The revealed level of the changes should be considered significant.

In this stage of calculations of steam power plant cycles by means of DIAGAR software, carried out for the design load conditions and with taking into account cleanless of heat transfer surfaces of recuperative low-pressure feed-water heaters the following conclusions can be drawn:

1. Increasing the ram temperature rise is a direct effect of presence of sediments on surface of recuperative feed-water heaters (characterized by certain value of the thermal resistance Rf). In the range up to Rf = 0.0005 m2K/W, the resistance results in a multiple increase of ram temperature rise.

2. The maximum degradation of all recuperative low-pressure feed-water heaters (at Rf = 0.0005 m2K/W) may result in the specific heat consumption increase by about 0.3%. It is the value which can be deemed significant for operation of high-output power generation units.

3. Thermal degradation of feed-water heaters of the lowest extraction pressure is accompanied by an additional thermal load imposed on the feed-water heaters of higher extraction pressures. Hence in the feed-water heaters of higher extraction pressures greater relative changes in sucked-in steam mass flow rate than in the heaters of lower extraction pressures, are observed. The relative changes in mass flow rate of steam sucked-in by the heater of the lowest extraction pressure do not exceed 16%, whereas the changes for the heater of the highest extraction pressure are contained in the range up to about 30%. The above described effects directly result in a drop of turbine-set efficiency, hence in a relevant increase of specific fuel consumption.

Therefore it is necessary to fil up an important information gap in the area of real thermal resistance values resulting from the fouling of recuperative low-pressure feed-water heaters used in steam power plants as the available data in question have not a comprehensive character.

This scientific research project (the ordered project No. PBZ-MEiN-4/2/2006) has been financed from science budget resources for the years 2007÷2009.

Bibliography

1. Butrymowicz D., Trela M.: The effect of impurities and inert gases on heat transfer during condensation (in Polish).11th Symposium on Heat and Mass Transfer, vol. 2, Szczyrk, 2001.
2. Butrymowicz D., Trela M.: Effects of fouling and inert gases on performance of recuperative feed-water heaters. Archives of Thermodynamics, No. 1-2,Vol. 23, 2001.
3. Gardzilewicz A., Głuch J., Uziębło W., Bogulicz M., Kurant B., Krzyślak P., Jamroż J., Jankowski T., Rutkowska K., Rogala I., Dzierzgowski J.: A software system for calculations of turbine thermal cycles (in Polish). Opracowania wewnętrzne Instytutu Maszyn Przepływowych PAN (Internal reports of IFFM), Gdańsk, 1985÷1997.
4. Gardzilewicz A., Uziębło W., Głuch J., Bogulicz M., Topolski J.: Modernization of the computer program for calculating thermal cycles, version 1998 (in Polish). Opracowanie wewnętrzne IMP PAN (Internal report of IFFM), No. 267/98, Gdańsk 1998.
5. Gardzilewicz A., Głuch J., Bogulicz M., Walkowiak R., Najwer M., Kiebdój J., Banasiewicz J.: Implementation of modern heat-and-flow diagnostics to turbine sets in TURÓW electric power station (in Polish). Proc.of The Conference ENERGETYKA'2004, Wrocław, 6÷8 November 2004
6. Krzyżanowski J., Głuch J.: Heat-and-flow diagnostics of power objects (in Polish). Wydawnictwo IMP PAN (IFFM Publishers), Gdańsk, 2004.
7. Butrymowicz D., Hajduk T., Karwacki J.: A method for measuring the fouling thermal resistance of heat exchangers (in Polish). 13th Symposium on Heat and Mass Exchange, Koszalin-Darłówko, 2007.
8. Butrymowicz D.: Analysis of possible measurement of thermal resistance of surface fouling of heat exchangers (in Polish). Opracowanie wewnętrzne Instytutu Maszyn Przepływowych PAN (Internal report of IFFM),, No. 281/1996, Gdańsk, 1996.
9. Zhang C.: Local and Overall Condensation Heat Transfer Behaviour in Horizontal Tube Bundles. Heat Transfer Engineering, Vol. 17, No 1, 1996.
10. Berman S.S.: Calculation of surface heat transfer equipment for condensation of steam from air-steam mixture (in Russian), Teploenergetika, No 7, 1959.
11. Trela M., Butrymowicz D., Matysko R.: Diagnostics of flow and thermal processes in power plant equipment. Chapter 7, Monograph on Diagnostics of New-Generation Thermal Power Plants, IFFM Publishers, Gdańsk, 2008.

POLISH MARITIME RESEARCH, Special issue 2009/S1; pp. 9-13
10.2478/v10012-008-0038-0

Specificity of automatic control of micro-turbines (steam or gas -driven and expanders) in dispersed generation system of heat and electric power

Zygfryd Domachowski

Abstract

This paper presents specific problems of automatic control of steam micro-turbines and expanders intended for the dispersed, combined generating of heat and electric power. The investigations concern ensurance of certainty of energy supply and its required quality.

Keywords: *micro-turbine, heat-and-electric power plant, structures, automatic control.*

Introduction

Dispersed electric power generation has many important advantages: it makes it possible to use local primary - energy sources (of water, wind, biomass or geothermal ones), it lowers electric power transmission losses, increases electric supply safety (in the case of state of emergency of large electric power system), improves stability conditions of electric power system (except of windmill electric generator farms). Application of biomass to electric power generation has an additional advantage: it facilitates the developing of coordinated economy, i.e. combined generation of heat and electric power.

On the other hand the dispersed electric power generation introduces certain problems dealing with cooperation of dispersed electric power sources with an external (large) electric power system. Apart from technical requirements concerning the switching-on of such dispersed sources to an external electric power system, the problems result from necessity to ensure suitable quality of electric energy (its frequency and voltage). The bigger they are the greater power developed by such source and the greater variability of its power. For this reason the greatest operational (control) difficulties are produced by windmill electric generator farms – their nominal power reaches from a few dozen to several hundred MW, and power fluctuation may be significant. In view of required quality of frequency control of electric power system the windmill electric power generating plants requires to be aided by conventional ones driven by water, steam or gas turbines [4], or by diesel engine.

Mini heat-and-electric power plants working on biomass, develop nominal electric power reaching from a few dozen, or even several, to a few hundred kW. Therefore from the point of view of frequency control their role in electric power system is incomparable with that of windmill electric generator farms. Nonetheless they should be also supported by conventional electric power sources due to the following reasons. Firstly, as a rule they do not take part in frequency control of electric power system since their controlled quantity is heat power, and electric power is an additional product whose quantity is associated with amount of produced heat. Secondly, total electric power of mini heat–and–electric power plants installed over a given territory, can be significant. Hence further considerations are focused only on selected variants of automatic control systems of mini heat–and–electric power plants and on specific operational aspects associated with them.

Specificity of a seperate electric power system fed by a microturbine

Mikroturbines can be used, and are used to delivering electricity and heat to:

- dwelling houses, especially individual houses,
- schools,
- hospitals,
- hotels,
- office buildings,
- small firms,
- consumers of heat and electric power on ships.

In such a role they are topics of various publications and patents, however it mainly concerns gas microturbines. From the point of view of electric power generation role of both types of microturbines (gas and steam driven) is analogous, therefore role of their automatic control systems is also the same. It makes that such considerations associated with a concept of automatic control of gas microturbine [2, 3, 6÷13] can be also related to a steam microturbine.

Steam microturbine first of all intended for heat delivering, delivers as much electric power as it results from amount of delivered heat. Therefore internal electric power system (internal electric network) fed by it, should be connected to an external electric power system in order - in the case of lack of balance between amount of electric

power produced by the microturbine and that absorbed by the internal electric power system -to supplement possible shortage from the external system or to deliver possible surplus to it, see Fig. 1.

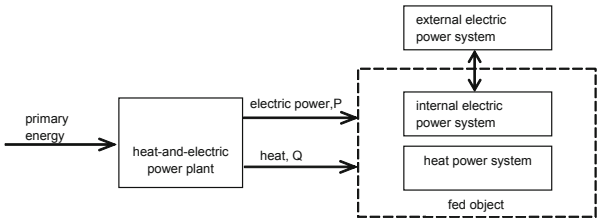

Fig.1. *Simplified schematic diagram of feeding an object with heat and electric power*

And, in land applications possible periodical breaks of connection between internal and external electric power system due to various emergency situations should be taken into account. On ships the internal electric power system is the only one. Its connection to an external electric power system may be only considered in the case of ship's stay in port. In such situation if amount of generated electric power (resulting from delivered heat amount) is smaller than the demanded (let's say critical) for feeding e.g. a refrigerator, necessary lighting, pumps, computers, then steam pressure control at outlet from turbine should be replaced by electric power control (current frequency control). For this reason the U.S. Patent [9] shows various structures of connection between a micro-gas turbine intended for the feeding of computer network with electric power and internal and external electric power systems.

In accordance with the concept described in the patent the internal electric power system is split into two parts: that unconditionally demanding to be fed (critical power demand) and the remaining part (non-critical power demand). The part of the internal electric power system, which is subjected to the critical feeding, is not connected to any external electric power system, but the remaining part of the internal electric power system is connected to it. Hence, in accordance with the concept presented in the patent in question in normal conditions the microturbine feeds separately (by separate converters) both the parts of the internal electric power system, see Fig. 2. In normal conditions to the internal system's part connected to an external electric power system only a surplus of electric power generated by the microturbine over that absorbed as critical demand, is transferred. Moreover, if the amount of electric power transferred by microturbine to that part of the internal electric power system is greater than the demanded, then the resulting surplus is directed to the external system; if it is smaller

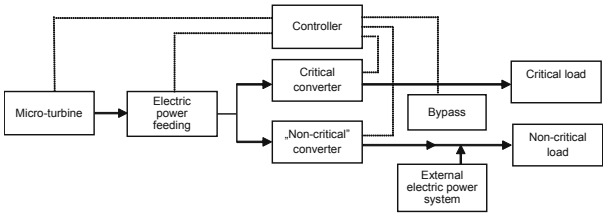

Fig.2. *General concept of connection between micro-turbine and internal and external electric power systems*

the demanded shortage is absorbed from the external system.

When internal electric power system is switched-off from external one then in the case of application of steam backpressure microturbine it is necessary to pass from steam pressure control at outlet from the turbine to electric power control (frequency). Schematic diagram of feeding the internal electric power system is presented in Fig. 3 (such concept is not covered by the patent in question. It concerns micro-gasturbines only).

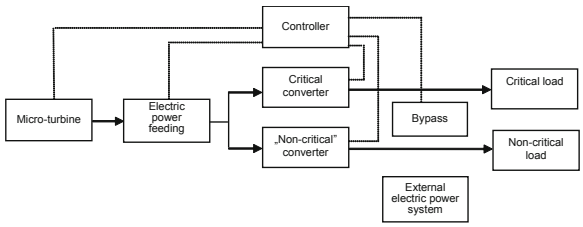

Fig. 3. *Concept of feeding the internal electric power system after its switching-off from the external system*

When microturbine is excluded from operation (for instance due to its failure, unserviceability, overhaul or repair) then the feeding of the internal electric power system is ensured by its connection to the external system, see Fig. 4. To the part of the internal power system, which constitutes non-critical load, electric power is transferred from the external system directly, and to the part which constitutes critical load – by means of a „non-critical" two-way converter (i.e that which allows for sending electric power in two directions). However, the direct feeding of both the parts of internal power system, i.e. without making use of any converters, is deemed more appropriate, see Fig. 5.

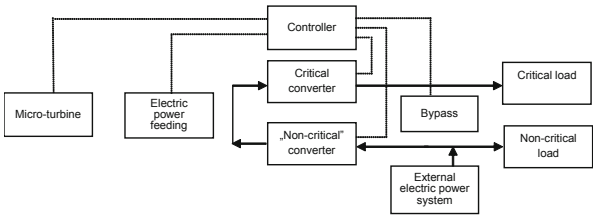

Fig.4. *Concept of feeding the internal electric power system after switching-off the micro-turbine*

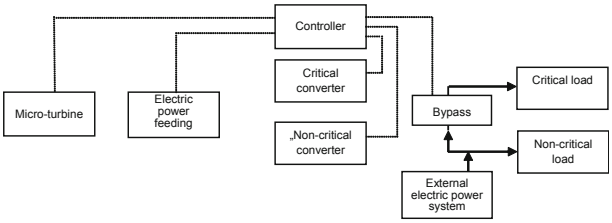

Fig.5*. Concept of feeding the internal electric power system directly from the external system after switching-off the micro-turbine*

Large objects can be fed, also for reliability reasons, by several microturbines operating in parallel. An example of such co-operation realized by four microturbines is presented in Fig. 6.

Electric current parameters in seperate electric power system

It is assumed that current parameters in the internal electric power system, there by parameters of electric

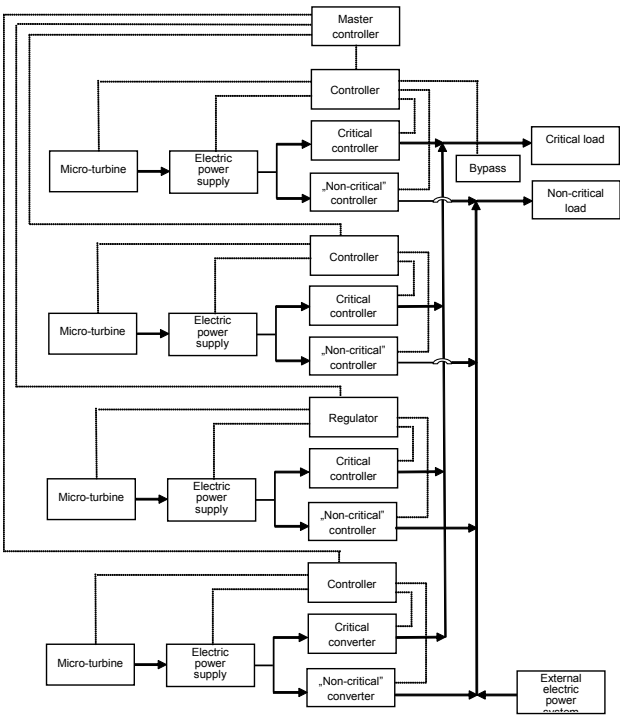

Fig. 6. *Example of feeding the internal electric power system, by means of four micro-turbines*

power delivered by microturbine are the same as standard ones in a low-voltage electric power distribution system, i.e. 50 Hz frequency (in Europe), and 230V voltage. However values of rotational speed of microturbine rotors are contained in the range of 45000÷120000 rpm, that corresponds to electric current frequency in the range of 750÷2000 Hz. Therefore it is necessary to apply an electric power converter at output from microturbine-driven generator so as to adjust parameters of the current delivered by the microturbine (frequency, voltage) to appropriate quantities relevant to low-voltage electric power system.

A concept of such converter is presented in Fig. 7. Alternating current of frequency in the range of 750÷2000 Hz, produced by microturbine -driven generator, is rectified (by rectifier as shown in Fig. 7). Direct current can feed consumers which require such feeding, as well as electric accumulators. The feeding of internal electric power system requires an inverter which converts direct current into alternating one of the parameters necessary for feeding the consumers in the internal electric power system (50 Hz frequency, 400V phase-to-phase voltage), to be applied.

Purposefulness of direct current (DC) application to seperate electric power systems fed with electric power obtained from renewable sources, has been also considered [1]. Such concept is presented in Fig. 8. In seperate electric power system DC voltage amounts to about 800V. Such system is fed from DC voltage sources

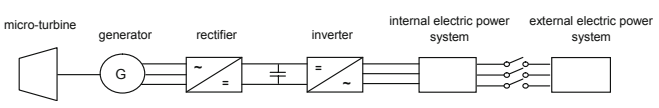

Fig.7. *Structure of connection of micro-turbine to internal and external electric power systems by means of converter and inverter*

(e.g. dispersed renewable sources) as well as -through rectifier -from external electric power system. An inverter is necessary to make delivering electric power from such seperate system to an external AC power system possible. For feeding AC consumers in the seperate internal DC power system individual inverters at their inputs are necessary.

Ship electric power system is an example of seperate system. Application of direct current to such system is deemed worth paying attention.

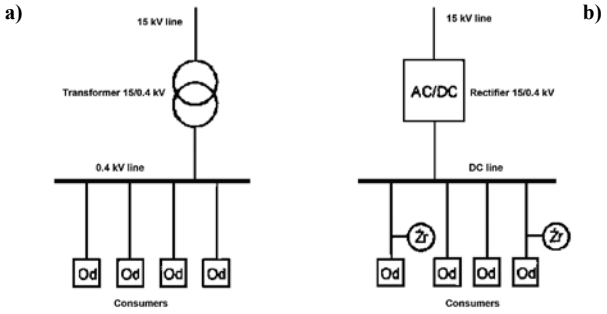

Fig.8. *A concept of replacement of alternating current* ***(a)*** *by direct current* ***(b)*** *in seperate internal electric power system*

Automatic control of heat generated by heat-and-electric power plant connected to external electric power system

Automatic control of heat-and-electric power plant is aimed at ensuring generation of demanded amount of heat of determined parameters. Amount of simultaneously generated electric power is associated with generated heat amount, but not subjected to control. Nonetheless in such conditions it should be intended to generate as large amount of electric power as possible. Hence, if heat delivered to an object is used both to space heating and service-water warming-up then two steam flows of different temperature values should be controlled. Simplified schematic diagram of automatic control system of heat-and-electric power plant, relevant to such situation, is presented in Fig. 9. Then to apply a multi-stage -extraction -backpressure turbine would be appropriate.

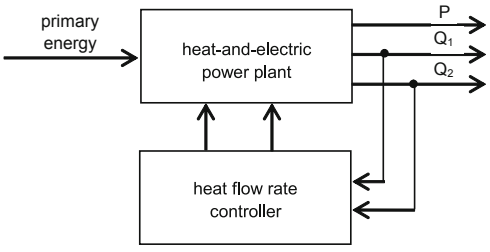

Fig. 9. *Simplified schematic diagram of automatic control system of heat flow rate for space heating (Q1) and service-water warming-up (Q2)*

In the case of application of backpressure turbine, only heat flow rate at turbine outlet is subjected to control (by controlling outlet steam pressure). It must correspond to the higher value out of the two temperature values: of service water and of space heating medium. In the case of floor heating it is reduced to choice of heating water temperature, from which limitation for amount of

generated electric power results. For this reason if a heat accumulator is applied to warming-up service water then steam pressure at outlet from turbine could be controlled with regard to space heating medium temperature. It would be then necessary to increase periodically the pressure in order to supercharge the heat accummulator.

When delivered heat is used only for service-water warming-up (in the periods when accommodations are not heated) then steam pressure at outlet from turbine has to correspond to a required value of service-water temperature.

If also other renewable sources (solar collectors, geothermal water) were used for delivering heat to an object then heat-and-electric power plant will be put in operation to supercharge heat accumulators, only if necessary.

Automatic control of heat generated by heat-and-electric power plant not connected to external electric power system

In the case of lack of connection between internal electric power system and external one as well as in the case of a break of the existing connection (e.g. in states of emergency of external electric power system) the heat-and-electric power plant is expected to deliver both required amount of heat and required amount of electric power [5]. In such situation two variants corresponding to two types of turbine assumed to be used in a given heat-and-electric power plant, should be considered.

Delivery control of heat and electric power if backpressure turbine is used

In backpressure turbine only one quantity can be subjected to automatic control, i.e. only one signal can be controlled. It can be either flow rate of delivered heat – the controlled signal is then steam pressure at outlet from turbine, or electric power – the controlled signal is then rotational speed of turbine-set rotor. In the considered situation (lack of connection between internal and external electric power systems) turbine-set electric output power must be controlled in order to ensure the required feeding of electric power consumers in internal electric power system. Amount of heat delivered by the turbine depends on its output power only.

If heat flow rate at outlet from the turbine is lower than the demanded (both for space heating and service-water warming-up) then the lacking heat amount is directly delivered from boiler by starting-up a reduction – and–cooling station (see the simplified schematic diagram of control of delivery system of heat and electric power, shown in Fig. 10).

During heating period, steam pressure at outlet from the turbine should correspond to a demanded temperature of working medium (in the case of floor heating); in this case the controller R_{p1} controls the reduction-and-cooling station SRS_1. Heat used to warming-up service water

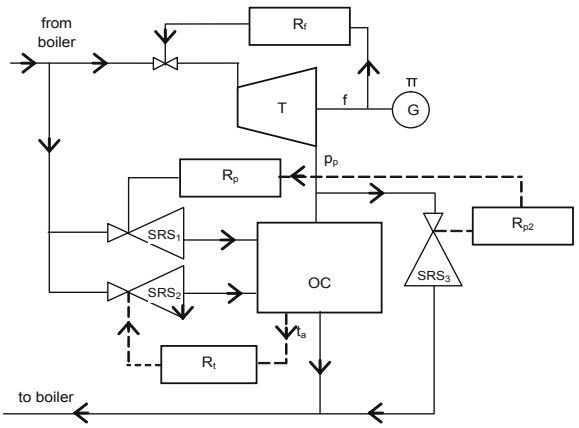

***Fig.10**. Simplified schematic diagram of control of delivery system of heat and electric power in heat –and –electric power plant fitted with backpressure turbine.*
***Notation**: T – turbine, G – electric generator, OC – heat consumers, SRS – reduction-and-cooling stations, f – frequency, p_p – steam pressure behind the turbine, t_a – water temperature in heat accumulator, R – controller.*

would be then delivered by means of the reduction-and-cooling station SRS_2 which feeds heat accumulator, being switched-on periodically. Outside the heating period steam pressure at oulet from the turbine should correspond to a demanded temperature of service water.

When heat amount resulting from quantityof generated electric power is greater than the demanded then steam surplus at outlet from the turbine is sent directly to boiler, bypassing the heat consumers, see Fig. 10; in this case the controller R_{p2} controls the reduction-and-cooling station SRS_3.

Delivery control of heat and electric power if extraction–and–backpressure turbine is used

In the extraction–and–backpressure turbine two quantities can be controlled for the reason of possible impact on two kinds of control valves: before the turbine and behind the extraction. Therefore, apart from electric power, steam pressure in the extraction or behind the turbine can be also controlled. Fig. 11 presents a concept of control of steam pressure in the extraction when the steam absorbed from the extraction is used to warming-up service water, and the steam taken from turbine's outlet is used to space heating. Flow rate of the steam used for warming-up service water, is subjected to control.To this end, the valves behind the extraction are used. Flow rate of the steam at outlet from the turbine, used to space heating, is not controlled.

When steam flow rate at outlet from the turbine is not sufficient to maintain temperature demanded for accommodations then the lacking amount of heat is absorbed from the extraction. To this end, the reduction–and–cooling station SRS_1, controlled by the behind the turbine pressure controller R_{p1}, see Fig.11.

When steam flow rate at outlet from the turbine is greater than the demanded for space heating then the steam surplus is sent directly to boiler -the controller R_{p2} in Fig. 11.

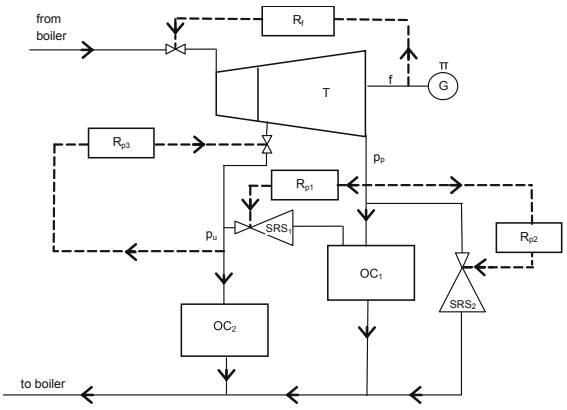

Fig.11. *Simplified schematic diagram of control of delivery system of heat and electric power in heat –and –electric power plant fitted with extraction-and-backpressure turbine of controlled flow rate of the steam used for warming-up service water.*
Notation*: T – turbine, G – electric generator, OC_1 – heat consumer for space heating, OC_2 – heat consumer for service water warming-up, SRS – reduction-and-cooling stations, f – frequency, pp – steam pressure behind the turbine, p_u -steam pressure in the extraction, R – pressure controller.*

In another variant the control valves behind the extraction can be applied to control steam flow rate at outlet from the turbine, used for space heating. Then, steam pressure at outlet from the turbine serves as the controlled signal. Such concept of delivery control of heat and electric power is presented in Fig. 12.

Steam pressure behind the extraction is subjected to control. Its change resulting from a change of flow rate of the steam used for space heating, triggers off action of the controller, R_p, onto control valves behind the turbine extraction. The steam used for warming-up service water is periodically taken from the turbine extraction. The service -water temperature controller R_t is applied to this end, see Fig.12.

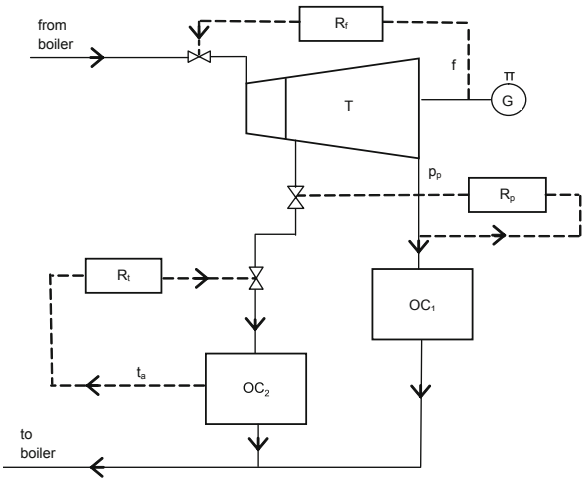

Fig.12. *Simplified schematic diagram of delivery control of heat and electric power in heat-and –electric power plant fitted with extraction-and-backpressure turbine of controlled flow rate of the steam used for space heating.*
Notation: *t_a – service water temperature in accumulator, R_t – temperature controller; as to the remaining symbols – see Fig. 11.*

Outside heating period, steam from turbine outlet should be directed to service-water heater when turbine extraction is shut-off; it corresponds to the backpressure turbine control whose concept has been presented in the preceding section.

Final remarks

Application of steam microturbines to the dispersed, combined generating system of heat and electric power, brings many specific problems in the area of automatic control. From this point of view various operational situations both dealing with microturbine set connection to an external electric power system and with its operation in a separate electric power system, have been reviewed. In both the above mentioned variants structure of microturbine automatic control system must ensure feeding the so called critical consumers with electric power. A concept of microturbine's automatic control system which fulfils the requirement has been presented in this paper. Structure of automatic control system for microturbines, both of backpressure and extraction-backpressure type, intended for the feeding heat consumers of two types and different steam pressure values, has been proposed and discussed.

Bibliography

1. Biczel P.: Direct current versus alternating current. Systems-Journal of Transdisciplinary Systems Science, Vol.13, special issue 1/2, 2008
2. Cruz T.V.G., de Mericia J.G.,.Veras C.G, Borges G.A.: Instrumentation, Architecture and Real-Time Control of Microturbine. Proc. of 18th International Congress of Mechanical Engineering,,Ouro Preto, MG, Brazil, 6÷11November 2005
3. Degobert Ph., Krenawan, X.Guilland S.: Micro-grid powered by photovoltaic and micro turbine. Proc. of International Conference on Renewable Energy and Power Quality, Palma de Mallorca, Spain, April 2006, (CD-ROM record)
4. Domachowski Z.: Counteracting Windpower Fluctuations within a Separate Electric Power Grid. Proc. of 5th ASME Turbo Expo 2007: Power for Land, Sea and Air, Montreal, Canada, 14÷17 May 2007, Paper No. GT 2007-28218
5. Domachowski Z., Klimacki Z.: Automatic control of frequency and active power of separate electric power system (in Polish). Prace Instytutu Maszyn Przepływowych Reports of Fluid Flow Machinery Institute, Polish Academy of Sciences), issue no. 92, 1990
6. Felthi O., Dessaint L.A., Al-Haddad K.: Modeling and Simulation of the Electric Part of a Grid Connected Micro Turbine. Proc. Power Engineering Society General Meeting, IEEE, 6÷10 June 2004
7. Hangwitz S.: Modelling of Microturbine Systems. Doctoral thesis, ISSN 0280-5316, Department of Automatic Control, Land Institute of Technology, May 2002
8. Jurando F., Cano A., Carpio J.: Biomass based microturbine plant and distribution network stability. Energy Conversion and Management, vol. 45, issue 17, October 2004.
9. Mackay R.: Microturbine Precise Power Systems. U.S. Patent 6 977 466 (granted on 20 December 2005)
10. Sacha A.K., Chowdhury S., Chowdhury S.P., Crossley P.A.: Microturbine Based Distributed Generator In Smart Grid Application. Proc. CRED Seminar 2008: Smart Grids for Distribution, Frankfurt, 23-24 June 2008.
11. Setiawan E.A.: Dynamic Behavior of a 30 kW Capstone Microturbine. Institut für Solare Energieversorgungstechnik, e.V. (ISET), Kassel, Germany, 2007
12. X.C.Shan, Hang Qide, Sun Yaofeng, Wang Zhenfeng: Design, fabrication and characterization o fan air-driven micro turbine device. Journal of Physics, Conference Series 34 (2006), International MEMS Conference 2006
13. Torres E., Larragneta J.M., Equia P., Mazon J., San Martin J.I., Zamora I.: Dynamic Performance of a Microturbine Connected to a Low Voltage Network. Departament of Electrical Engineering, ETUI – Bilbao, UPV/EHU, 2006
14. Woodward: Comprehensive Steam Turbine Control for Various Applications. Application Sheet 51 237.

POLISH MARITIME RESEARCH, Special issue 2009/S1; pp. 14-21
10.2478/v10012-008-0039-z

Polish aspects in the modern design solutions of steam turbine flow systems

Andrzej Gardzilewicz,
Dariusz Obrzut,
Mariusz Szymaniak

Abstract

This paper presents new solutions of turbine stages which have been applied to high-power steam turbine flow systems. The structures, elaborated in Poland, were designed with the use of the authors' original computational software and verified by measurements performed on real turbine sets.

***Keywords**: steam turbine, power cycles, flow systems, efficiency, errosion.*

Introduction

Most steam turbines operating in Poland were produced by Zamech Works, Elblag. For power industry needs domestic solutions were elaborated and also licence designs, mainly from Russia, were adapted. For past years it was managed to elaborate a relatively modern production process based on own computer design systems. The programs have been based first of all on co-operation with Polish scientific research institutes. It would appear that after taking over the Zamech Turbines Division by the ABB, ALSTOM, the worldwide recognized concerns, realization of Polish designs will be eliminated. In line with the new philosophy the works in Elblag took over immediately the most modern design and technological solutions of the concern and started to use foreign numerical calculation programs. However the fact of keeping Polish engineers still at work in the enterprise, has resulted in that Polish turbine solutions have been still coming into being. In this paper are described two design solutions elaborated in co-operation with the Fluid Flow Machinery Institute, Polish Academy of Sciences, Gdansk. They deal with new turbine stages: high-loaded ones and those before regenerative extraction.

Examples of realization of new stages of steam turbine

High-loaded stages

Impulse stages intended for operating under high loads, which ALSTOM, Elblag, has applied to 7CK-65 turbine set in the Zielona Gora Electric Power Station, can be deemed the best example of the modern solutions presently realized in Poland. Their superiority over other solutions of the concern has consisted in that the blading system of the turbine of 65 MW electric power and 135 MW heat power, could be accommodated in one common cylinder, that is schematically shown in Fig. 1 [1].

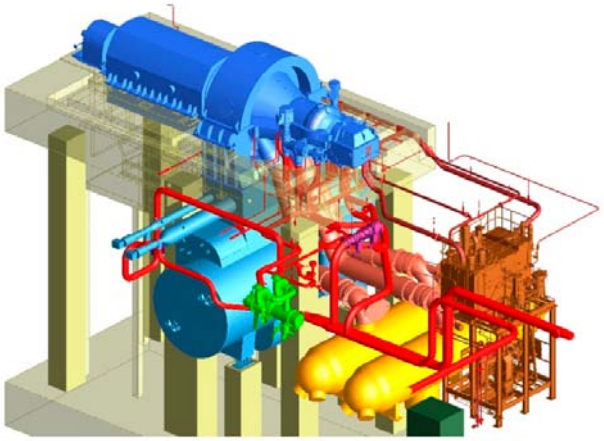

***Fig.1** Machinery devices of 7CK-65 steam turbine unit installed in Zielona Gora Electric Power Station [1].*

It was achieved at maintaining its high efficiency, improved availability, and obviously, material savings. The minimized number of 23 stages resulted from the application of new profiles permitting to operate under high loads, to majority of rings of guide vane and rotor blades. Geometry of the profiles had to be changed the higher loads to be realized. They had to guarantee a little changed kinematics of steam flow as compared with conventional solutions. This results from a change of inlet and outlet angles as shown in Fig. 2, acc. Yamamoto [2].

As can be observed in Fig. 2 the rotor blade profiles of highly loaded stages make flow passages longer,

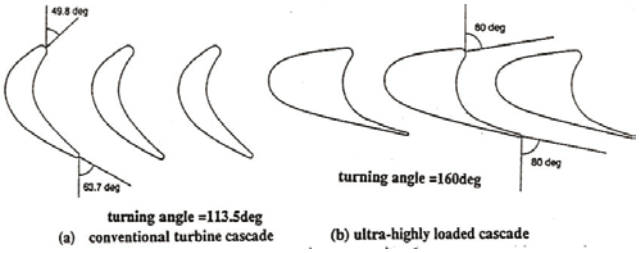

***Fig. 2** Comparison of rotor blade ring cascades: **a)** conventional and **b)** highly loaded, acc. [2].*

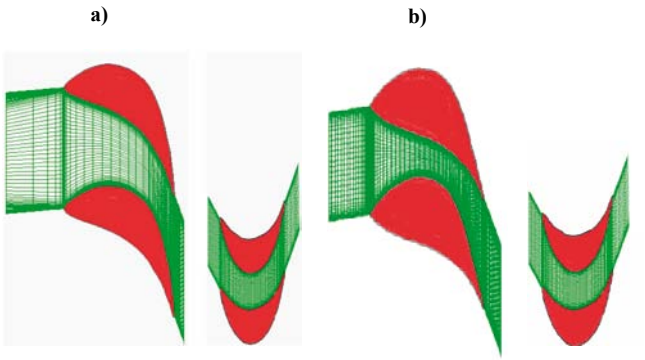

*Fig.3 Geometry of guide vane and rotor blade rings of the turbine stages: **a)** conventional and **b)** high-loaded*

that is resulted from a distinctly larger change of flow turning angle in blade rings. The so large changes of flow direction reaching even 160^0 are realized first of all due to change in suction (concave) side contours of profiles, as described in detail by Amos [3].

The larger flow turning angles result obviously in a greater loss of energy. In the tests performed on the new designed stages the turning angles were limited to the range of $130\div140^0$. In this case the guide vane ring profiles operate at outlet angles in the range of $10\div12^0$ and the rotor ring profiles – in the range of $16\div18^0$. Forms of the new profiles resulted from optimization of conventional impulse profiles elaborated in ALSTOM, Elblag, in co-operation with the von Karman's Institute, Brussels. Their geometry is schematically shown in Fig. 3.

The performed numerical analyses confirmed that the new profiles have been applicable to the assigned aims [4]. The relevant flow calculations were carried out by using the CFD FlowER program and 3D model

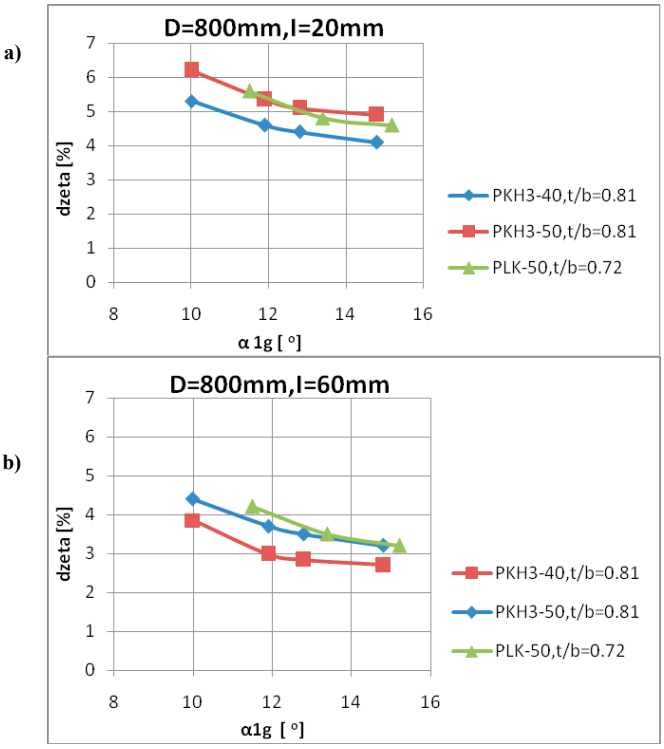

*Fig.4. Comparison of energy losses in function of the angle α1 for cylindrical blade ring cascades of; **a)** PKH3-40 profiles and **b)** PLK-50 profiles, acc. [4].*

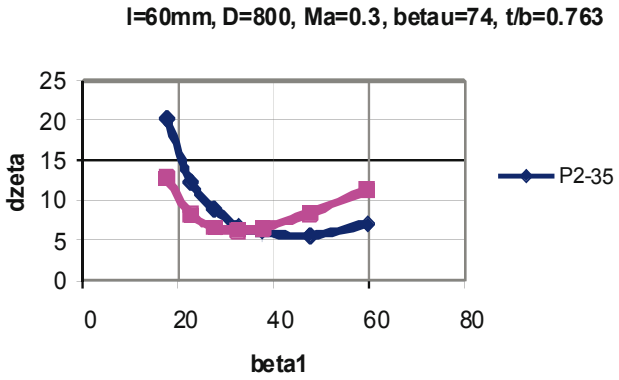

Fig.5. Comparison of energy losses for P2-35 and P2V-35 profiles in function of the inlet angle beta 1, acc. [4]

which takes into account viscosity of medium [5]. The calculations dealt with single ring of guide vane and rotor blades for geometry and operational conditions appropriate for operation in heat power turbine. It was observed that the losses within the cascades of guide vane blades of the new, PKH3 profiles, at the small values of the outlet angle $\alpha_1 \approx 11^0\div13^0$ and the velocities corresponding with higher loads, were lower by more than 1%, as compared with those recorded in the PLK typical impulse blade rings, Fig. 4.

In the PKH3-profile blade rings the lower level of flow losses resulted not only from the performed efficiency-orientated optimization of form of the profiles but also change of their geometry. In the new, „thicker" guide vane blade profiles it was possible to limit breadth of the ring at maintaining similar values of strength parameters. Such operation leads additionally to limitation of secondary and edge losses at the same

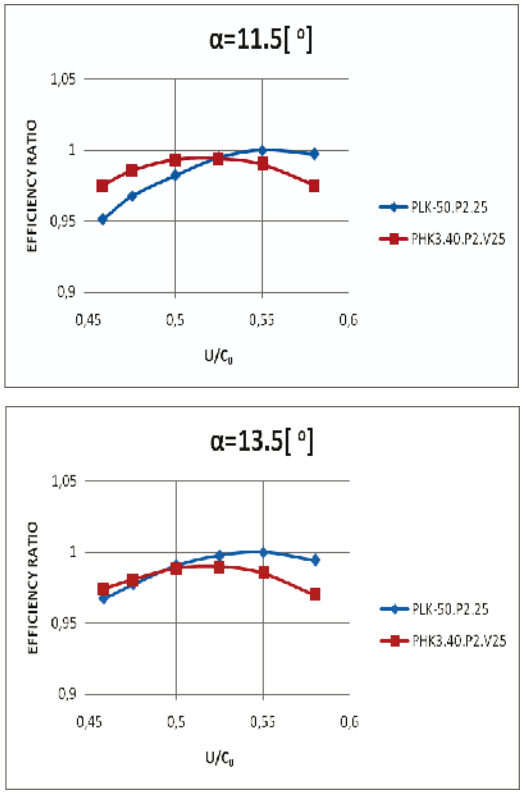

Fig.6 Change of efficiency in function of loads for the group of three cylindrical stages with PKH-3/P2V and PLK-P2 profiles at different values of the inlet angle, α1, acc. [4].

length of blades. It should be stressed that values of the optimum-efficient relative pitch of the new-profile rings exceeded 0.8, whereas values of the conventional relative pitch of guide vane rings were kept on the level of 0.7. It corresponds with a lower number of blades.

A little lower losses than those for P2 conventional profiles were also obtained for new rings of rotor blades of P2V profiles. The lower losses concerned flows at smaller inlet and outlet angles, characteristic for higher values of stage load. Comparison of the new and old profiles showed that the lowering of losses was especially distinct for values of the inlet angle $\beta_1 < 27^0$, that corresponded with values of the outlet angle $\beta_2 < 18^0$. The observed differences exceeded 2% in favour of the new profiles, however the level of minimum losses for greater angles corresponding with lower loads on conventional rings, was lower by 0.5%, (see Fig. 5).

The positive results of analysis of steam flow through rings of PKH3/P2V profiles encouraged to perform successive numerical tests. They dealt with investigations of turbine stages. In this case was searched for an optimum efficiency-orientated geometry of three cylindrical stages fitted with the new and conventional profiles, suitable for operational conditions of the first group of stages of the designed heat power turbine. It was revealed that the stages with PKH3 P2V profiles were more efficient than those with PLK P2 profiles at the same assumed diameter $D_w = 800$ mm, in the range of greater loads at the applied angle $\alpha_1 \sim 11.5^0$ (see Fig.6). In the diagram the loads are determined by the ratio u/co. The curve of efficiency change in the new stages appeared more „flat" as compared with the characteristics of typical impulse stages. The superior features are not observed at greater values of inlet angles, i.e. on the level of 13.5^0.

The relative pitch values of the calculated stages at which the highest efficiency was obtained, was determined on the level of 0.8 for the new, PKH3 guide vanes, and for the old, PLK ones on 0.7, at the similar pitch values for both rotors, on the level of 0.7. It resulted from the optimization process of mutual orientation of blades.

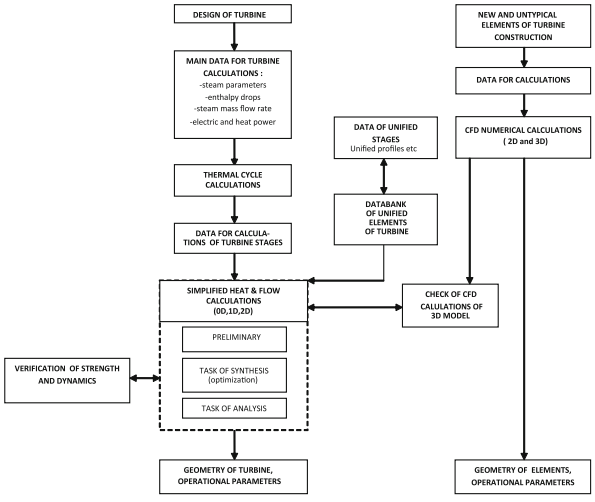

Fig.7 *CAD system for high-loaded turbine stages, acc. [6].*

Also in this case a favourable impact on efficiency was given by the smaller breadth assumed for the new guide vane profiles, that additionally made length of turbine flow passage, shorter. As above mentioned, the turbine stages with the new blade rings which permit higher loads to be applied, were practically installed in 7CK-65 turbine construction. Relevant design calculations were carried out with the use of the CAD system elaborated in Poland, whose schematic diagram is shown in Fig. 7 [6].

Data concerning thermodynamical parameters of the stages were determined from thermal cycle calculations of the turbine unit, with taking into account parameters of boiler, water cooling system, as well as the electric and heat power assumed for the unit. From preliminary calculations of the turbine (0D model) it has resulted that cylindrical stages could be used for three groups of stages. The following basic gabarites were determined for them: diameters, blade heights, as well as number of stages. The data were used as the basis for detail design calculations (synthesis) and check calculations (analysis) which were rperformed by means of simplified programs for 1D and 2D model. In the programs solutions of non-viscous-flow equations were corrected by means of coefficients obtained from CFD numerical calculations for blade rings with new profiles, in accordance with the concept presented in [7].

Efficiency optimization procedures built-in the programs, made it possible to determine passage geometry, as well as number of blades and their most favourable orientation in particular stage rings. In the calculations the producer's design standards concerning diameters, overlaps as well as solutions of sealing were taken into account [8].

The increasing of stage loads made it possible to reduce number of cylindrical stages in the turbine from 20 to 16. It was achieved at a high flow efficiency confirmed by numerical calculations of 3D model [9]. As obtained from the tests, the efficiency was -by a little more than 1% -different from the maximum value available in the case of conventional impulse stages.

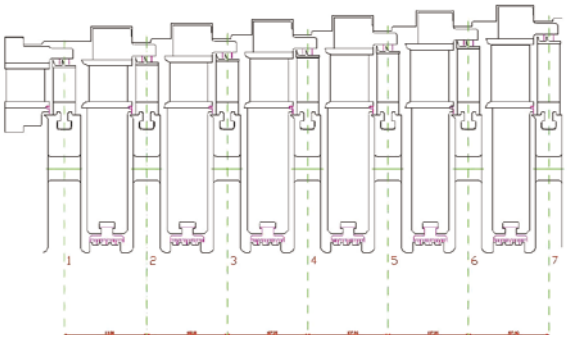

Fig.8 *Axial cross-section of 1st group blade system of 7CK-65 heat power turbine, acc. [8]*

In Fig. 8 the computer drawing of the flow system of 1st group cylindrical stages is presented.

The drawing was automatically generated on the basis of heat–and-flow calculations just after design

verification of particular rings by means of strength and dynamics calculations [8]. As a result of the lowering of number of cylindrical stages it was possible to resign easily from an additional cylinder originally planned in the turbine. A photo of the turbine set and its axial cross-section covering also two steam -flow control stages intended for heating the extractions is shown in Fig. 9.

The calculations for the designed flow system of the turbine were verified experimentally in the heat-and-power station. To this end the routine guarantee tests of the entire turbine set were supplemented by thermal measurements in compliance with the concept given

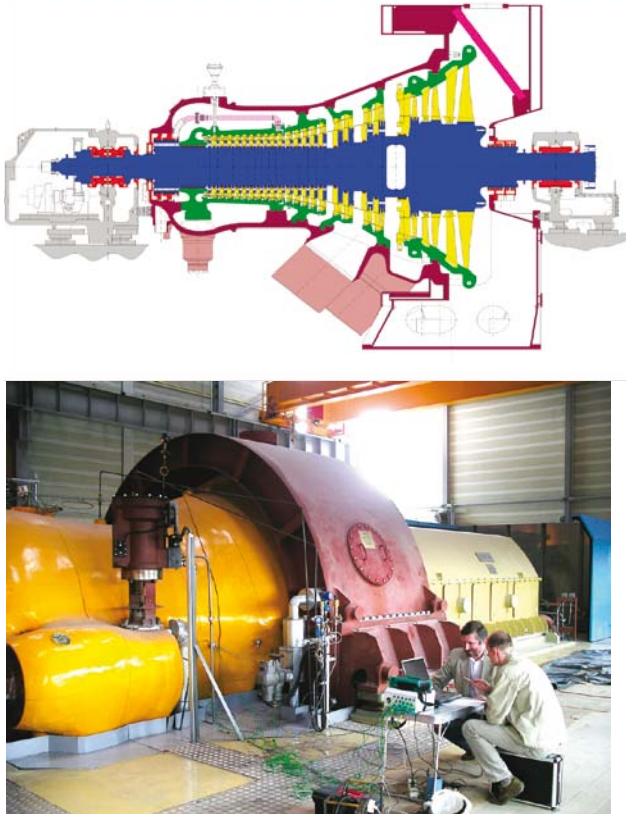

Fig.9 *Photo and axial cross-section of 7CK-65 steam turbine set, [4].*

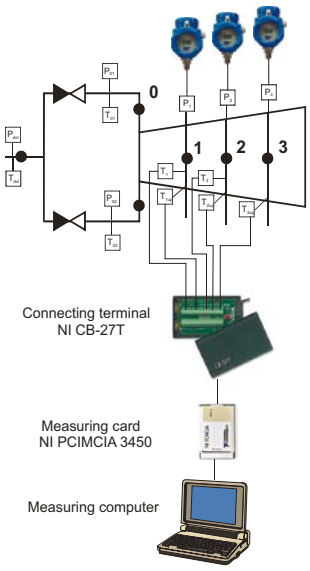

Fig.10 *Schematic diagram of the measuring system intended for the testing of the cylindrical stages of 7CK-65 turbine, acc.[11].*

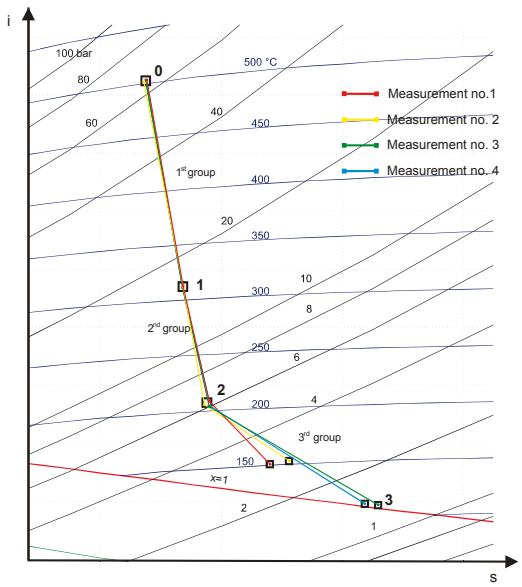

Fig.11 *Run of steam expansion line for 7 CK-65 turbine, acc. [10].*

in [10]. Schematic diagram of the measuring system intended for the testing of cylindrical stages is shown in Fig. 10, acc. [11].

The measured pressure and temperature values made it possible to determine steam enthalpy and expansion line in this part of the turbine (Fig. 11). The tests covered series of four measurements in various operational conditions. The performed analysis showed that the measurement errors in estimating efficiency of two first groups of the turbine's stages did not exceed 1%. The third group of the turbine's stages was excluded from the analysis because during the tests its operational parameters appeared greatly variable. It was caused by the fact that to this group the steam leaking from seals, largely changing the blade system parameters, was delivered.

Tab. 1 presents comparison of calculated and measured values for 1st groups of cylindrical stages in nominal conditions.

Tab. 1 *Comparison of calculated and measured values for 1st groups of cylindrical stages in nominal conditions*

	As measured	As calculated
Inlet pressure [MPa]	6.287	6.287
Inlet temperature [oC]	498	498
Outlet pressure [MPa]	1.553	1.553
Outlet temperature [oC]	310.1	307.5
Efficiency of the group of stages [-]	0.879	0.892
Mass flow rate [kg/s]	51.05	51.35

Only 1.5% differences in efficiency were obtained at a very high conformity of the calculated mass flow rate with that measured with the use of an area reducer. They were only a little smaller from measurement errors. As the analysis showed, the higher value of calculated efficiency resulted from the fact that non-stationary processes were not taken into account [9] during determination of the correction coefficients used in the design programs. The 7CK-65 one-cylinder turbine of 16 stages fitted with the new profiles has faultlessly operated for over seven years.

New solutions of stages before extraction

In construction of turbine stages to introduce clearance (gaps) between moving and motionless elements in order to ensure their co-operation is necessary. Steam fluxes flowing through such gaps do not transfer work to rotor, which results in loss of energy. The phenomenon is especially intensive in low-pressure parts of turbine where large gaps over unshrouded rotor blades are present and fast flowing steam makes medium outflow to regenerative extraction difficult. In the blade system whirl and stagnation zones are then formed, that was confirmed by probing measurements carried out on real turbines (see Fig. 12), acc. [12]. In order to eliminate the intensive fluxes it was proposed to introduce, to the stages placed before regenerative extraction, a ring which will direct the leaking steam to the heat exchanger directly, Fig.13. The relevant solution was claimed to Polish patent office [13] and sucessfully implemented in LP parts of 200 MW turbines with Bauman's stages [14].

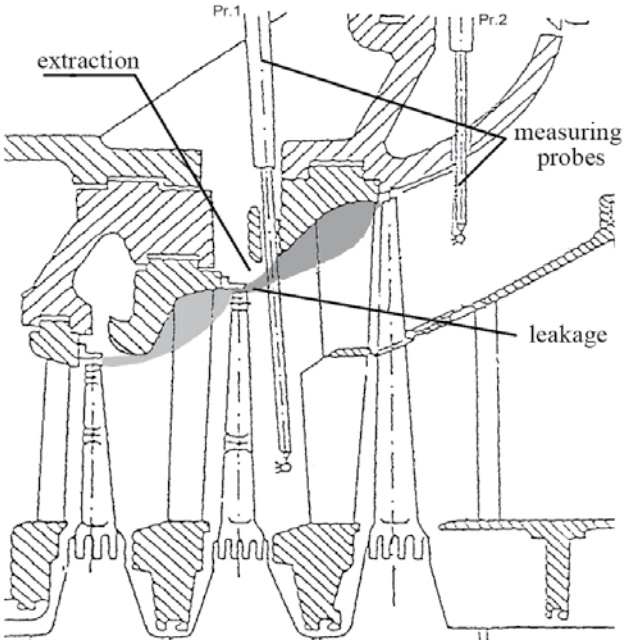

Fig. 12 *Low-pressure part of 200 MW turbine with measurement instrumentation. Separation zones in leakage area are shown in grey. wg [12].*

Advantages of application of the ring, with a view of turbine efficiency and operation, consisted in:

- elimination of whirl zones in the stage behind extraction both in meridional and circumferential plane;
- elimination of the mixing of two fluxes: of main flow and leaking flow;
- the making use of higher energy of leaking steam in the first, usually underheated, regenerative extraction;
- the lowering of moistness losses and errosion damage by effective separation of water drops to the extraction; its low cost as compared with other solutions.

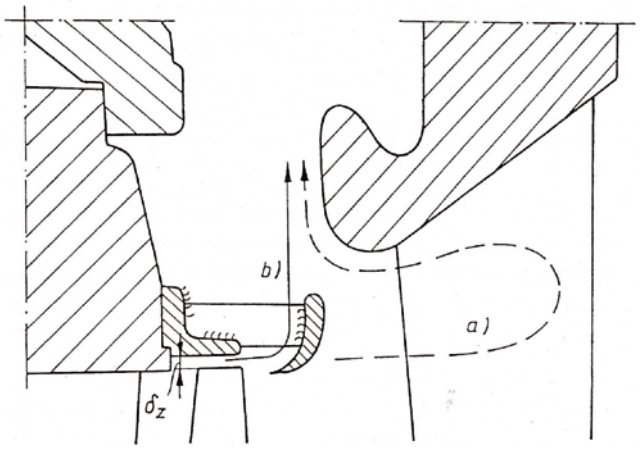

Fig.13 *New solution of turbine stage before extraction, acc. Patent no. P 160-805*

Both the performed theoretical investigations and measurements have demonstrated superiority of application of the new solution. Owing to it, shrouding seals -much more expensive and difficult in the case of realization of long blades -could be eliminated.

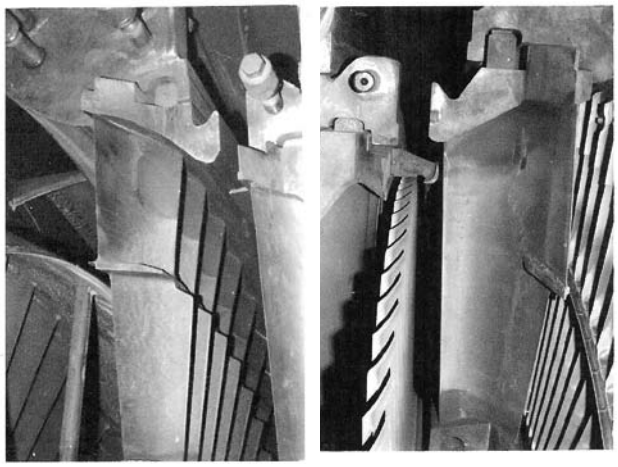

Fig.14 *Photos of 200MW turbine Bauman's stage in versions before (left) and after (right) its modernization, acc. [14].*

Photos of the turbine blade system in the versions before and after introduction of the ring are presented in Fig. 14. Salt sediments in the stagnation zones, eliminated after introduction of the ring, can be there observed.

In the years 1994÷2006 the solution was implemented in fourty 200 MW turbines in Poland and Ukraine. The average power increase of 600 kW/unit was obtained. The rings operated in the turbines faultlessly, that was confirmed by the observations carried out during operation [15].

The successful implementations have contributed to application of the considered solution also to the most modern design of LP parts fitted with ND 41A ALSTOM outlet, used for modernization of 200 MW turbines. In this case the decision on the application has been taken not so much due to profits in efficiency as to decrease faster erosion of inlet edge of blades of the last rotor stage, spread over 2/3 of their length (see Fig.15). This region was reached by water drops seperated in the next-to-last stage and intensively splashed by leakage flux. The recorded erosion damage are specially dangerous in unhardened areas shown in Fig. 15, acc. [16].

Fig.15 *Photos of inlet edge erosion of the blade of the last rotor stage after 40 000 h service, acc. [16].*

Fig. 16 presents the concept of introduction of the rings to the modernized LP part of 200 MW turbines, acc. [17].

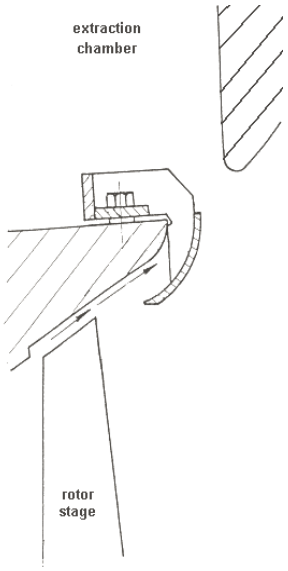

Fig.16 *Concept of introduction of the ring to the LP part of 200 MW turbine modernized in ALSTOM Works, acc. [17]*

After performing some additional analyses the patent was implemented to the power unit no.5 of Kozienice Electric Power Station. The analyses concerned detail heat-and-flow calculations in which values of its operational parameters before and after modernization were compared to each other. The CFD numerical calculations were carried out by means of the FlowER software [5]. For both the cases identical steam flow boundary conditions which resulted from the probing measurements carried out on the real power unit [18], were assumed. They covered distributions of static pressure, total pressure, temperature and steam flow angles before and behind stages, for a set value of steam mass flow rate. Description of the applied calculation methods can be found in [19].

The calculated total pressure distributions and streamlines prior assembling the rings in the diffuser between 3rd and 4th stage are presented in Fig. 17. The images distinctly show how the leakage blocks the steam flowing toward extraction.

In the performed analysis concerning the modernization the ring's form most favourable for efficiency was determined by using multi-variant numerical calculations. The following quantites were optimized: diameter of the pipe the ring was made of, its length, inlet edge orientation angle and its location with respect to rotor blade. The location was crucial for final choice as it had to guarantee that any intensive leakage is eliminated from the main steam flux at only minor disturbance of it. Some characteristic images of the distributions of flow parameters for the calculated variants, are given in Fig. 18.

Total pressure distribution and streamlines in the diffuser and extraction chamber for a selected variant are presented in Fig. 19. The leakage flows to the extraction chamber and after being braked it rather smoothly splits into the flow to the heat exchanger and the continued flow through the blade system. For the ring's position selected for nominal conditions, 3 kPa rise of pressure in the extraction chamber with respect to the initial version, was recorded. Also, the inflow to the guide vanes ring of the last stage has been favourably ordered, that is illustrated by the uniformly arranged stremlines. As calculated, the phenomenon resulted in the stage efficiency increase by over 1%. The shift of the ring inlet from the edge of the rotor blade should ensure effective sucking-off the water accummulated in this zone due to action of centrifugal forces, and to direct it into regenerative extraction and reduce erosion this way.

The performed calculations made it possible to assess forces acting on the ring, which were the basis for strength and dynamic verification. The recorded loads appeared

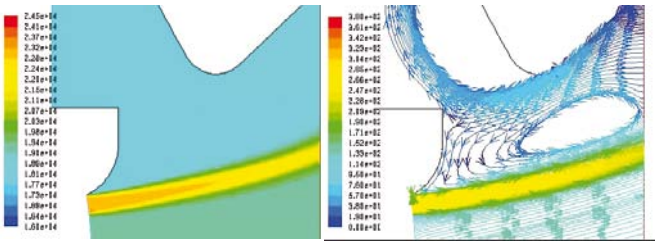

Fig. 17. *Total pressure distrbution (left) and streamlines(right) in the interstage diffuser, close to regenerative extraction, prior assembling the ring, acc. [18].*

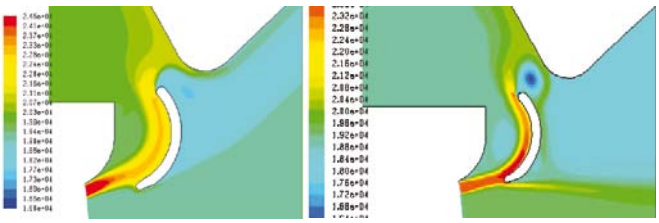

Fig. 18. *Distributions of steam flow total pressure close to extraction in turbine for selected calculation variants.*

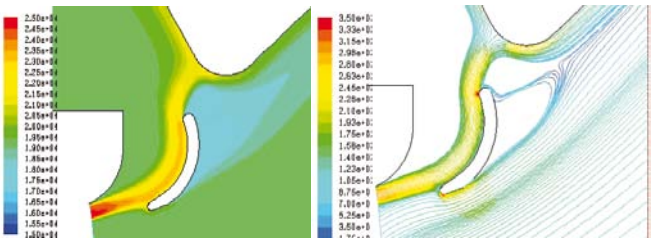

Fig.19. *Distrbutions of total pressure (left) and streamlines(right) in the interstage diffuser, close to regenerative extraction, after assembling the ring, acc. [18].*

rather small and danger of resonances effectively eliminated by proper choice of number of ribs fastening the rings to clamp [20], which was taken into account in the final design.

The significant changes in extraction chamber pressure and the last stage efficiency were used to assess energy profits to be obtained from application of the patent in question. They were assessed by calculations of thermal balance of the entire turbine set, performed with the use of the thoroughly tested DIAGAR software [21]. Main data for the above mentioned calculations were taken from measurements of thermodynamic parameters prepared on the basis of the guarantee tests [22].

Schematic diagram of thermal cycle of the power unit, i.e. 200 MW power unit no.5 at Kozienice Electric Power Station, is presented together with depicted measurement points in Fig. 20.

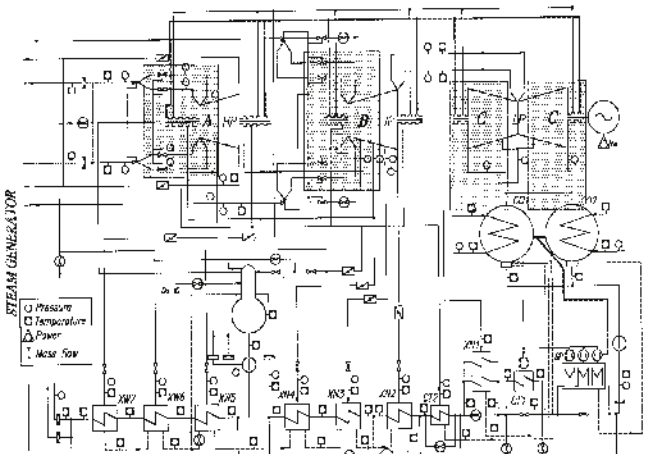

Fig. 20. *Schematic diagram of heat-and-flow cycle of the power unit, i.e. 200 MW power unit No.5 at Kozienice Electric Power Station, with depicted measurement points, acc. [22].*

Changes of output power and specific heat consumption in the cycle after implementation of the patent to the modernized turbine fitted with ND41 outlet in function of output power and condenser pressure, are shown in Fig. 21.

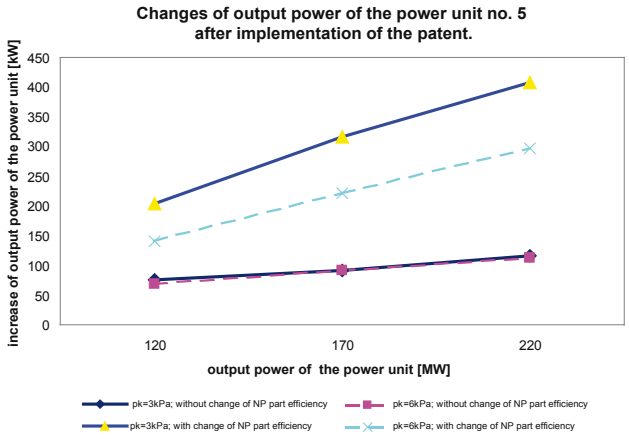

Fig.21 *Changes of output power and specific heat consumption for various loads of the turbine set after implementation of the patent in question, acc. [19].*

As can be observed in the figure, within the turbine load range of 120÷220 MW and the condenser pressure range of 3÷6 kPa the decrease of specific heat consumption amounts to 11÷16 kJ/kWh, which results in the output power increase of 200÷400 kW. The equivalent increase of the turbine-set efficiency is in the range of 0.1÷0.2% which can not be measured during routine guarantee tests.

The efficiency rise effects can be only determined indirectly during measurements after modernization. It concerns the easily measurable rise of feed-water temperature in the first heat exchanger, by 3^0C. Measurements of distribution of thermodynamical parameters can be used in interstage spaces, which can be realized by the probing method only. Such measurements are planned to be performed soon on the turbine set no. 5 at Kozienice Electric Power Station (see Fig. 22). Within the scope of the measurements control of erosion damage growth in the last stage rotor blades as well as inlet area of the rings, is provided for.

Fig.22. *The ring placed inside 225 MW turbine*

Bibliography

1 Łuniewicz B., Kietlinski K., Obrzut D., Szyrejko Cz., Gardzilewicz A.: 7CK turbine for gas-steam power unit at Zielona Gora Heat and Electric Power Station (in Polish). Mat. Conf. „Technical, Economic, and Environmental Aspects of Combined Cycle Power Plant", Gdansk University of Technology, Gdansk 2004

2 Yamamoto A., Matsunama T., Outa E.: Three Dimensional Flows and Losses in an Ultra-Highly Loaded Turbine . ASME Turbomachinery Conf. Hawaji 2003

3 Amos I.G. et al.: Design and off-design optimisation of highly loaded industrial gas turbine stages. Applied Thermal Engineering 24, 2004

4 Obrzut D.: Design of turbine highly loaded impulse stages with the use of modern computational techniques (in Polish). Doctoral thesis, Gdansk University of Technology, Gdansk, 2009, (in the press)

5 S. Yershov, A. Rusanov, A. Gardzilewicz, P. Lampart, J. Świrydczuk: Numerical simulation of 3d flow in axial turbomachines, Task Quarterly,Vol. 2/2, pp. 319-347, 1998

6 A. Gardzilewicz: Contemporary problems of design, construction and diagnostics of steam turbines (in Polish). Zeszyty Naukowe IMP PAN (Scientific Bulletins of FFM Institute, Polish Academy of Sciences), no.502/1461/99, Gdansk 1999

7 Gardzilewicz A., Lampart P., Świrydczuk J., Łuniewicz B., Obrzut D.: A mixed 1D/3D approach to design of turbomachinery blading system. Proc. Summer School on CFD for Turbomachinery Applications, September 2001, Gdansk.

8 Collective work under supervision of Obrzut D.: Heat-and-flow design calculations of 7CK-65 turbine for Zielona Gora Heat and Electric Power Station. Shortened strength calculations (in Polish). Int. publ. ALSTOM Power, Elblag 2002/2003.
9 J. Świrydczuk, A. Gardzilewicz: CFD numerical calculations of 7CK-65 turbine cylindrical stages (in Polish) . Publ. Diagnostyka Maszyn 22/04, Gdansk, 2004
10 D. Obrzut: A concept of measurement verification of design calculations of turbine impulse stages (in Polish).Int. publ. ABB-ALSTOM, Elblag 2000
11 A. Gardzilewicz, S. Marcinkowski, J. Karwacki, D. Obrzut: Heat-and-Flow Tests of 7CK-65 turbine at Zielona Gora Heat and Electric Power Station (in Polish). Publ. Diagnostyka Maszyn, no.01/05, Gdansk 2005
12 Gardzilewicz A.. Marcinkowski St., Rogala I.: Realization of the tests on steam flow through LP part of 13K-215 turbine of the power unit no. 8 at Kozienice Electric Power Station (in Polish). Publ. IMP PAN, no. 123/90, Gdansk 1990
13 Gardzilewicz A., Marcinkowski St.: A turbine stage (in Polish). Patent no. P 160-805, Polish Patent Office, Warszawa 1993
14 Gardzilewicz A., Marcinkowski St.: On a design solution of steam turbine stage before extraction (in Polish). Zagadnienia Maszyn Przepływowych (Problems of Fluid Flow Machinery), Jubilee Publ. IMP PAN (FFM Institute, Polish Academy of Sciences), Gdansk 1993
15 Gardzilewicz A., Marcinkowski St., Sobera H., Jozefowicz Z.: Service experience from application of the patent no. P160-805 to 13K-215 steam turbines (in Polish). Energetyka, no. 3, Warszawa 1994
16 Marcinkowski St., Gardzilewicz A., Szymaniak M.: Examination and analysis of erosion hazard to outlet stages of 200 MW turbine of the power unit no. 3 at Kozienice Electric Power Station (in Polish). Publ. 06/08, Diagnostyka Maszyn, Gdansk 2008
17 Gardzilewicz A., Karcz M., Marcinkowski St., Bielecki M., Badur J., Malec A.,
18 Banaszkiewicz M.: Proposal of modernization of a steam turbine stage before extraction, CFD and CSF analysis.TASK-Quarterly 6, no. 4, 2002
19 St. Marcinkowski, A. Gardzilewicz: Test reports and results of measurements of steam flow through LP part of modernized 13K-215 turbine at Kozienice Electric Power Station (in Polish). Ext. Publ., no. 3113/98, IMP PAN (FFM Institute, Polish Academy of Sciences), for Diagnostyka Maszyn, Gdansk 1996
20 Gardzilewicz A., Szymaniak M., Pałżewicz A., Głuch J.: Concept of a new solution of before-extraction stage of the turbine set no. 5 at Kozienice Electric Power Station. Heat-and-flow calculations (in Polish). Publ. IMP PAN (FFM Institute, Polish Academy of Sciences), no. 563/08, Gdansk 2008
21 J. Badur, D. Sławinski: Strength and dynamics calculations of the ring according to the patent no. P 160-805, for 13K-225 turbine fitted with ND41 outlet (in Polish). Publ. Diagnostyka Maszyn, no. 05/08, Gdansk 2008
22 Gardzilewicz A., Bogulicz M., Głuch J., Uziębło W.: Modernization of the thermal calculation module of DIAGAR software, v.2002 (in Polish). Publ. Diagnostyka Maszyn, no. 28/02, Gdansk 2002
23 Report on the guarantee measurements of 200 MW turbines at Kozienice Electric Power Station, performed after modernization (in Polish). Arch. mat. INWAT, Łodź 1999÷2002

POLISH MARITIME RESEARCH, Special issue 2009/S1; pp. 22-26
10.2478/v10012-008-0040-6

Selected problems of determining an efficient operation standard in contemporary heat-and-flow diagnostics

Jerzy Głuch

Abstract

In this paper are specified causes of ambiguities and difficulties in determining an efficient operation standard for land and marine turbine power plants. Two of them, namely: lowering values of working media inlet parameters and changes in configuration of connections between component devices of thermal cycles, have been analyzed. As a remedy for resulting difficulties a thermal cycle computational model of modular structure has been proposed. As showed, the tuning of the computational model with respect to correct measurements by elaborating individual corrections for calculation coefficients of computational methods used for particular devices ensures good accuracy of determination of unserviceability symptoms in these conditions. Introduction to the modular computational model – of control modules making use of valve opening indicators in DCS system ensures good accuracy also in the case of changes in structure of complex power object.

Keywords: *steam turbines, operation of turbines, power units, thermal measurements, thermal diagnostics, diagnostic relations*

Introduction

Heat-and-flow diagnostics belongs to such forms of process diagnostics, in which the diagnostic method based on application of a standard, turns out to be useful, Fig. 1. As it belongs to process diagnostics its main task is to assess efficient run of energy transformation in turbine thermal cycles [2, 5, 8, 10, 12, 13, 15, 21]. Such standard is that of efficient work of operationally undegraded object [5, 10, 15].

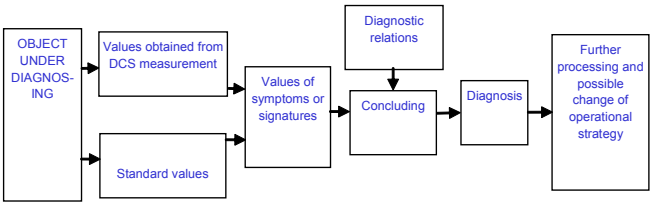

Fig. 1*. Schematic diagram of diagnosing process based on a standard*

Heat-and-flow diagnostics is intended for the determining of efficient operation of power plants fitted with thermal turbines. Turbine engines are applied to land and marine power plants. In the case of steam turbine power plant, its equipment with many measuring instruments is characteristic both in land applications, [4, 7, 9, 10, 11, 14, 16, 20], Fig. 2, and marine ones [3, 6], Fig. 3. The equipment is available in the frame of Distributed Control System (DCS) [1, 14, 16, 17, 18, 19]. It makes good prospects for diagnosing objects of both kinds by using an efficient operation standard.

Inefficient work of steam power plant results from operational degradation of geometry of component devices of thermal cycle. Control of efficient run of energy transformations in power plant constists in examining signatures consisted of inefficient work symptoms. Every symptom determines deviation of value of heat-and-flow parameter corresponding to it (mass flow, pressure, temperature), or characteristics (e.g. efficiency, steam flow capacity of particular component elements) from a reference value characteristic for undegraded object.

The above presented description seems to be simple but only in the case of object working in stable conditions and with its unchangeable structure. Yet steam turbine power plant (both land and marine one) is characteristic of:

- varying conditions of the loading of the power plant, and of its environment,
- dependence of power plant operational parameters on changes in its loading and environment,
- dependence of power unit's operational parameters on operational degradation of geometry of component devices.

It leads to difficulties in making diagnosis.

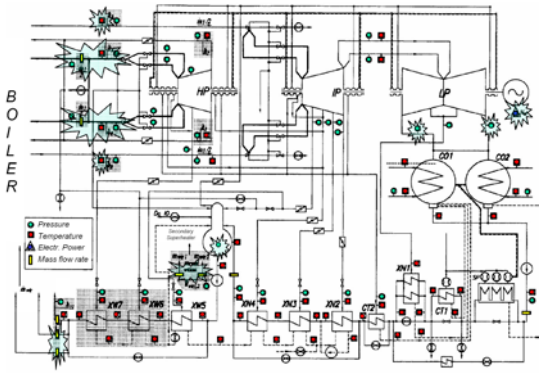

Fig. 2. *An example of thermal cycle configuration and arrangement of measurement instruments in a high -power unit of an electric power station*

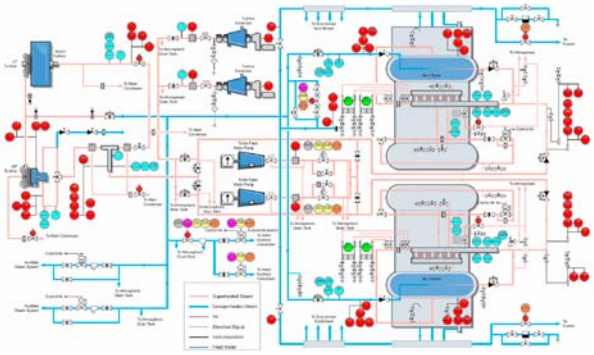

Fig. 3. *An example of arrangement of control -measurement instruments (represented by colour circles) in steam power plant of one of contemporary steam turbine ships [6]*

To obtain an unambiguous diagnosis, symptoms and signatures should be so formed as to get them depending on all characteristic states of operation. As acquisition of measurement results is performed with taking into account all the states it means that the same requirement is imposed on the standard. Therefore the standard-based diagnostics requires to have:

- an efficient operation standard which reflects dependence of changes of parameters on current load state,
- an efficient operation standard which reflects structure of a given object.

Such aims are fulfilled by a standard of functional type, having modular structure, which makes it possible:

- to identify measurement points,
- to imitate (reproduce) object's structure and,
- to calculate distribution of measured parameters in function of power unit's load and environmental conditions.

Hence every change in mode of operation leads to determination of a new reference state, i.e. a new standard.

The first of the considered situations which complicate diagnosis making, arises when periodical limitations of power unit operational parameters occur or when configuration of connections between the unit's devices should be periodically changed. The second situation takes place when a fault measurement gauge should be replaced by a new one.

The third case concerns a machine in which only some of its degraded component devices were repaired.

A seperate problem is to elaborate a standard, i.e. a reference state for on–line diagnostics. This paper is aimed at analyzing the first of the considered disturbances in operation of steam turbine plants. In the case of land power plants limitations of parameters may occur if there is a need to operate a non-fully serviceable object provided it is approved by its manufacturer. In practice are more and more often met circumstances to change configuration of feed component devices, which occur in the case of significant power limitation of the power unit. In the case of ship power plants the necessity to continue ship voyage under limited steam boiler parameters sometimes appears. In some cases it is necessary to keep ship propulsion system working at delivery of power from only one turbine cylinder. For these considerations 200 MW power unit cycle whose schematic diagram is presented in Fig.2, was selected. For this cycle influence of limitations of parameters and selected changes in configuration were analyzed, and selected results of simulation calculations have been presented here.

Investigated object

In Fig. 2 schematic thermal diagram of the 200 MW power unit is presented. The arrangement of measurement instruments intended for measuring the heat-and-flow parameters such as: pressure, temeperature, mass flow rates and – additionally– also electric ouput power, is given. Majority of the parameters is dependent on load state and environmental conditions of the object. And, a part of them just indicates the load and environmental conditions, and to consider them as independent parameters, is possible. For the 200 MW condensation steam power unit the following parameters belong to the dependent ones:

- electric generator output power or live steam mass flow rate, alternatively,
- live steam pressure,
- live steam temperature,
- interstage superheat temperature,
- condensation pressure,
- pressure in the degasifier (since the constant -pressure degasifier is applied),
- rate of water jet to live steam superheater,
- rate of water jet to reheat steam superheater.

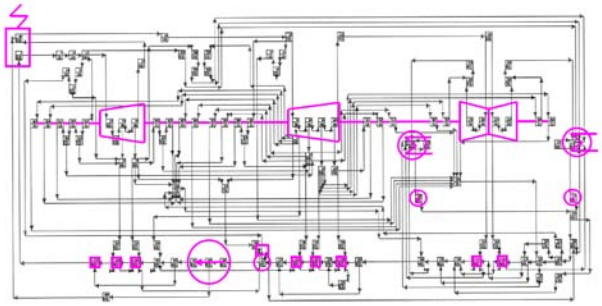

Fig. 4. *Illustration of numerical calculation scheme of the power unit [5, 10]*

The measurement points of these quanities are indicated by irregular asterisks in the schematic diagram, Fig.2. Results of the measurements can be used to calculate the cycle efficiency characteristics. Measurement results of the dependent parameters together with the so determnied characteristics can be taken as current values in heat-and-flow diagnostics. They next serve for determining inefficient operation symptoms.

The efficient operation standard can be determined computationally. For this purpose the steam power plant calculation model [5, 8, 10, 15] as well as the DIAGAR numerical calculation program [5] intended for balancing thermal cycles and performing their diagnostics, can be used. Fig.4 shows graphically the calculation model of the power plant presented in Fig. 2. Every square symbolizes a calculation procedure for particular component devices of the cycle, which makes use of geometrical and flow data of a given device, whereas the connecting lines reproduce structure of the power plant. With the use of the schematic diagram measurement points of heat-and-flow parameters can be identified. After introduction of independent parameters to the calculations, by hand or directly from DCS system, dependent values, including those associated

with measurement points, are calculated. Reference (standard) values are determined by taking into account undegraded geometry of component devices.

The calculation program fulfils role of the efficient operation standard. It is a kind of functional standard. It makes it possible to calculate reference values in function of changes of independent parameters. Structure of the model is flexible and allows to introduce modifications. Partial calculation models of the devices are susceptible to tuning [8, 10]; they can be tuned on the basis of correct experimental results and are characterized by accurate, i.e. convergent with the experiment, calculation results of heat-and-flow quantities [10, 15]. The tuning of model consists in determination of corrections to experimental coefficients appearing in calculation methods. The corrections take into account all phenomena which cause differences between measurement results and relevant calculation results. Such corrections for two flow coefficients: μ_1 and μ_2, and two velocity coefficients: φ and ψ, were prepared for turbine stages, as well as the heat transfer coefficient k – for heat exchangers [10, 15]. The calculation model tuned with their use satisfies the above mentioned requirements for efficient operation standards.

Application of efficient operation standard in the case of external limitations imposed on power unit operational parameters

In service conditions such situations -usually resulting from minor failures -happen that power generation objects operate at limited inlet parameters of working media because of cost of long -lasting standby periods. This has been observed in land electric power stations. In the cases known to this author live and reheat steam temperatures were decreased (sometimes even by 30^0 C) because of overruning repairs of boiler superheaters. In marine conditions similar phenemena can also occur if they happen during voyage which should be continued without generating excessive risk to safety of the ship and its crew. In each of the above mentioned events to get approval to do it from the side of manufacturers of crucial devices (first of all – boiler and turbine) is necessary.

The above mentioned case of limitation of live and reheat steam temperatures is exemplified by a fragment of line of expansion within turbine, Fig. 5. The nominal temperature t_{00} was lowered to that t'_{00}. This resulted in change of run of the expansion line from the nominal state (continuous purple line) to the transient state (dashed line). Only minor influence on operation of the valves and control stage can be observed. In both the states the efficiency characteristics of the non-regulated part of the turbine are only slightly different. However pressure distribution within the turbine is changed distinctly. Such state of the power unit can be reproduced in the calculation model of the DIAGAR program. Hence, an efficient operation standard can be elaborated on the basis of the calculation model.

The tuning of the calculation model at limited inlet parameters is excessively time-consuming and unprofitable. Periods of such power plant operation are limited and the time-consuming process of the tuning cannot be then started. Therefore tuning-up and corrections for the nominal state of operation at different loads should be used.

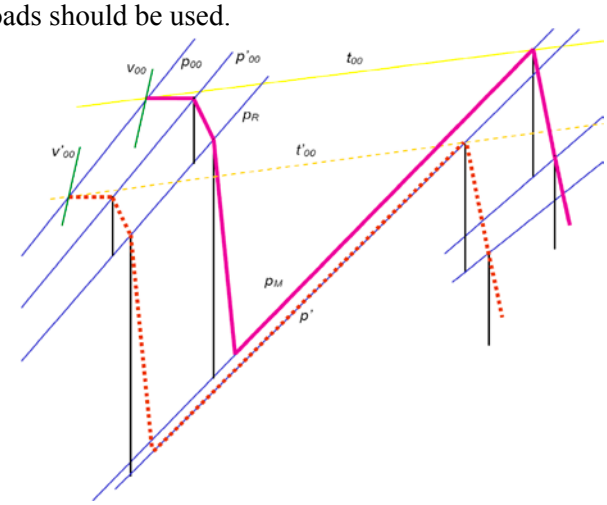

Fig. 5. Simplified schematic diagram of steam flow changes at inlets to HP and IP cylinders in the case of limited superheating temperatures

The corrections of the above mentioned coefficients of turbine stages and the heat transfer coefficients k for heat exchangers can be performed either individually or globally. The global approach consists in introducing the correction in function of the independent parameters of the cycle, as expressed by the below given relations (1)÷(5), [5, 10]:

The individual corrections (6)÷(10) are functions of the local parameters, i.e.: generalized losses – for the velocity coefficients, as well as blade geometrical parameters and Reynolds number – for the flow coefficients, and functions of the heating steam and feed water inlet parameters – for the heat transfer coefficients k for heat exchangers [10, 15]:

$$\frac{\Delta\varphi}{\varphi_{obl}} = f(p_{00}, t_{00}) \tag{1}$$

$$\frac{\Delta\psi}{\psi_{obl}} = f(p_{00}, t_{00}) \tag{2}$$

$$\frac{\Delta\mu_1}{\mu_{1obl}} = f(p_{00}, t_{00}) \tag{3}$$

$$\frac{\Delta\mu_2}{\mu_{2obl}} = f(p_{00}, t_{00}) \tag{4}$$

$$\frac{\Delta k}{k_{obl}} = f(p_{00}, t_{00}) \tag{5}$$

By making use of the global corrections and owing to compliance with experiment, to perform more accurate calculations in conditions of power plant normal load as compared with application of local corrections, is possible. However the global corrections have also

$$\frac{\Delta\varphi}{\varphi_{obl}} = f(x_1, x_2) \tag{6}$$

$$\frac{\Delta\psi}{\psi_{obl}} = f(x_1, x_2) \tag{7}$$

$$\frac{\Delta\mu_1}{\mu_{1obl}} = f\left(x_{1t}, BC_1, L_1, t_1, \mathrm{Re}_1\right) \quad (8)$$

$$\frac{\Delta\mu_2}{\mu_{2obl}} = f\left(x_{2t}, BC_2, L_2, t_2, \mathrm{Re}_2\right) \quad (9)$$

$$\frac{\Delta k}{k_{obl}} = f\left(p_p, i_p, p_{w1}, i_{w1}\right) \quad (10)$$

disadvantages resulting from their elaboration on the basis of the narrow changeability range of independent parameters, Fig. 6.

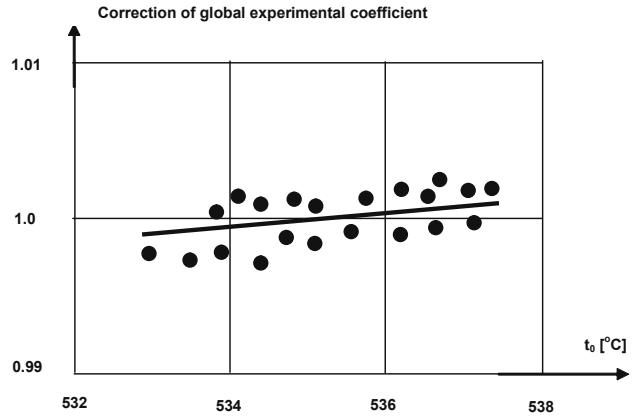

Fig. 6. *Example of experimental ranges of live steam changes in conditions of normal turbine load to obtain global correction relations,[15]*

The narrow range results from requirements of producers of equipment, especially boilers and turbines, who recommend to maintain values of the parameters relatively constant. It concerns live steam pressure as well as temperatures of primary and secondary superheating. And, the corrections result from regression relations. If the range used for determining the regression relations is exceeded the obtained calculation results will be loaded by large errors reaching even a few dozen percent [5, 10].

The local corrections make it possible to perform more accurate calculations in conditions of large changes of independent parameters, which distinctly exceed the ranges used in tuning the model. It results from only minor exceedance of ranges of independent variables of correction functions, Fig. 7, even at large changes of independent parameters of power plant [5, 10]. In this case linear correction functions are especially favourable [15]. The expected value of calculation errors does not exceed 1% [15].

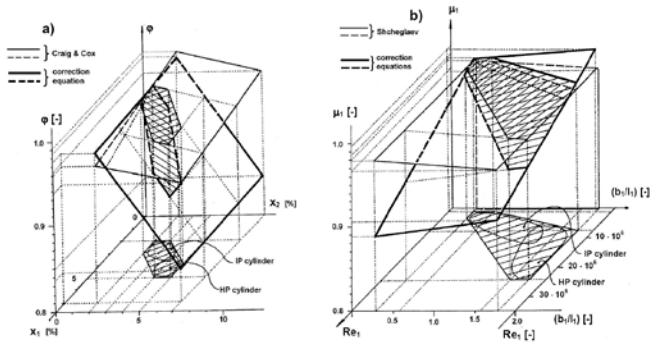

Fig. 7. *Example areas of application of individual correction relations for HP and IP cylinders of steam turbine:* ***(a)*** *– for velocity coefficients, φ;* ***(b)*** *– for flow coefficients, μ1, [10, 15]*

Hence, the application of local correction makes it possible to calculate reference values and values of symptoms with a satsifactory accuracy in conditions of significant limitations of power plant independent parameters. As a matter of fact symptom determination error is greater than that in conditions of normal load but it makes it possible to use the so determined symptoms for diagnosing efficient operation of steam turbine cycles even in the so changed operational conditions.

Application of efficient operation standard in the case of cycle configuration changes

In operational practice cycle configuration changes can be met more often than the lowering of independent parameters. For land power plants for instance it concerns mode of feeding the degasifier, Fig. 8, or unsealing the valves in bypasses of heat exchangers, Fig. 9. Configuration changes often result from short current overhauls of component devices of power unit or also from producing low power. For marine power plants a change in utilization of steam for overall ship purposes or change in electric output power of turbogenerators may lead to changes in configuration of the cycle.

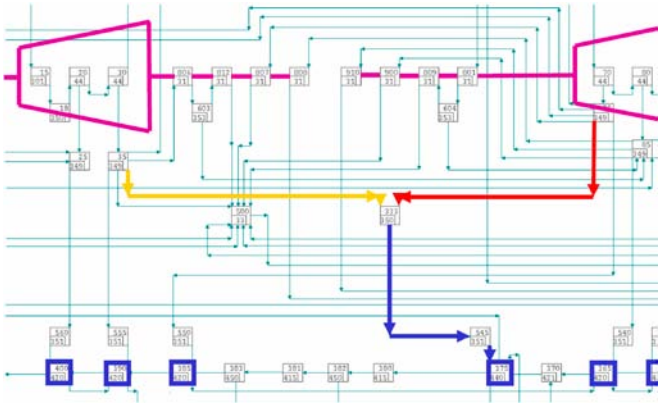

Fig. 8. *A fragment of schematic diagram of power unit numerical calculations, which illustrates reproducing the cycle configuration change which consists in choice of various extractions (No. II marked 35/349, or No. III marked 75/349) for feeding the degasifier (marked 375/440), [5, 10]*

In the case of possible power plant operation at configuration changes of connections between component devices, calculation procedure of reference state parameters should take into account their occurence. The above mentioned numerical calculation program DIAGAR [5] fulfils such condition. Due to its modular structure which makes it possible to reproduce power unit's structure it can contain modules intended for the

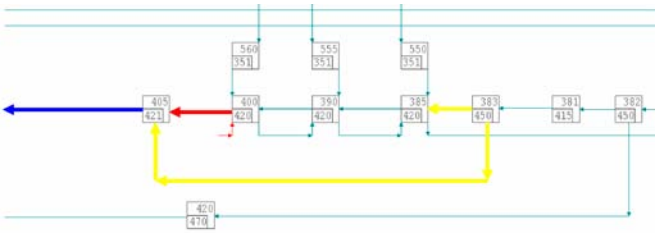

Fig. 9. *A fragment of schematic diagram of power unit numerical calculations, which illustrates reproducing the cycle configuration change which consists in activation of the bypass of HP regeneration exchangers – yellow line, [5, 10]*

controlling of working media flow to various devices of the power unit. The control modules of the program can be commenced manually by DIAGAR system operator, or automatically by reading valve opening indicators of DCS system. Values of dependent parameters necessary to determine inefficient operation symptoms are then calculated by such system adequately to an operational state of steam turbine power plant.

Significance of reproduction of power object structure is illustrated by the numbers which determine selected parameters of power plant and its efficiency indices, presented in Tab. 1. They are obtained by means of simulation calculations of the chosen power unit of 200 MW output. Characteristics of component devices comply with reference conditions and are not subjected to changes; the changes concern only inlet parameters or configuration. The first column deals with the operation in conditions of nominal configuration of the power unit, which consists a.o. in feeding the degasifier from the extraction III and closing all bypasses of heat exchangers. Three successive columns deal with changes in the cycle. The second one reproduces the operation of the cycle at lowered temperatures of live and reheat steam. The third one reproduces the operation of the cycle at feeding the degasifier from the extraction II. And the fourth one reproduces the operation at partial opening the bypass of HP regeneration exchangers.

Tab. 1. *Changes of parameters and characteristics of 200MW power unit in the case of introduction of configuration changes with respect to nominal one*

Descrition	Symbol	Units	Nominal configuration	Changed inlet parameters or configuration		
				Lowered temperatures: t_{00} and t_M	Feeding the degasifier from the extraction II	HP bypass active
Power	N	MW	196.700	196.700	196.700	196.700
Live steam pressure	p_{00}	MPa	12.500	12.500	12.500	12.500
Live steam temperature	t_{00}	°C	539.000	500.000	539.000	539.000
Reheat steam temperature	t_M	°C	539.000	500.000	539.000	539.000
Condensation pressure	p_c	kPa	9.770	9.770	9.770	9.770
Specific heat consumption	q_j	kJ/ kWh	9221.000	9309.000	9238.000	9266.000
HPcyl. efficiency	η_{HP}	-	0.695	0.695	0.695	0.695
IP cyl. efficiency	η_{IP}	-	0.889	0.889	0.889	0.889
LP cyl. efficiency	η_{LP}	-	0.801	0.801	0.801	0.801
Feed water temp. after the last HP heater	$t_{aft\ HP}$	°C	219.000	219.000	219.000	210.000
Terminal temp. differ. of the last HP heater	Γ_{HP}	°C	0.107	0.107	0.107	0.107

Values of the parameters in Tab. 1 indicate that the only quantity susceptible to changes is the specific heat consumption qj. In a content-related way it is justified because only the parameters assumed nominal and only the nominal configuration ensure to reach maximum value of object's efficiency (i.e. the lowest specific heat consumption). The remaining quantities and characteristics determined by calculation are not subjected to changes. It shows that the use of the DIAGAR system calculation model as an efficient operation standard is correct even in changed external conditions and for operation of the cycle with changed configuration of connections between component devices.

Summary

The above presented analysis and selected results of simulation calculations indicate that there are applicable solutions which make it possible to solve certain problems concerning the power plant reference state of power objects, including marine ones. The problem is important for heat-and-flow diagnostics carried out with the use of object's efficient operation standard.

In this paper the problem of influence of limitation of values of working media inlet parameters and changes in configuration of connections between component devices of thermal cycles – with respect to conditions deemed nominal – on determining a reference state in the case of correct geometry of thermal cycle component devices, was analyzed.

It was stated that the use of the modular calculation model as an efficient operation standard makes it possible to determine the reference values in the described changeable conditions. Such model tuned to a diagnosed power plant on the basis of correct measurements at nominal configuration will comply with accuracy criteria required for that standard also in the case of changed cycle configuration.

In the case of limitation of working media inlet parameters, corrections to experimental coefficients of calculation methods should be then functions of local parameters in the surrounding of the device modeled by them. Then even large changes in power plant independent operational parameters make only slight impact on values of variables of the corrections. In simulation calculations no significant errors in determining characteristics of component devices, are observed, Tab. 1.

The modular calculation model for reproducing a modified structure of power plant should contain special modules to control calculations, depending on current cycle configuration. Control parameters can be inserted by hand. However the use of information received from contemporary DCS systems makes it possible to automate the process by gaining data from valve opening indicators. In the case of correct geometry of component devices, modification of object's structure does not change their correct characteristics, that is illustrated by the values given in Tab. 1.

Comparison of the values for the nominal configuration, given in Tab. 1, with those for the changed configuration and independent parameters shows that the using of the modular calculation model as an efficient operation standard is correct even in the case of changed external conditions and the operation with changed configuration of connections between component devices.

Bibliography

1. Abernethy R. B., Benedict R. P., Dowdell R. B.: ASME Measurement Uncertainty, Transactions of ASME, Journal of Fluids Engineering, June 1985, ASME 1985
2. Doel D. L.: Sample Analyses Including Interpretation of Residual Error, VKI Lectures Gas Turbine Condition Monitoring & Fault Diagnosis, Ed. Sieverding & Mathhioudakis, ISSN0377-8312, January 13-17, Rhode Saint Genese, Belgium, Unit 4,
3. Dzida M.: On the possible increasing of efficiency of ship power plant with the system combined of marine diesel engine, gas turbine and steam turbine, at the main engine – steam turbine mode operation, Polish Maritime Research, 1/2009, Vol. 16, Gdańsk, 2009
4. Fodemski T. R., et al.: Heat measurements, Part I and II (in Polish). WNT (Scientific Technical Publishing House),Warsaw 2001
5. Gardzilewicz A., Głuch J., Bogulicz M., Uziębło W.: Correctness control of heat-and-flow measurment data gained from DCS systems of steam electric power plants (in Polish). Materials of 5th Conference on industrial process diagnostics DPP'2003, Władysławowo, 15÷17.09.2003
6. Głuch J.: Set of lectures for steam turbine power plant engineers. Unpublished internal report of Ship Automation and Turbine Propulsion Department, Faculty of Ocean Engineering and Ship Technology, Gdańsk University of Technology, Gdańsk, 2005.
7. Głuch J.: On searching-out incorrect measurements in DCS systems of power objects (in Polish). Materials of The Scientific Conference „Mechanika 2005", Gdańsk, 04.02.2005
8. Głuch J.: Application of Artificial Neural Networks (ANN) as Multiple Degradation Classifiers in Thermal and Flow Diagnostics, TASK Quarterly 2005 No. 9, Gdańsk, 2005
9. Głuch J.: Control of heat-and-flow measurements in DCS systems of complex power objects (in Polish). Materials of The DPP'05 Conference, Rajgród, 12÷14.09.2005, Pomiary Automatyka Kontrola, Special issue, 09/2005
10. Głuch J.: A method of heat-and-flow diagnostics, which makes it possible to recognize location and degree of degradation of power turbine sets (in Polish), Series „Monographs", No. 81, Wydawnictwo Politechniki Gdańskiej (Publishing House of Gdańsk University of Technology), Gdańsk, 2007
11. Głuch J.: Fault detection in measuring systems of power plants, Polish Maritime Research, 4/2008, Gdańsk, December 2008
12. Kosowski K.: Some aspects of vibration control; Part I: Active and passive control, Polish Maritime Research, 4/2004 (42), Vol. 11, Gdańsk, 2004
13. Kosowski K.: Some aspects of vibration control; Part II: An optimal active controller, Polish Maritime Research, 1/2005 (43), Vol. 12, Gdańsk, 2005
14. Kościelny J. M.: Development directions of decentralized automation systems (DCS) (in Polish), Pomiary Automatyka Kontrola No. 6/1998
15. Krzyżanowski J., Głuch J.: Heat-and-flow diagnostics of power objects (in Polish). Wydawnictwo Inst. Masz. Przepł. PAN (Publishing House of Institute of Fluid Flow Machinery, Polish Academy of Sciences), Gdańsk, 2004
16. Makal J.: Measurement uncertainty of multi-channel measuring system (in Polish). Pomiary Automatyka Kontrola, No. 9/2001
17. Polska Norma PR (Polish Standards): PN-EN 60953-1: PR: PN-IEC953-1, PR: PN-EN 60953-2: PR: PN-IEC953-2. Requirements for thermal acceptance tests of steam turbines. Sheet 1 and 2: Methods:A and B (in Polish), December 1998.
18. PTC6: Performance Test Code 6 on Steam Turbines ASME PTC6-2001, 1996 (Revision of ASME PTC6-1976).
19. Romessis C., Mathioudakis K.: Jet Engine Sensor Validation with Probabilistic Neural Networks. Materials of 5-th European Conference on Turbomachinery, Prague, March 17÷21, 2003
20. Ślęzak-Żołna J.: On the Application of the Artificial Neural Network Method to a Neural Simulator of Steam Turbine Power Plant, Polish Maritime Research, 1/2006, Gdańsk, January 2006
21. Żółtowski B., Ćwik Z.: Lexicon of technical diagnostics (in Polish). Wydawnictwo Uczelniane Akademii Techniczno-Rolniczej (Publishing House of Technical and Agricultural Academy of Bydgoszcz), Bydgoszcz, 1996.

Nomenclature

b, BC – profile chord,
i – enthalpy,
k – heat transfer coefficient,
l – blade length,
p – pressure,
p_{00} – live steam pressure,
p_C – condensation pressure,
p_M – reheat steam pressure,
q_j – specific heat consumption,
t – working medium temperature or cascade pitch,
t_{00} – live steam temperature,
$t_{aft\ HP}$ – feed water temperature after the last HP heater,
t_M – reheat steam temperature,
x_1 – generalised primary profile losses,
x_2 – generalised secondary profile losses,
x_t – steam dryness at the end of isentropic expansion,
Δ – deviation between actual and reference values,
Γ_{HP} – terminal temperature difference of the last HP heater,
φ – nozzle blade velocity coefficient,
ψ – rotor blade velocity coefficient,
μ – blade flow coefficient,
η – efficiency.

Indices:

1 – stands for nozzle blade cascade,
2 – for rotor blade cascade,
HP – for HP turbine cylinder,
IP – for IP turbine cylinder,
LP – for LP turbine cylinder,
obl – for calculated values,
p – for steam,
w – for water.

POLISH MARITIME RESEARCH, Special issue 2009/S1; pp. 28-33
10.2478/v10012-008-0041-5

Design analysis of Tesla micro-turbine operating on a low-boiling medium

Piotr Lampart, Krzysztof Kosowski,
Marian Piwowarski, Łukasz Jędrzejewski

Abstract

This paper presents results of the design analysis of a Tesla bladeless turbine intended for a co-generating micro-power plant of heat capacity 20 kW, which operates in an organic Rankine cycle on a low-boiling medium. Numerical calculations of flow in several Tesla turbine models were performed for a range of design parameters. Results of investigations exhibit interesting features in the distribution of flow parameters within the turbine interdisk space. The calculated flow efficiency of the investigated Tesla turbine models show that the best obtained solutions can be competitive as compared with classical small bladed turbines.

Keywords: Tesla turbine, axial flow bladed turbine, flow efficiency, CFD calculations, RANS model

Introduction

It is a rather common opinion that bladed turbines are unbeatable as compared with Tesla turbines in the range of large power outputs. However, at very small outputs some superiority of bladeless turbines can be expected, Fig. 1. In a majority of published cases, rotational speeds of Tesla turbine rotors appear lower than those of bladed turbines, which makes the selection of an electric generator easier.

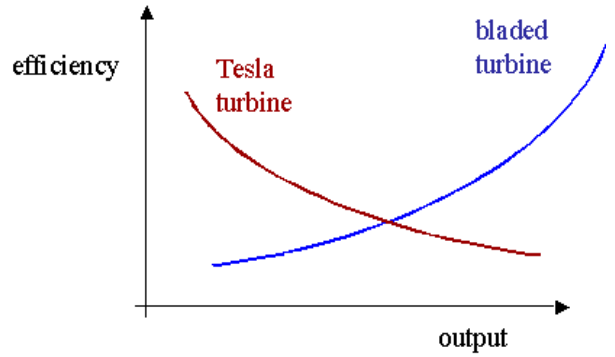

Fig.1 *Pictorial comparison of efficiency of small bladed and Tesla turbines*

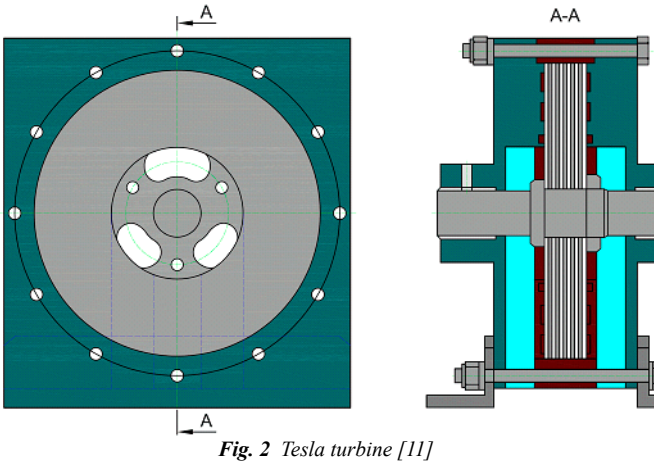

Fig. 2 *Tesla turbine [11]*

The first bladeless turbine was designed and manufactured by Nikola Tesla (in 1913) [11]. The design makes use of the effects which occur in the boundary layer flow between the rotating disks placed very close to one another (Fig. 2). The gas flowing spirally from the outer to inner part transfers energy to the rotating disks. The supply usually takes place from several nozzles discretely located along the circumference. The medium flows out through the holes in the disks situated near the turbine shaft.

Distances between disks are very small. The highest value of efficiency appears when they are approximately equal to the double boundary layer thickness [9]. The efficiency of the Tesla turbine depends on many parameters, namely on: pressure, temperature, inlet medium velocity, number, diameter, thickness and distance between the disks as well as on the state of the disk surface, rotational speed of the rotor, flow kinematics at the inlet to and outlet from the turbine, etc. In the subject-matter literature, examples of experimental research referring to the following models of Tesla micro-turbines can be found:

- ~3.0kW output power, 15000 rpm, 32% efficiency, [5];
- ~1.0kW output power, 12000 rpm, 24% efficiency, [1];
- ~1.5kW output power, 12000 rpm, 23% efficiency, [8, 9];
- ~50W output power, 1000 rpm, 21% efficiency, [7];
- ~1.5kW output power, 12000 rpm, 49% efficiency, [3].

Experimental works aimed first of all at establishing relationships between the turbine efficiency and parameters given below:

- distance between the micro-turbine disks;
- number and diameter of the micro-turbine disks;
- number of inlet nozzles to the micro-turbine;
- rotational speed of the rotor;
- medium inlet pressure;

- medium inlet temperature;
- medium inlet velocity and inlet angle;
- corrosion and erosion of micro-turbine elements;
- constructional materials (composites, ceramic materials, bronzes, aluminium alloys);
- kind of medium flowing through the micro-turbine (air, biogas, organic agents, exhaust gases, multi-phase media, etc).

Main design features and operational parameters of Tesla turbines published in the literature referenced in this paper are presented in Tab. 1. Not only turbines but also compressors, pumps and gas turbine sets can be built on the basis of the same working principle.

Preliminary design analysis

CFD calculations of various models of Tesla disk turbines were carried out on the basis of the RANS model supplemented by the k-ω SST turbulence model available in the computer programme Fluent [12]. Numerical discretisation of the set of fundamental equations is performed using the finite volume method. The "segregated" solver with the sequential solving of the governing equations as well as the SIMPLE algorithm for correction of pressure and velocity are applied. Discretisation of convection fluxes is performed using an "upwind" scheme of the 2nd order accuracy. The time-domain discretisation is made by an "implicit" scheme. The calculations are carried out until the stationary state is reached, lowering the residua of particular equations by 4÷6 orders of magnitude.

The calculation domain was prepared by means of the software Gambit [14]. The models of Tesla turbines contain the inlet nozzle, a half of the single interdisk space (under the assumption on flow symmetry in a central plane) as well as the outlet area. The models analyzed in this work represent a simplification of real geometry of Tesla turbines. The outlet area was simplified in a way to allow the medium outflow from the turbine flow passage along the entire circumference of the shaft. The presence of the tip clearance was neglected. The calculations were carried out in a fixed (motionless) reference frame, with turbine disk walls kept in rotational motion. In accordance with the assumed turbulence model, the calculation grid

Tab. 1. *Specification of Tesla turbine design solutions*

No	Outer diam. of disk	Disk thickness	Interdisk distance	Inner diam. of disk	Number of disks	Rotational speed	Moment	Power	Medium	Inlet pressure	Inlet temperature	Nozzle diameter	Nozzle surface area	Nozzle angle	Efficiency
	D_1	t	b	D_2	z	n	T	N		p_0	t	D	S	α	η
	[m]	[m]	[m]	[m]	[-]	[rpm]	[Nm]	[kW]		[kPa]	[ºC]	[m]	[mm^2]	[º]	[-]
1	-	-	-	-	6	18000	-	2,983	Air	615,29	-	-	-	-	0,35
2	-	-	-	-	-	8193	-	8,650	Air	593,00	-	-	-	-	-
3	0,17780	0,0024	0,0016	-	7	10000	-	-	Air	861,84	-	-	-	15	0,232
4	0,17780	0,0024	0,001	-	11	9200	-	-	Air	377,14	-	-	-	10	0,258
5	0,20320	0,0005	0,0005	0,0335	24	17000	-	-	Air	615,29	-	-	-	20	0,35
6	0,30480	0,0008	0,0008	0,07620	45	1100	-	0,447	Air	227,53	20,5	-	121	15	0,16
7	0,30480	0,0008	0,0008	0,07620	45	6218	-	3,430	Gas	275,79	444	-	-	15	0,123
8	0,30480	0,0008	0,0008	0,07620	45	6284	-	3,206	Biomass	275,79	391,6	-	-	15	0,11
9	0,30480	0,0008	0,0008	0,07620	45	6500	-	9,247	Saturated vapour	689,48	170	-	-	15	0,137
10	0,25240	0,0016	0,0016	-	9	6300	-	-	Air	-	-	-	206,67	15	0,41
11	-	-	-	-	-	15000	-	2,983	-	-	-	-	-	-	0,32
12	-	-	-	-	-	12000	-	0,969	-	-	-	-	-	-	0,24
13	-	-	-	-	-	12000	-	1,491	-	-	-	-	-	-	0,23
14	-	-	-	-	-	1000	-	0,045	-	-	-	-	-	-	0,21
15	-	-	-	-	-	120000	-	1,491	-	-	-	-	-	-	0,49
16	0,30480	0,0008	0,0008	-	45	12000	-	4,4-50	Vapour/ exhaust gas	689,48	537,78	0,0191	-	-	0,25
17	0,24765	0,0048	0,0016	-	7	-	-	14,914	-	-	-	-	-	-	-
18	0,40000	-	-	-	26	5400	-	-	-	-	150	-	-	-	-
19	0,25400	-	-	-	-	-	-	74,569	-	-	-	-	-	-	-
20	0,45720	-	-	-	-	-	-	149,138	-	-	-	-	-	-	-
21	1,52400	-	-	-	-	-	-	503,341	-	-	-	-	-	-	-
22	0,24765	-	-	-	25	-	216	82,026	-	-	-	-	-	-	-
23	0,15240	0,0009	0,0012	-	7	1290	17,27	-	-	-	-	-	-	-	-
24	0,15240	-	-	-	-	3000	17,27	-	-	517,11	-	-	-	-	-
25	-	-	-	-	-	9240	-	2,908	Air	723,95	444	-	-	15	-
26	-	-	-	-	-	10200	-	9,694	Air	723,95	-	-	-	15	-
27	0,11430	-	-	-	-	24000	-	0,250	Vapour	1034,2	-	-	-	-	-
28	0,25400	-	-	-	29	18000	-	96,940	-	-	-	-	-	-	-
29	0,07620	-	-	-	15	10500	-	0,153	-	448,16	-	-	-	-	0,31

at the disk wall was refined so as to obtain the y_+ value equal to 1 ÷ 2. This is a structural mesh divided into blocks, which contains 400 000 ÷ 500 000 finite volumes, depending on a turbine model. The calculation grid was also refined in the inlet and outlet regions. Fig. 3 presents images of the calculation area for several turbine models with one, two and four inlet nozzles. Geometrical parameters of particular investigated models are given in Tab. 2.

Thermodynamic parameters assumed for CFD calculations were found from preliminary 1D model calculations, making use of data from literature sources. It is assumed that the considered Tesla turbine models consist of 11 rotating disks (12 flow channels of the interdisk space). The outer diameter of the disk is equal to 10 cm. The nominal operating conditions are for the mass flow rate of 0.13 kg/s and pressure drop from 14.8 bar to 1.9 bar. Solkatherm®SES36S was assumed to be a working medium. The perfect gas model was chosen for the calculations, assuming the individual gas constant and specific heat as average values from the given expansion range. Values of dynamic viscosity and heat conductivity coefficient were assumed in a similar way. Pressure boundary conditions relevant to compressible flow solution were assumed. However, it should be noted that the perfect gas model assumed for the calculations may be a poor approximation of working medium properties, especially for flow velocities close to the sonic velocity. The calculations were carried out for a range of operating conditions (by changing the available pressure drop) for two rotational speeds of the rotor, namely: 18 000 rpm and 9 000 rpm.

Contours of static pressure and velocity for the investigated turbine models 1-3 are presented in Figs. 4, 5

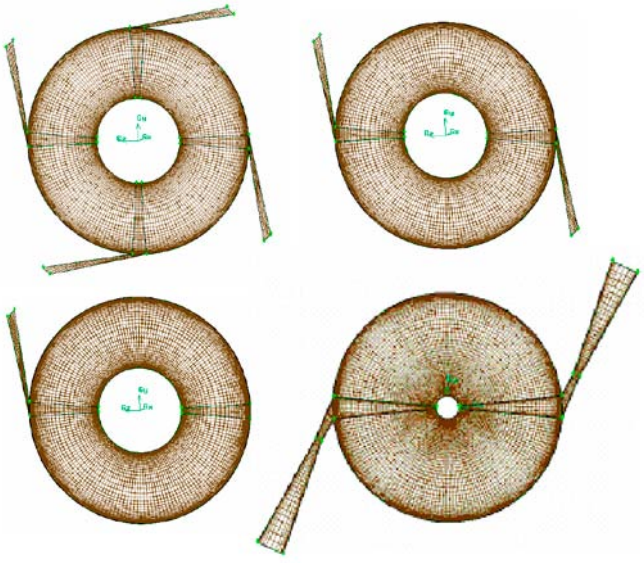

Fig. 3 *The calculation domain for four models of the Tesla turbine*

Tab. 2 *Geometrical parameters of Tesla turbine models*

	Model 1	Model 2	Model 3	Model 4
Number of supplying nozzles	1	2	4	2
Outer radius [m]	0.05	0.05	0.05	0.05
Inner radius [m]	0.02	0.02	0.02	0.005
Breadth of gap [m]	0.001	0.0005	0.00025	0.0005
Breadth of inlet [m]	0.003	0.003	0.003	0.008

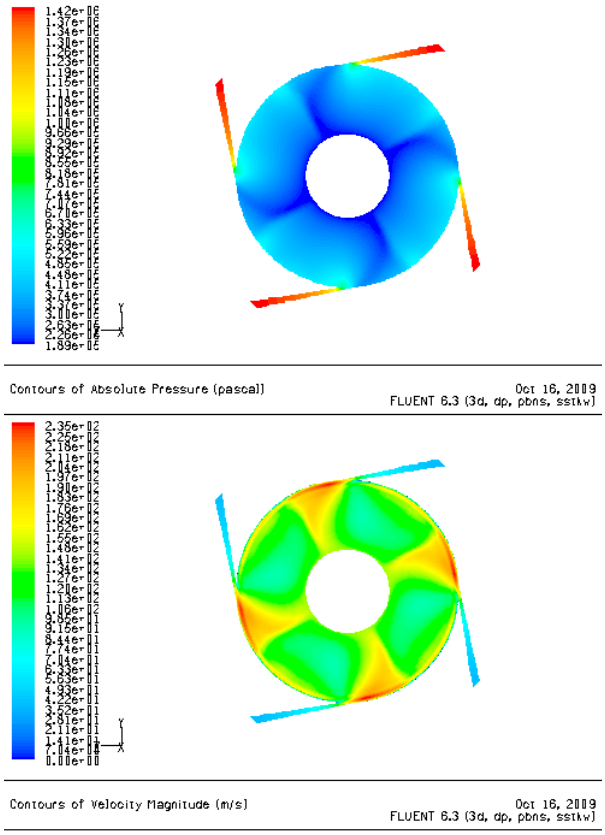

Fig. 4. *Contours of static pressure and velocity in flow through the four-nozzle model of the Tesla turbine; δ=0.25mm, n=18 000, pin= 14,8 bar, T_{in}=410K, G = 0,132 kg/s, P = 1177 W.*

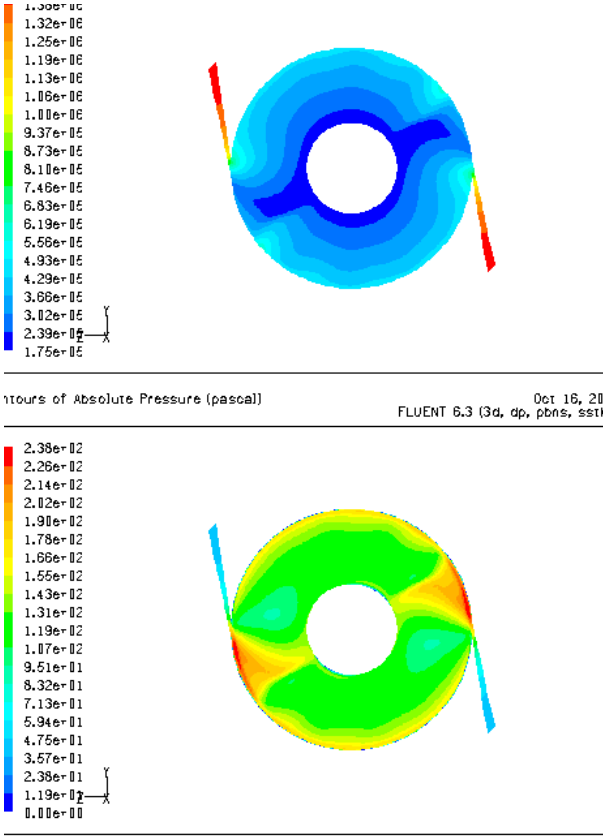

Fig. 5. *Contours of static pressure and velocity in flow through the two-nozzle model of the Tesla turbine; δ=0.5mm, n=18 000, pin= 14,8 bar, T_{in}=410K, G = 0,124 kg/s, P = 1102 W.*

and 6. The numbers below the figures show the interdisk gap, rotational speed, inlet pressure and temperature (at the outlet pressure of 1.9 bar) as well as the resultant values – rate of mass flow through 12 interdisk passages and output power generated on both sides of 11 rotating disks. It results from the pressure contours that a part of the available pressure drop is accomplished in the nozzle, the other part takes place in the interdisk space, i.e. in the rotor. In the case of higher loads, configurations of isolines characteristic for the occurrence of shock waves are observed some distance downstream of the inlet nozzle. When a shock wave occurs, an increase of pressure and a decrease of flow velocity takes place. Streamline patterns for the four-nozzle and two-nozzle models operating under part-load conditions (inlet pressure at 7.8 bar) are presented in Fig. 7. It is clear that fluid elements make more than three or four rotations within the interdisk space before they reach the outlet section.

A sample distribution of static pressure and velocity in flow through the model 4 of Tesla turbine (of a small shaft diameter) is presented in Fig.8. Such a system is characterized by a high reaction, which means that practically the whole pressure drop takes place in the interdisk space of the rotor and that the velocity at the nozzle exit is relatively low. This is due to the vortex motion induced in the interdisk space, which results from the conservation of angular momentum. Thus, flow transition to smaller diameters towards the outlet section causes a velocity increase and a pressure drop. This situation is unfavourable as far as the efficiency is considered – high outlet energy means high flow losses.

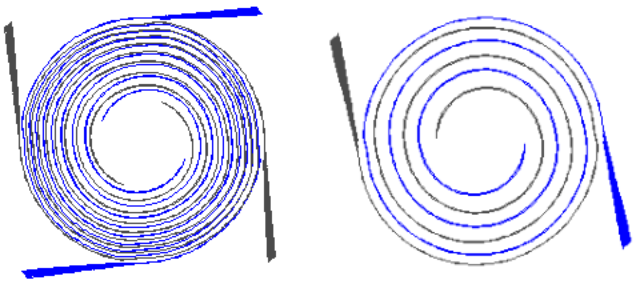

Fig. 7. Streamlines in flow through the four-nozzle and two-nozzle models of the Tesla turbine; n=18 000, pin= 7,8 bar, T_{in}=390K.

Therefore, the outlet section of a disk turbine should be located at an appropriately large diameter.

The power output, inlet pressure required, flow efficiency and reaction of three investigated models of 11-disk (12-passage) turbine are presented in Figs. 9, 10 and 11 as a function of mass flow rate. The model with four nozzles gives the largest power and flow efficiency. Values of power and efficiency obtained from the two-nozzle model are slightly lower. The respective values for the single-nozzle model are considerably lower. The change in rotational speed from 9000 rpm to 18000 rpm leads to a significant power and efficiency increase. For the rotational speed of n=18000 rpm, at the nominal pressure drop from 14.8 to 1.9 bar, which refers to the nominal flow rate of about 0.13 kg/s, the output power of the investigated models of 11-disk turbine amounts to about 1020 W for a single-nozzle model, increasing to 1100 W for the two-nozzle model, to 1180 W for the four-nozzle model. At n=18000 rpm, the calculated efficiency

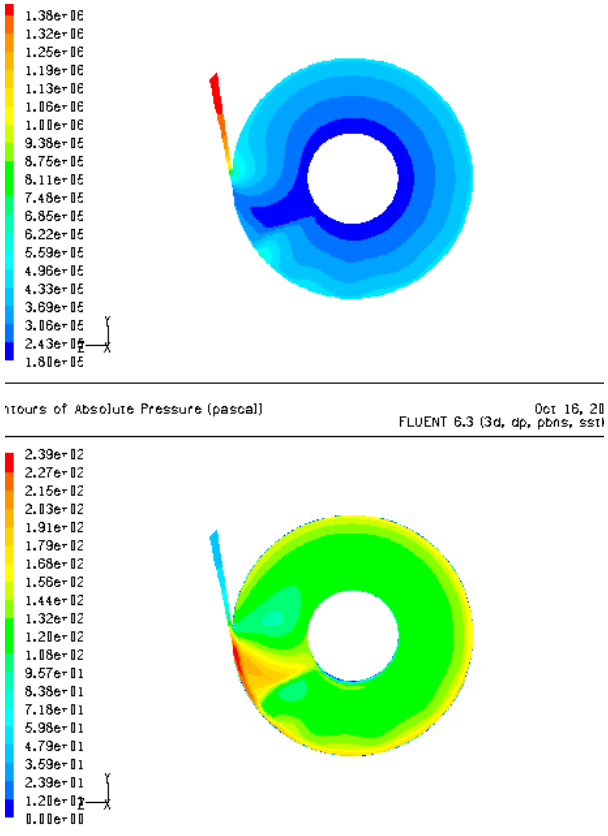

Fig. 6 Contours of static pressure and velocity as well as form of pathlines in flow through Tesla turbine model; δ=1mm, n=18 000, pin= 10,8 bar, T_{in}=390K, G' = 0,024 kg/s, P' = 109,7 W

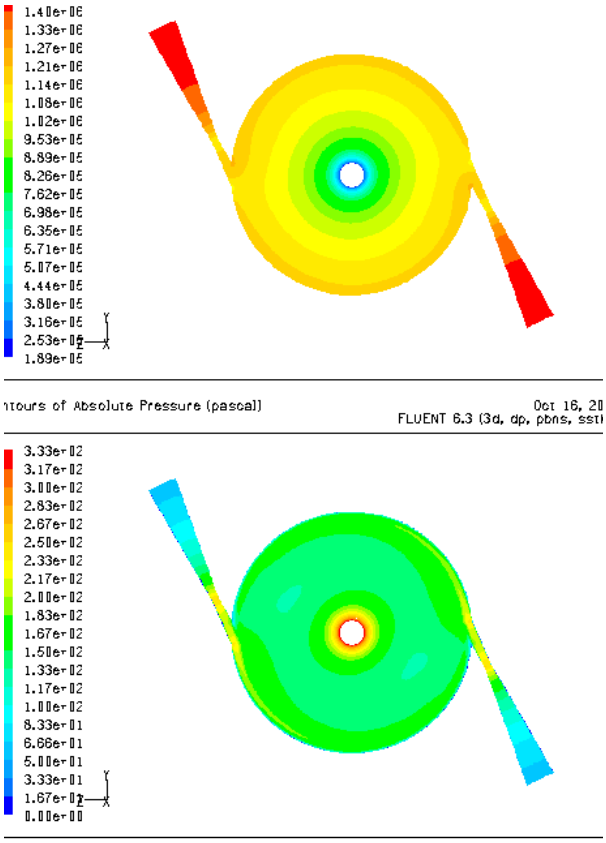

Fig. 8. Contours of static pressure and velocity in flow through the model 4 of the Tesla turbine with a small shaft small diameter; δ=0.5mm, n=18 000, pin= 14,8 bar, T_{in}=410K.

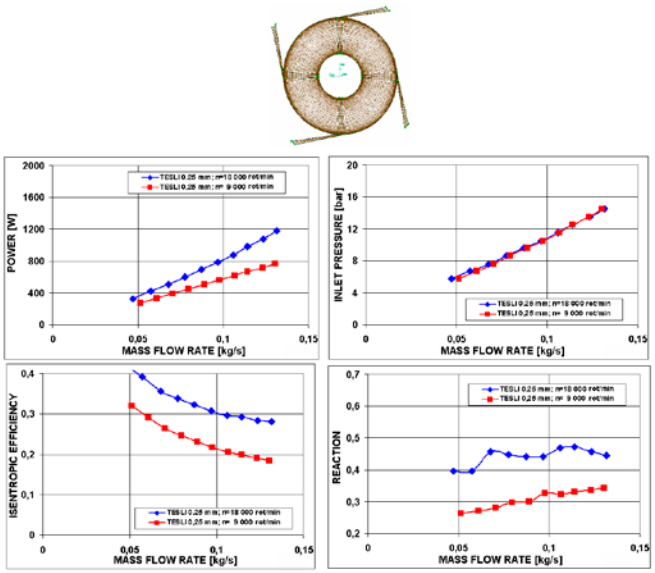

Fig. 9. The power output, inlet pressure, flow efficiency and reaction of an 11-disk turbine as a function of flow rate; the system supplied from four nozzles -δ=0.25mm.

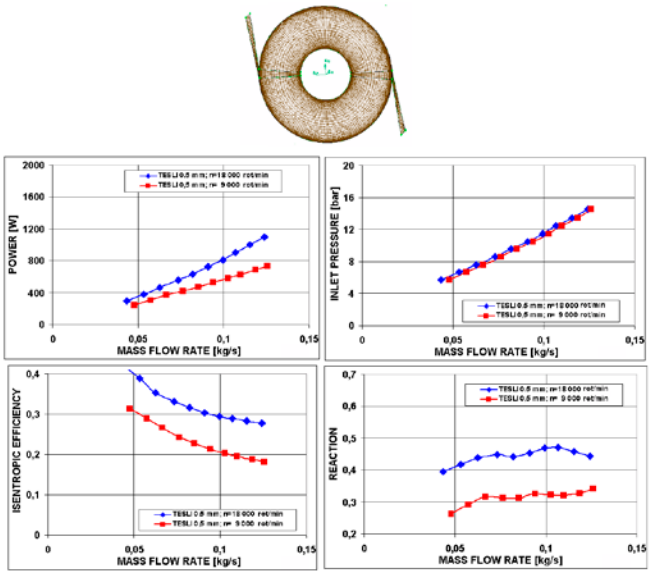

Fig. 10. The power output, inlet pressure, flow efficiency and reaction of an 11-disk turbine as a function of flow rate; the system supplied from two nozzles -δ=0.5mm.

of the models at the nominal operating conditions is equal to 25.5% for the single-nozzle model, increasing to 27% for the two-nozzle model, to 28% for the four-nozzle model. For the rotational speed of n=9000 rpm, at the nominal flow rate of 0.13 kg/s (and nominal pressure drop from 14.8 to 1.9 bar) the output power of the investigated models of 11-disk turbine amounts to about 700 W for a single-nozzle model, increasing to 760 W for the two-nozzle model, to 780 W for the four-nozzle model. At n=9000 rpm, the calculated efficiency of the models at the nominal operating conditions is equal to 17% for the single-nozzle model, increasing to 18.2% for the two-nozzle model, to 18.5% for the four-nozzle model. It is also important to note that for lower loads below nominal operating conditions the flow efficiency is increased. The reaction of the models at n=18000 rpm varies within the

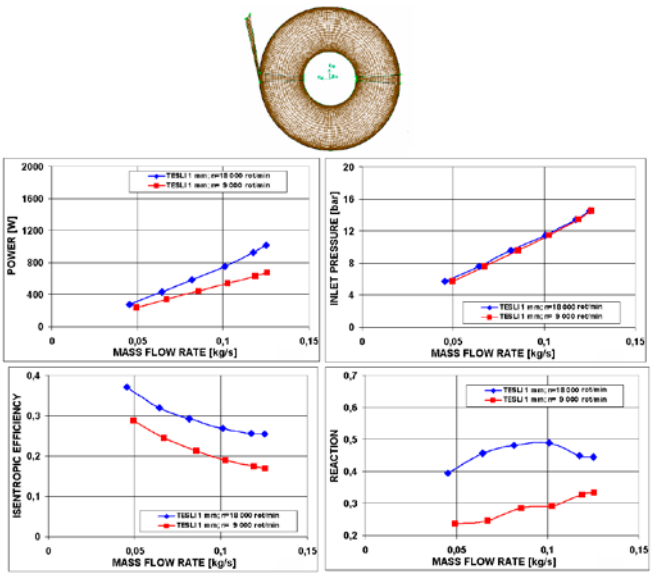

Fig. 11. The power output, inlet pressure, flow efficiency and reaction of an 11-disk turbine as a function of flow rate; the system supplied from one nozzle -δ=1mm.

range of 0.4 ÷ 0.5, at n=9000 rpm changing between 0.25 ÷ 0.35. The characteristics of the model no. 4 are here omitted because of a low value of flow efficiency. The internal efficiency of this model is not greater than 10% over the whole range of investigated loads.

Closing remarks and direction of future works

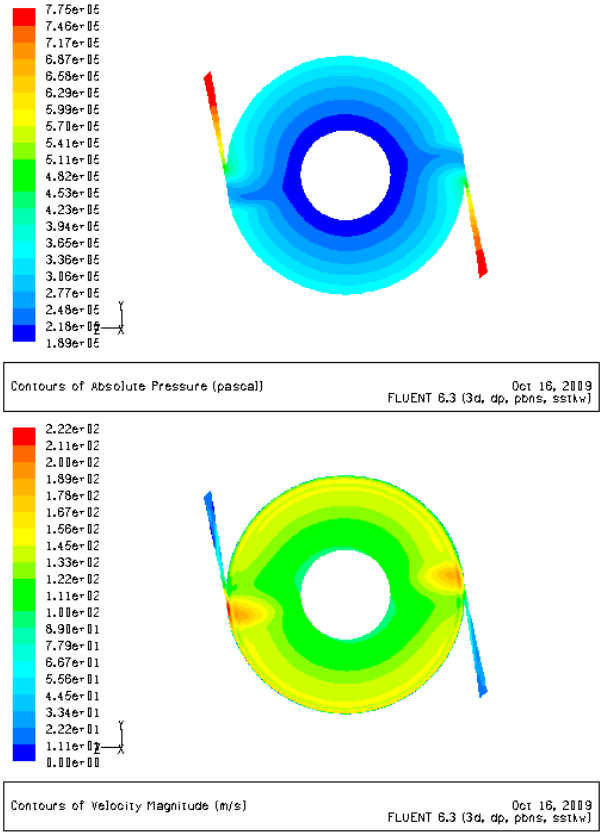

Fig. 12. Contours of static pressure and velocity in flow through the large diameter two-nozzle model of the Tesla turbine; d=32mm, δ=0.5mm, n=9 000, pin= 7,8 bar, Tin=390K, G = 0,119 kg/s, P = 1312 W

The flow efficiency of the investigated models 1-3 of a Tesla turbine obtained by means of numerical calculations from the code Fluent fall within the range of efficiency values quoted in Introduction based on the literature search. The calculations also highlight some features of operation of the Tesla turbine from a point of view different than that presented in a majority of publications. First of all, the Tesla turbine operates as a reaction turbine with a large pressure drop within the interdisk space. The diameter of the outflow area from the intersdisk space should be still large enough to avoid large outflow velocities. It can also be expected that the lengthening of the friction path within the interdisk space would result in a more effective power transfer.

The above conclusions lead to an idea of increased disk diameter of the Tesla turbine, also accompanied by a decreased cross-section area of the inlet passages. To verify this idea, preliminary calculations were performed for two variants of disk diameter of the two-nozzle model of the Tesla turbine scaled up to 16 cm and 32 cm. In both cases the distance between the disks was equal to 0,5 mm. The supply of medium was accomplished by means of two nozzles located opposite to each other. Sample distributions of pressure and velocity fields in the interdisk space of the Tesla turbine model with the outer diameter equal to 32 cm are shown in Fig. 12, whereas power and efficiency characteristics are displayed in Fig. 13. Within the presented range of mass flow rate (between 0.1 and 0.4 kg/s) and pressure drop (between 7.8 and 14.8 bar) the calculated flow efficiencies oscillate around 50%.

It seems justified to conclude that precise optimization of the Tesla turbine design and geometrical parameters could ensure values of the output power and efficiency similar to those achieved by small bladed turbines. However, the rotational speed of the Tesla turbine rotor is several times lower as compared with small bladed turbines of rotational speed 100 000 rpm. This makes the Tesla turbine an attractive proposal for small heat and power stations, e.g. of heat capacity 20 kW.

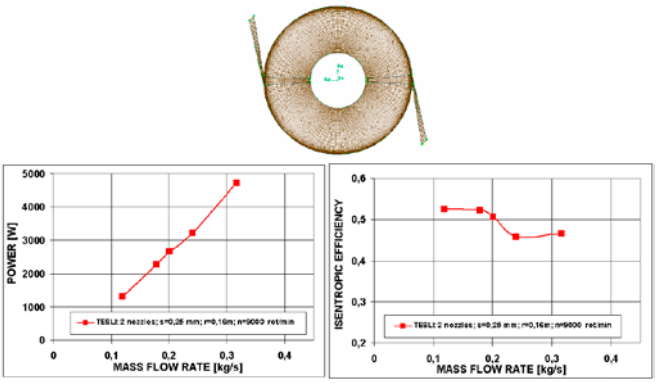

Fig. 13 *The power output and efficiency of an 11-disk turbine of a large shaft diameter (32 cm) as a function of flow rate; the system supplied from two nozzles -δ=0.5mm.*

Bibliography

1. Beans, W.E.: „Investigation Into the Performance Characteristics of a Friction Turbine". Journal of Spacecraft, January 1966
2. Cairnes W. M. J.: „The Tesla Disc Turbine". Camden Miniature Steam Services, 2001
3. Davydov, A. B., and Sherstyuk, A.N.: „Experimental Research on a Disc Microturbine". Russian Engineering Journal, Issue 8, 1980
4. Gingery V.: „Building the Tesla Turbine". ISBN 1-878087-29-0, David J. Gingery Publishing, 2004;
5. Gruber, Earl L.: „An Investigation of a Turbine with a Multiple Disc Rotor". Thesis, Arizona State University, Tempe, Arizona, 1960
6. Ladino F. R.: „Numerical Simulation of the Flow Field in a Friction-Type Turbine (Tesla Turbine)". Diploma Thesis, Institute of Thermal Powerplants, Vienna University of Technology, 2004
7. North, Richard, C.: „An Investigation of the Tesla Turbine". Thesis, University of Maryland, 1969;
8. Rice, Warren: „An Analytical and Experimental Investigation of Multiple-Disk Turbines". Journal of Engineering for Power, Trans. ASME, January 1965
9. Rice, Warren: „Tesla Turbomachinery". Conference Proceedings of the 4th International Tesla Symposium, Serbian Academy of Sciences and Arts, Belgrade, Yugoslavia, September 22-25, 1991
10. Schmidt D. D.: „Final Report on Biomass Boundary Layer Turbine Power " Energy Innovations Small Grant, EISG Final Report, Appendix A FAR 00-06, 2002
11. Tesla Nikola: „Turbine". Patent no: 1,061,206., United States Patent Office, Nikola Tesla, of New York N. Y., Patented May 6, 1913;
12. Fluent Inc.: Fluent/UNS/Rampant.„User's Guide", 2000
13. Fluent Inc.: Gambit. „User's Guide". 2000.
14. http://phoenixnavigation.com/ (Phoenix Navigation & Guidance Inc. Munising, Michigan and Phoenix Turbine Builders Club)

POLISH MARITIME RESEARCH, Special issue 2009/S1; pp. 34-38
10.2478/v10012-008-0042-4

Design analysis of turbines for co-generating micro-power plant working in accordance with organic Rankine's cycle

Jarosław Mikielewicz,
Marian Piwowarski,
Krzysztof Kosowski.

Abstract

This paper presents results of a design analysis of turbines for co-generating micro-power plant working in accordance with organic Rankine's cycle and using biofuel. The heat power range from 25 kW to 100 kW with corresponding available electric power from 2kW to 12kW, was considered. Designs of axial-flow turbines (single-stage and multi-stage ones, also those partially fed), radial-flow and axial-radial -flow ones, were analyzed. Particular variants of the solutions were compared to each other.

Keywords: *micro power plant, microturbines, organic Rankine cycle, turbine design*

Introduction

In the subject-matter literature steam micro-turbines are considered to be such devices which produce output power of the order of a few kW or even W. For last years greater and greater interest paid to such machines and their dynamic development has been observed. Hybrid co-generating systems, either three-generating or combined gas-steam ones can be most often met [1-3,10-13,16,18-21,24,25,27]. Steam turbines may find application to micro-power plants which co-generate electric power and heat. A micro-power plant based on water steam turbine, described in [14], can serve as an example. The system delivers electric power amounting from 0,5k W to 4,6 kW as well as heat power - from 2 kW to 25 kW. In the literature can be met examples of steam micro-turbines of much lower values of output power, built with the use of the MEMS technology (Micro-Electro Mechanical System) [6÷8]. Apart from the traditional medium, i.e.water vapour, also low-boiling media, as a rule organic ones, are taken into consideration. In this case the Organic Rankine Cycle (ORC) is dealt with. For many years such installations of electric power output of the order of several hundred kW or MW have been used in power plants based on geothermal sources [4,5,17,26]. On the market are already available the co-generating systems working on organic media, e.g. the power plant of 300÷600 kW electric power and 1500÷2800 kW heat power, or that of 200÷1000 kW electric power and 1000÷6000 kW heat power [9]. However only a few examples can be found of ORC installations of output power smaller than 100 kW, which operate in co-generating systems (e.g. the ORC-CHP system intended for biomass combustion [23], or the systems generating: 72 kW [22] or 30 kW [15] of electric power). Under research are: a turbine set of 5÷12 kW electric power at 70÷115ºC inlet temperature of working medium (R134a, R245fa, R22, R6xx, R7xx) [15], and a power plant working on n-pentane and developing 1.5÷3 kW power (at 90÷100ºC vapour temperature) [21].

Problems faced by designers of such turbines are associated with very small volumetric flow rate of working medium. It leads to small values of height of flow-part blades (hence to increased loss of flow rate) and high values of rotor speed, namely from a few dozen to over a hundred thousand rpm, usually.

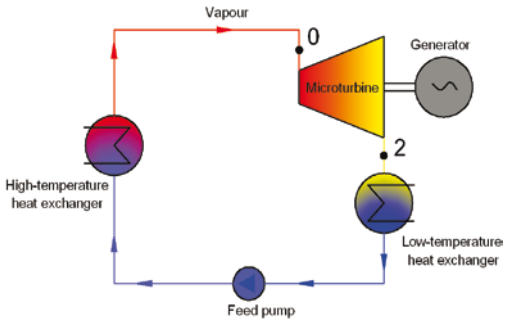

Fig. 1*. Schematic diagram of micro-power plant cycle*

In all the considered variants the power plants operated on the Solkatherm®SES36 working medium. Calulations were performed in compliance with the power plant schematic diagram shown in Fig. 1, for four values of the cycle's thermal power: 25 kW, 50 kW, 75 kW and 100 kW. Particular variants, depending on a heat power value, differred from each other only by value of working medium flow rate, and its parameters at turbine inlet, as well as pressure behind the turbine were the same for all the considered cases:

-the pressure at turbine inlet, $p_0 = 1464$ kPa,

-the temperature at turbine inlet, $t_0 = 140\ ^0$C,

-the pressure behind the turbine, $p_2 = 189$ kPa.

Within the frame of performed design analyses the following types of microturbines were taken into account:

- single-stage axial-flow turbine,
- two-stage axial-flow turbine,
- four-stage axial-flow turbine,
- single-stage radial-flow turbine,
- single-stage radial-axial-flow turbine.

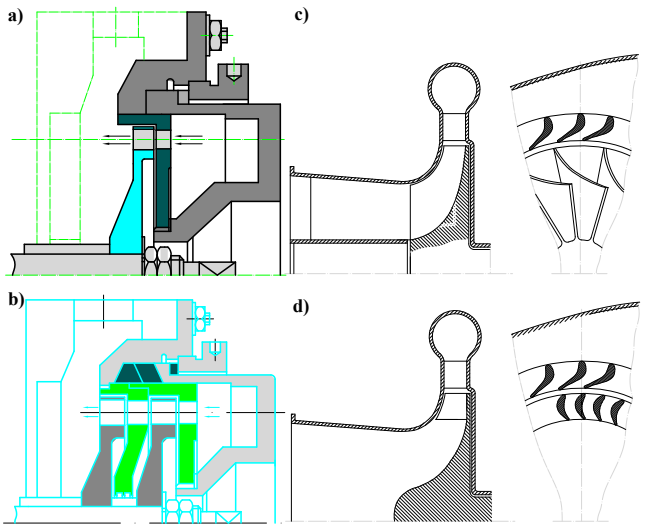

*Fig. 2. Examples of the considered constructional types of micro-turbines: **a)** single-stage axial-flow turbine, **b)** two-stage axial-flow turbine, **c)** radial-axial-flow turbine, **d)** radial-flow turbine*

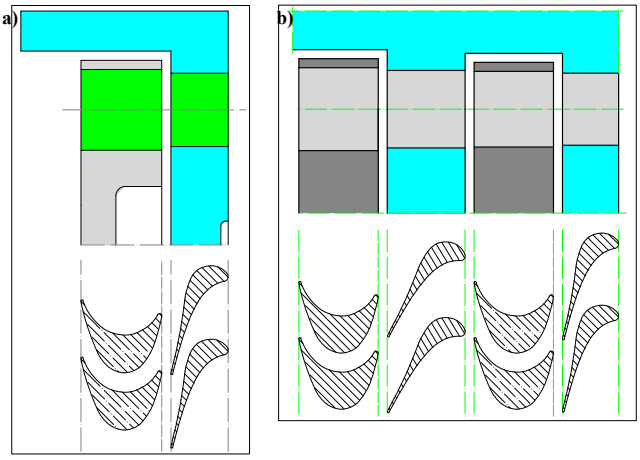

*Fig. 3. Examples of flow part of micro-turbines: **a)** single-stage axial-flow turbine, **b)** two-stage axial-flow turbine*

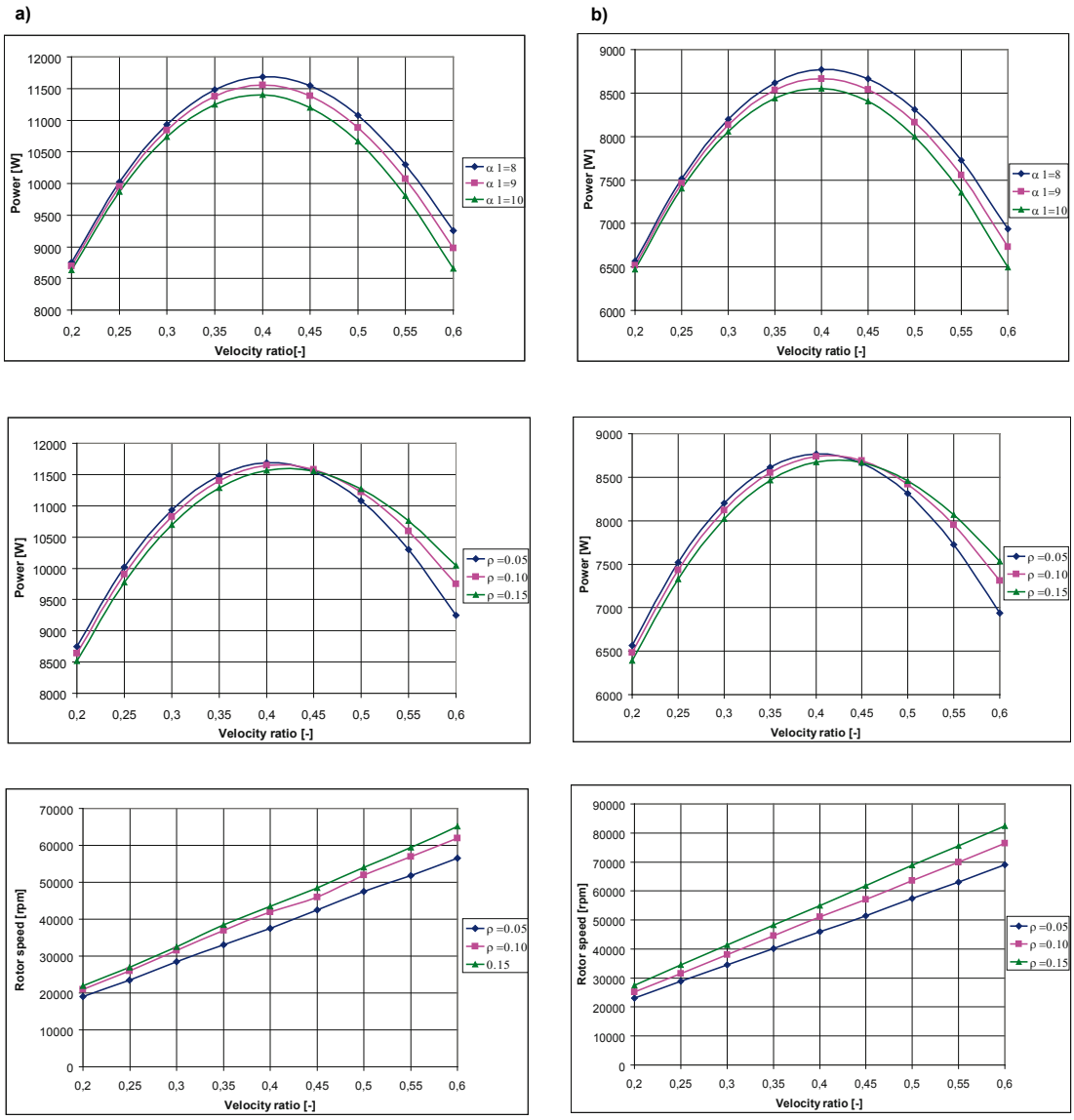

*Fig. 4. Examples of design characteristics of single-stage axial –flow turbine: turbine output power in function of velocity ratio for three assumed values of the angle α_1, turbine output power in function of velocity ratio for three assumed values of the reactivity ρ, rotor speed in function of velocity ratio for three assumed values of the reactivityρ, **a)** plant's heat power – 100 kW, **b)** plant's heat power – 75 kW*

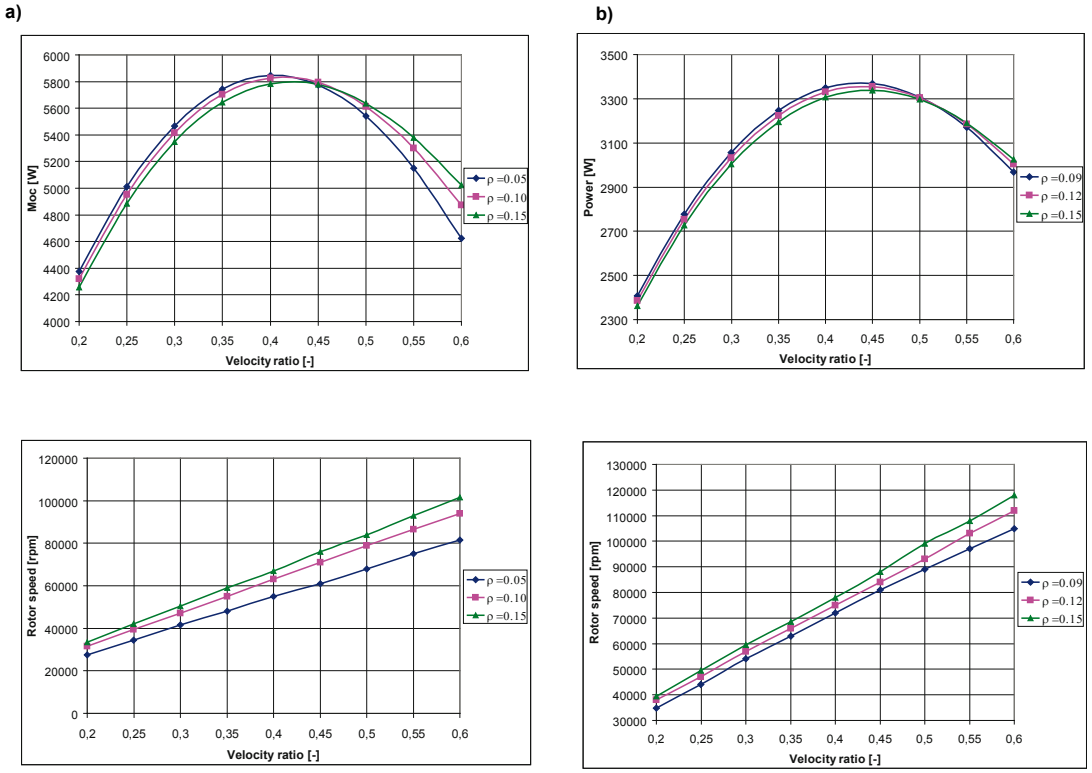

Fig. 5. *Examples of design characteristics of single-stage axial-flow turbine: turbine output power in function of velocity ratio for three assumed values of the reactivity ρ, rotor speed in function of velocity ratio for three assumed values of the reactivity ρ,*
a) *plant's heat power – 50 kW,* ***b)*** *plant's heat power – 25 kW*

Examples of the considered design solutions are presented in Fig. 2. For all the variants preliminary optimization of main design parameters was performed and appropriate blade profiles were selected. Examples of the flow part of single-stage and two-stage axial-flow turbines are given in Fig. 3.

Results of design analyses of micro-turbines

Calculations of flow-part of turbine were performed by assuming different sets of values of main design parameters such as: velocity ratio, reactivity and outlet angle of guide vanes grid. Examples of design characteristics are presented in Fig. 4 for plant's heat power values: 100 kW and 75 kW, and in Fig. 5 for plant's heat power values: 50kW and 25kW. For the greatest heat power value (100 kW) of the considered co-generating systems, the electric power value of ~11,5 kW can be obtained at the rotor speed of about 45000 rpm. For the smallest considered heat power value (25 kW) the above mentioned quantities amount to about 3.35 kW and 80000 rpm, respectively.

Possible elaboration of series of types of turbines which would be suitable for the power range of 25 kW ÷ 100 kW and of the same design and similar gabarites, has been also considered. It was decided that all turbines, regardless of their power, would be built of the same rotor and the only difference would consist in adjusting the feeding arc of vane blades grid, respectively. It was assumed that the 100 kW turbine would operate with full feeding arc, hence turbines of smaller power values would operate with smaller feeding arcs, respectively. Examples of design characteristics of single-stage axial-flow turbines working with partial feeding are presented in Fig. 6. Application of feeding arc makes that power values of turbines working with partial feeding are smaller than those of turbines with full feeding (compare Fig.4 and Fig.5 with Fig.6), however in the variants of smaller power values rotor speed values were significantly lower, e.g. for the plant's heat power of 25 kW, when partial feeding has been applied, the turbine's electric power decreased from 3,35 kW to 2.65 kW, but with accompanying drop of rotor speed from about 80000 rpm to about 40000 rpm. Significantly lower production costs would be reached as a result of standardization, application of rotors of the same design to all variants, and possible selection of a generator intended for lower rotational speeds (definite influence on price of turbine set).

Similar design calculations were carried out for the remaining constructional types of turbines in question; their results are presented in Tab. 1. For the presented solutions suitable electric generators were selected; their main particulars are attached also in Tab. 1.

For the variant of 100 kW heat power of the power plant the largest electric power values (~ 12,3 kW) were obtained in the case of application of the radial turbine or two-stage axial-flow turbine. In most considered cases the radial-flow turbine as well as two-stage axial-flow turbine turned out to be the most profitable as regards the obtained electric power value. From this point of view the radial–axial–flow turbine appeared the worst.

a)

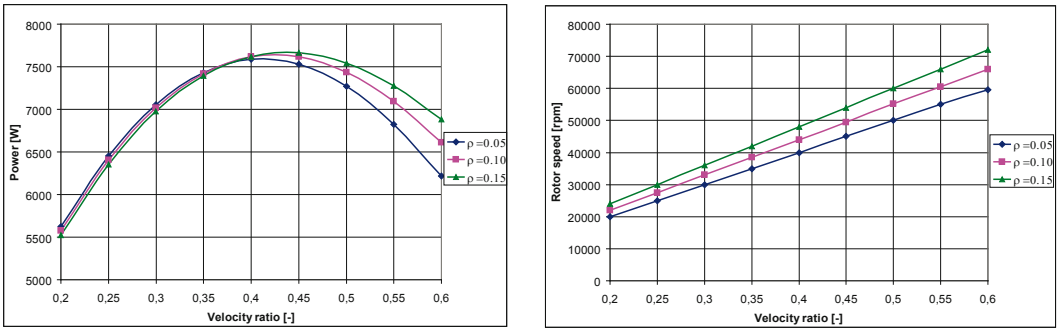

b)

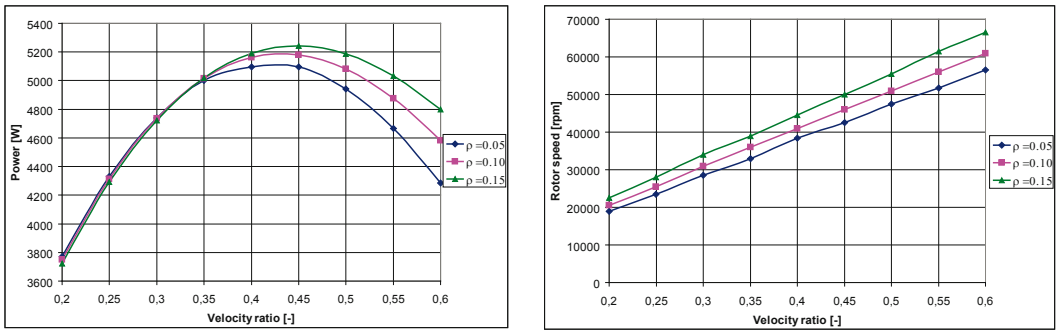

c)

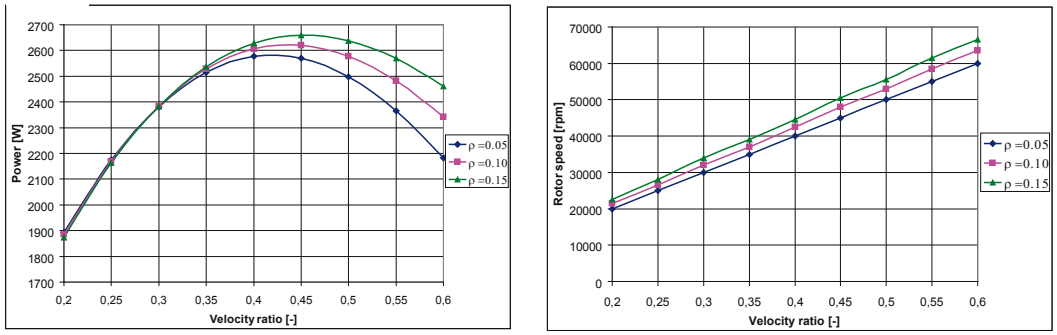

Fig. 6. *Examples of design characteristics of single-stage axial-flow turbine with partial feeding: turbine output power in function of velocity ratio for three assumed values of the reactivity ρ, rotor speed in function of velocity ratio for three assumed values of the reactivity ρ*
plant's heat power – 75 kW, feeding arc of ~ 0,75
plant's heat power – 50 kW, feeding arc of ~ 0,50
plant's heat power – 25 kW, feeding arc of ~ 0,25

Summary

Calculations of a few dozen of variants of turbines of various constructional types and different values of main design parameters, were performed. The following turbines were taken into consideration: single-stage axial-flow turbines, two-stage axial-flow turbines, radial-flow turbines and radial-axial-flow turbines. It was demonstrated that in the case of co-generating micro-power plant working with low-boiling medium (in accordance with the ORC principle) the following electric power values are possible to be obtained depending on a heat power value of the system:

-10,4 kW ÷ 12,8 kW (for 100 kW heat power),

-7,6 kW ÷ 9,4 kW (for 75 kW heat power),

-5,0 kW ÷ 6,1 kW (for 50 kW heat power),

-2,4 kW ÷ 3,3 kW (for 25 kW heat power).

Rotor speed values of the considered micro-turbines were relatively high as they amounted to from 21000 rpm to 134 000 rpm depending on working medium mass flow rate, constructional type of turbine and choice of its main design parameters. For many variants one managed to select suitable electric generators. However, because of high rotational speeds, novel innovative design, material and technological solutions should be applied in developing power plants of the kind.

Acknowledgements

These authors would like to express their thanks to Mr Koronowicz J., M.Sc., and Mr Bykuc S., M.Sc. from Institute of Fluid Flow Machinery, Polish Academy of Sciences, for their help in selecting electric generators.

Bibliography

1. Campanari S., Boncompagni L., Macchi E.: „Microturbines and Trigeneration: Optimization Strategies and Multiple Engine Configuration Effects".Journal of Engineering for Gas Turbines and Power, Vol. 126, JANUARY 2004
2. Campanari S., Macchi E.: „Technical and Tariff Scenarios Effect on Microturbine Trigenerative Applications". Journal of Engineering for Gas Turbines and Power, Vol. 126, January 2004
3. Colombo L. P. M., Armanasco F., Perego O.: „Experimentation on a Cogenerative System Based on a Microturbine". Applied Thermal Engineering 27, 2007
4. Duvia A., Gaia M.: „ORC Plants for Power Production from Biomas from 0.4MWe to 1.5MWe: Technology, Efficiency, Practical Experiences and Economy".7th Holzenergie Synopsium, Zurich 2002
5. Duvia A., Tavolo S.: „Application of ORC Units in the Pellet Production Field: Technical-Economic Considerations and Overview of the Operational Results of an ORC Plant in the Industry Installed in Mudau (Germany)" 7th Holzenergie Synopsium, Zurich 2002
6. Fréchette Luc G., Stuart A. Jacobson, Kenneth S. Breuer1, Fredric F. Ehrich, Reza Ghodssi2, Ravi Khanna, Chee Wei Wong, Xin Zhang, Martin A. Schmidt and Alan H. Epstein: „Demonstration of a Microfabricated High-Speed Turbine Supported on Gas Bearings". Solid-State Sensor and Actuator Workshop, Hilton Head Is., SC, June 4-8, 2000
7. Fréchette L. G., Lee C., Arslan S. Yuan-Chun Liu: „Preliminary Design of a MEMS Steam Turbine Power Plant on a Chip". 3rd Workshop on Micro & Nano Tech. for Power Generation & Energy Conv. (PowerMEMS'03), Makuhari, Japan, 4-5 Dec. 2003
8. Fréchette L. G., Lee C., Arslan S.: „Development of a MEMS-Based Rankine Cycle Steam Turbine For Power Generation". 4th Workshop on Micro and Nano Technology for Power Gene. & Energy Conv. Apps (Power MEMS'04), Kyoto, Japan, pp. 92-95, Nov. 28-30, 2004
9. Gailfuß M.: „Private meets Public – Small scale CHP". Technological Developments, Workshop BHKW-Infozentrum Rastatt 09.09.2003, Berlin, 2003
10. Haught D.: „Final ATS Annual Program Review Meeting". Clean Energy for 21st Century, Alexandria, VA, December 4-6, 2000
11. Hedman B. A.: „The Potential for Combined Heat and Power (CHP)". An Underserved Market for Combined Heat and Power, Energy and Environmental Analysis, Inc., September 19, 2005
12. Ho J.C., Chua K.J., Chou S.K.: „Performance study of a microturbine system for cogeneration application". Renewable Energy 29, 2004
13. Horlock J. H.: „Advanced Gas Turbine Cycles". An imprint of Elsevier Science, Amsterdam, Boston, Heidelberg, London, New York, Oxford, Paris, San Diego, San Francisco, Singapore, Sydney, Tokyo, 2003
14. Hoval: Close-ups: „Visions become reality" (in Polish). Information for clients and co-workers of Hoval Group, July 2004
15. Infinity Turbine LLC, phone (608) 238-6001, November 7, 2008
16. Logan Earl, Jr. Roy R.: „Handbook of Turbomachinery". Second Edition, Arizona State University, Marcel Dekker Inc., New York, Basel, 2003
17. McMahan A. C., Klein S. A., Reindl D. T.: „Design and Optimization of Parabolic Trough Organic Rankine Cycle Powerplants". University of Wisconsin – Madison Solar Energy Laboratory July 12, 2006
18. Mills D.: „Advances in solar thermal electricity technology".Solar Energy 76, 2004
19. Nexus Energy Group: „Catalogue of CHP Technologies". Introduction to CHP Catalogue of Technologies, U.S. Environmental Protection Agency Combined Heat and Power Partnership, Arlington, Virginia, 2002
20. ONSITE SYCOM: „Review of Combined Heat and Power Technologies". Office of Industrial Technologies, Office of Energy Efficiency and Renewable Energy, U.S. Department of Energy, October 1999
21. Riffat S. B., Zhao X.: „A Novel Hybrid Heat Pipe Solar Collector/CHP System". Project no. ENK5-CT-2001-20544, Thematic Network on Combined Heat and Power, United Kingdom, 2004
22. Rosfjord T., Tredway W., Chen A., Mulugeta J., Bhatia T.: „Advanced Microturbine Systems". Final Report for Tasks 1 Through 4 and Task 6, Report Number DOE/CH/11060-1 prepared for The U.S. Department of Energy, Office of Distributed Energy, 2007
23. Simader G. R., Krawinkler R., Trnka G.: „Micro CHP systems: state-of-the-art". Deliverable 8 (D8) of Green Lodges Project, EIE/04/252/S07.38608, Vienna 2006
24. Spentzas S.: „Optimization of a Cogeneration System in the Automotive Industry". SAE 2006 World Congress, 2006
25. Staunton R. H., Ozpineci B.: „ Microturbine Power Conversion Technology Review". OAK Ridge National Laboratory, ORNL/TM-2003/74, April 8, 2003
26. Turboden Company Profile: „Organic Rankine Cycle (ORC) concept". University of Wisconsin – Madison Solar Energy Laboratory July 12, 2006, 101;
27. Wolf Jonas et al.: „Micro and Small Scale CHP from Biomass (<300kWe)". Technology Paper 2, OPET RES-e – NNE5/37/2002, Networks Put You in Touch with Innovative Energy Technologies, April 2004.

Tab. 1. *Specification of main particulars of turbo-generators*

No.	Type of turbine	Particular	Unit	Power plant of 100 kW heat power	Power plant of 75 kW heat power		Power plant of 50 kW heat power		Power plant of 25 kW heat power	
					Full feeding	Partial feeding	Full feeding	Partial feeding	Full feeding	Partial feeding
1	single-stage axial-flow	Average diameter	[m]	0,055	0,048	0,055	0,035	0,055	0,025	0,055
		Length of rotor blade	[m]	0,0058	0,005	0,0058	0,0037	0,0058	0,0027	0,0058
		Power of turbine	[W]	11688	8768	7586	5826	5098	3248	2577
		Rotational speed	[rpm]	40000	46000	40000	63000	40000	76000	40000
		Length of generator	[m]	0,12	0,1	0,1	0,085	0,10	0,085	0,085
		Outer diameter of generator's stator	[m]	0,06	0,055	0,060	0,055	0,055	0,055	0,055
2	two-stage axial-flow	Average diameter	[m]	0,04	0,035	0,04	0,029	0,04	0,02	0,04
		Length of rotor blade (1st stage)	[m]	0,0042	0,0036	0,0042	0,0029	0,0042	0,0021	0,0042
		Length of rotor blade (2nd stage)	[m]	0,0046	0,0038	0,0046	0,0031	0,0046	0,0023	0,0046
		Power of turbine	[W]	12273	9241	8756	6167	5794	3102	2927
		Rotational speed	[rpm]	33600	38500	33600	47000	33600	67000	33600
		Length of generator	[m]	0,126	0,12	0,12	0,100	0,0120	0,085	0,085
		Outer diameter of generator's stator	[m]	0,07	0,060	0,060	0,055	0,055	0,055	0,055
3	radial-axial-flow	Outer diameter of rotor blades grid	[m]	0,0517	0,0402	-	0,0324	-	0,0224	-
		Power of turbine	[W]	10426	7643	-	4974	-	2367	-
		Rotational speed	[rpm]	62081	78846	-	96566	Max. catalogue value: 80 000	136565	
		Length of generator	[m]	0,12	0,1	-		-		-
		Outer diameter of generator's stator	[m]	0,055	0,055	-		-		-
4	radial-flow	Outer diameter of rotor blades grid, d1	[m]	0,061	0,053	-	0,043	-	0,03	-
		Power of turbine	[W]	12306	9231	-	6154	-	3077	-
		Rotational speed	[rpm]	49076	56663	-	69397	-	98143	
		Length of generator	[m]	0,12	0,1	-	0,085	-		-
		Outer diameter of generator's stator	[m]	0,06	0,055	-	0,055	-		-

POLISH MARITIME RESEARCH, Special issue 2009/S1; pp. 39-44
10.2478/v10012-008-0044-2

Evaluation of technical efficiency of heat and electric power generation

Hanna Piwowarska,
Marian Piwowarski

Abstract

This paper presents an evaluation of technical efficiency and time-dependent changes in productivity of Polish professional electric power and heat & electric power stations by using Data Envelopment Analysis non-parametric method. The research covered the enterprises whose total available electric power amounted to about 98% of that of all professional thermal electric power stations in this country. The analysis has concerned the years 2000÷2004. Impact was considered of such factors as: scale of enterprise activity, form of ownership as well as type of carried out activity, on technical efficiency and time-dependent productivity changes. Changes in productivity of the power generation sector were determined by means of Malmquist index.

Keywords*: Data Envelopment Analysis (DEA), technical efficiency, Malmquist index, thermal power generation*

Introduction

An important factor which determines enterprise competitiveness level is optimum use of its resources to generate higher profits. In other words, the obtaining of higher economic efficiency by an enterprise impacts its competitiveness level. One of the economic efficiency components is technical efficiency which is understood as the achieving of the highest output in presence of a determined number of production factors. Level of the technical efficiency is influenced by a.o. technical progress and economic scale.

One of the methods for measuring the technical efficiency is the Data Envelopment Analysis (DEA) based on the linear programming where appropriate technical efficiency levels are obtained by determining optimum values of objective function at certain constraints imposed on it.

The sector of heat and electric power generation industry, crucial for Polish economy, was selected for this analysis. More comprehensive research into technical efficiency of power production eneterprises has been lacking so far. In this paper an evaluation of relative technical efficiency (as well as its components) of domestic professional electric power and heat & electric power stations is performed by using the DEA method, and of time-dependent changes in their productivity in the years 2000÷2004 - by applying the Malmquist productivity index.

For power industry enterprises effective use of their resources, i.e. increasing technical efficiency level, is of special importance. In the case of the industry sector technological changes and rationalization of internal organization are of a great influence on technical efficiency level.

Technical efficiency and productivity

Technical efficiency determines enterprise capability of achieving maximum level of effects at given inputs or consuming minimum amount of inputs to achieve assumed effects, at a given technology, i.e. structure of production inputs.

Economists are unanimous that the technical efficiency is the most important efficiency component as its level is influenced mainly by technical progress and better use of applied technology.

The reaching of maximum technical efficiency means that from a given combination of resources an enterprise manufactures the maximum possible amount of goods and services, in other words it cannot increase amount of its effects without increasing amount of its inputs or reduce its inputs without reducing its effects, which is unambiguous to the statement that resources are not wasted during production process. And, the technical efficiency measure orientated towards inputs shows to which degree to reduce consumption of inputs without reducing amount of effects, is possible. However the technical efficiency measure orientated towards effects shows by which amount the generated effects can be increased without engaging any greater amount of inputs. The technical efficiency can be assessed independing on prices.

A way of measuring the eneterprise technical efficiency consists in relating an observed level of production at given inputs to their potential level. And, the potential level is determined by limit values, i.e. minimum amount of component inputs (or their combimation) necessary to produce a given amount of effects (or their combination). Distance from the analyzed enterprise production level to the curve which shows relevant limit values is a measure of technical inefficiency. If the point which symbolizes current production of a given enterprise lays on the limit curve then the enterprise is assumed fully efficient; and if the point lays below the curve then the enterprise is considered technically inefficient. The ratio of observed output and potential output at given inputs and definite technological conditions constitutes the efficiency level of the enterprise in question.

The components of total technical efficiency are as follows:

$$TE \equiv PTE \times SE \tag{1}$$

where:

TE - technical efficiency;
PTE - purely technical efficiency;
SE - scale efficiency;

TE, PTE and SE - take values from the interval <0÷1>.

The purely technical efficiency is the part of technical efficiency, which cannot be considered as that caused by deviations from the most favourable scale of enterprise activity.

The enterprise productivity is the ratio of quantity or value of one or several categories of the effects generated to a certain quantity or value of one or several caregories of the inputs by means of which the effects have been obtained.

Description of Data Envelopment Analysis (DEA) method

The DEA method is aimed at measuring efficiency of a certain number of enterprises. Entities belonging to a considered group are compared to each other. The DEA method finds the best entities and shows to which degree others are inefficient as compared with those fully efficient.

The investigations presented in [2], [4] have formed a background to relative efficiency evaluation.Their authors have introduced the Data Envelopment Analysis method which consitutes operational research methodology based on linear programming technique and aimed at measuring relative efficiency of the decision making unit (DMU) when it is difficult to compare general efficiency measures in situation of many kinds of component inputs and effects.

The DEA method belongs to non-parametric ones. Hence, in contrast to the parametric methods, it does not necessitates a functional relation between inputs and effects to be determined, neglects inflation influence on results, does not make taking into account prices of production factors in technical efficiency calculations, necessary.

The Efficiency Measurement System (EMS), version 1.3, a special computer software (elaborated by Universität Dortmund, Germany, and kindly released for scientific use) was used to perform the technical efficiency analysis for the industrial sector in question. This paper presents the technical efficiency analysis based on DEA measures orientated towards inputs, which show how far it can be reduced without worsening the effects. The DEA model orientated towards inputs, written as a linear programming problem, is of the following form:

$$\min\left\{\Theta \middle| \left(\Theta X^k, Y^k\right) \in T\right\} \tag{2}$$

In the model, T stands for the set of production capabilities, defined on the basis of available empirical data about n objects; X^k, Y^k -vector of k-th entity inputs and effects, respectively. The parametr Θ determines technical efficiency level of a given object and simultaneously informs which perentage of inputs would suffice to be kept in the enterprise to obtain present effects in the case of using the technology implemented in the enterprises deemed efficient. Solving the above mention problem consists in finding minimum value of Θ. The value of Θ for the most efficient objects is equal to 1, for the remaining ones the value is adequate to the efficiency level achieved by them and is smaller than 1.

In calculating the efficiency a kind of economic scale can be assumed, namely it used to be assumed that either constant scale effects or variable ones occur. Depending on that, different results as to different kinds of efficiency, can be obtained. Let's attribute the following symbols to the different efficiency measures depending on an assumed kind of economic scale:

- M_CRS - stands for the efficiency measure in the case of constant scale effects;
- M_VRS - stands for the efficiency measure in the case of variable scale effects.

If the measures differ from each other then one will be able to conclude as to occurrence of scale effects in a considered sector. It can be assessed by means of the following measure:

$$\text{E_S_VRS} = \text{M_CRS} / \text{M_VRS} \tag{3}$$

If it yields a value smaller than 1, then the entity in question can be said inefficient with respect to scale.

In this paper comparisons of time-dependent productivity were performed by using the Malmquist index. The index applicable to comparing changes in efficiency has the following form:

$$M_o^G\left(x^t, y^t, x^{t+1}, y^{t+1}\right) = \left[\frac{D_o^t\left(x^{t+1}, y^{t+1}\right)}{D_o^t\left(x^t, y^t\right)} \frac{D_o^{t+1}\left(x^{t+1}, y^{t+1}\right)}{D_o^{t+1}\left(x^t, y^t\right)}\right]^{1/2} \tag{4}$$

where:

$D_o^t\left(x^{t+1}, y^{t+1}\right)$ -the efficiency in the case of making use of t-th year technology for data from (t+1)-th year,

$D_o^t\left(x^t, y^t\right)$ -the entity's efficiency in the period t in the case of making use of the then available technology and data from the period t.

$D_o^{t+1}\left(x^{t+1}, y^{t+1}\right)$ -the entity's efficiency in the period (t+1).

$D_o^{t+1}\left(x^t, y^t\right)$ -the efficiency in the case of making use of (t+1)-th year technology for data from t-th year.

And, the notion of technology is deemed to represent a level of technological development of a given enterprise in a given period. Such approach to the technology makes it possible a.o. to investigate productivity improvement resulting from technological development.

When $M_o^G\left(x^t, y^t, x^{t+1}, y^{t+1}\right)$ is equal to or smaller than 1, then productivity increases, remains constant, or decreases, respectively, in the period (t+1), as compared with that in the period t.

Data and results of the investigations

In this work 39 eneterprises were analyzed for the years 2000÷2001 and 38 for the years 2002÷2004. And, 27 heat & electric power stations and their complexes were analyzed for the years 2000÷2001 and 26 of them for the years 2002÷2004. Also 9 electric power stations and their complexes were analyzed in this work. Three complexes combining electric power stations and heat & electric power stations were taken into consideration as well.

The model's variables were selected on the basis of the literature sources dealing with DEA method application to analyzing technical efficiency in the power industry sector. The model was so formed as to comply with specificity of Polish electric power industry.

In this work for every investigated entity six categories of input data to DEA model were assigned, four of which concerned inputs and two – effects. The input categories taken into account were:

- mean yearly number of employees [number of persons];
- available electric output power [MW];
- available heat output power [MW];
- amount of chemical energy loading contained in fuel, e.g. coal, consumed to produce heat and electric power [TJ].

Amount of sold heat energy, counted in [TJ], and amount of sold electric energy [TJ] appear in the model as the effects.

In this work efficiency measures for the successive years: 2000, 2001, 2002, 2003 and 2004, were calculated. As these authors have been obliged to respect confidentiality of the input data achieved from the enterprises the obtained results were assigned only to symbols of particular enterprises. The example results of estimation of the efficiency measures are given in Tab. 1.

The technical efficiency measures orientated towards inputs inform on which perentage of inputs would be sufficient to produce such amounts of heat and electric energy as to operate as efficiently as the electric power stations which obtained the highest marks. For instance to get 70% measure value in a given year means that to produce the same amount of energy by using 70% of inputs for this aim will be possible if only the enterprise in question uses its resources as efficiently as the best enterprises among the analyzed ones. The productivity analysis is more suitable to present time-dependent changes in results of the sector's operation than the presenting of mean measures of relative efficiency as the latter quantity may increase whereas the productivity may decrease. Apparent improvement expressed in the form of mean relative efficiency tells mainly about degree of differentiation of enterprises with a view of their skill in using inputs to transform it into effects. Whereas changes in productivity shows whether relation of effects to inputs has really increased or not. Diag.1 shows the mean measure of Malmquist index, taken from the measures as well as their components for all the investigated entities in the years 2000÷2004.

Tab. 1. *Technical efficiency measures orientated towards inputs obtained by means of DEA model for the years 2000÷2004, at the scale effects assumed constant (M_CRS)*

Symbol of entity	Year				
	2000	2001	2002	2003	2004
F1	100,00%	100,00%	100,00%	96,79%	100,00%
F2	91,62%	87,60%	92,86%	92,76%	95,39%
F3	95,50%	84,66%	79,88%	74,23%	73,81%
F4	83,77%	81,11%	76,28%	71,74%	70,77%
F5	100,00%	100,00%	100,00%	100,00%	100,00%
F6	82,66%	77,50%	76,02%	73,84%	72,96%
F7	100,00%	100,00%	100,00%	100,00%	100,00%
F8	100,00%	100,00%	100,00%	100,00%	100,00%
F9	98,25%	90,21%	94,79%	90,87%	92,50%
F10	91,80%	88,39%	90,46%	81,28%	87,18%
F11	100,00%	100,00%	100,00%	100,00%	100,00%
F12	83,32%	95,64%	100,00%	97,01%	100,00%
F13	100,00%	100,00%	97,64%	100,00%	100,00%
F14	86,06%	80,82%	87,03%	100,00%	100,00%
F15	100,00%	100,00%	100,00%	100,00%	100,00%
F16	100,00%	100,00%	100,00%	100,00%	100,00%
F17	100,00%	92,21%	91,82%	88,58%	90,64%
F18	85,49%	87,87%	84,97%	89,27%	86,64%
F19	89,60%	91,34%	93,13%	90,52%	90,33%
F20	65,58%	67,36%	71,89%	78,10%	69,10%
F21	96,28%	93,24%	89,78%	96,21%	94,85%
F22	100,00%	100,00%	99,98%	99,89%	100,00%
F23	62,45%	65,34%	67,58%	60,99%	63,82%
F24	100,00%	100,00%	100,00%	100,00%	100,00%
F25	96,95%	97,15%	100,00%	100,00%	100,00%
F26	81,74%	81,62%	83,47%	93,29%	97,95%
F27	98,85%	97,93%	89,32%	86,56%	88,17%
F28	100,00%	100,00%	89,37%	85,29%	83,30%
F29	70,78%	73,70%	76,44%	82,48%	93,09%
F30	100,00%	100,00%	95,47%	100,00%	100,00%
F31	84,02%	91,42%	100,00%	100,00%	100,00%
F32	50,69%	65,80%	65,52%	73,74%	81,13%
F33	98,86%	81,55%	54,96%	69,75%	70,17%
F34	57,30%	59,47%	100,00%	100,00%	100,00%
F35	100,00%	100,00%	76,36%	78,21%	80,11%
F36	74,87%	79,50%	72,77%	57,95%	68,57%
F37	72,79%	74,32%	76,98%	100,00%	100,00%
F38	76,13%	71,13%	81,53%	73,48%	74,04%
F39	83,28%	83,71%			

The performed analysis of Malmquist index shows that the high productivity level for the year 2001 has resulted from the large amount of heat energy sold in this period, that can be explained a.o. by different atmospheric conditions, namely low temperature values. And, for the years 2002÷2003 the low level of the index (abt. 0,6%) resulting from economy slowing-down, can be observed. In the year 2004 the productivity increase is greater than in the preceding years. And, changes in relative technical efficiency, as well as technological progress resulting from technological changes in the subsector of electric power generation, have been to a similar extent responsible for the increase. The technological progress, a component of the productivity index, results in that the limit line

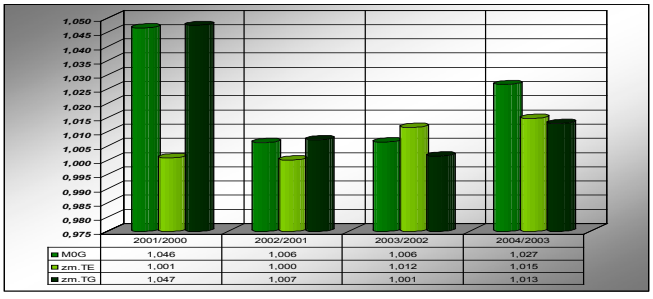

Fig. 1. *Mean measures of the Malmquist index (M0G) and its components: the relative efficiency (zm. TE) as well as the technological progress (zm. TG), observed in the professional heat & electric power and electric power stations for the years 2000÷2004.*

of the set of production capabilities moves upward in the diagram. It tells about changes in general tendencies for the investigated group of entities. The mean yearly increase of productivity of the investigated professional thermal electric power and heat & power stations installed in Poland in the years 2000÷2004, was equal to 2,1%. For comparison, in China the mean productivity increase for the years 1995÷2000, measured by TFP index, amounted also to 2,1%, whereas in Australia was equal on average to 1,6% for the years 1981÷1991.

The observed mean yearly increase, on 2,1% level, of productivity of the investigated power industry enterprises was mainly caused by technological progress. The productivity increase of the domestic power industry sector resulted from employment rationalization as well as modernization of permanent assets, and installation of modern devices in electric power and heat & electric power stations. As a result, higher efficiency of their equipment, manifested by lower specific fuel consumption for power generation, was obtained.

In the investigated period the productivity increase was also influenced, apart from atmospheric conditions and economy trends, by other factors such as political decisions as to rebuilding and modernizing the power sources installed in this country, as well as multi-year continuation of the long-term contract system not including any requirements as to introducing improvements to the power industry enterprises, that could not be conductive to taking care of increasing energy generation efficiency in the enterprises.

Apart from the general changes in productivity of the sector in question also impact of internal factors on efficiency and time-dependent changes in productivity were analyzed for the investigated group of enterprises. The factors selected for the analysis were as follows: scale of enterprise activity, form of ownership, as well as type of carried-out activity. Verification of impact of scale factor on activity results shows whether the making use of a greater scale of activity by power generation enterprise does allow to achieve inputs savings and this way higher efficiency measures. The influence analysis of ownership form verifies the opinion whether private power industry enterprises are more efficient and faster developing than the state ones. And, the activity type factor, i.e. differentiation of enterprises with a view of prevailing share of either heat power or electric power production in a given enterprise, reveals differences in specificity of activity of the enterprises.

In order to analyze impact of size of the considered enterprises on their efficiency, and of changes in their productivity they have been split into three groups: those of the total available heat and electric power: below 500 MW, between 500 and 1500 MW, and over 1500 MW. Mean values of particular efficiency categories were then calculated and time-dependent changes in productivity for the particular groups were evaluated (see Tab. 2 and Tab. 3). As results from the analyses the enterprises of the total available power below 500 MW have achieved the lowest scale efficiency measures in the particular years, however the mean measure of their scale efficiency has increased in the years 2000÷2004. For the entities the scale efficiency constitutes an important element of the total technical efficiency, and the efficiency limit line in the case of assuming changeable scale effects, is the most distant from that in the case of constant scale effects. The group forms the main source of scale inefficiency

Tab. 2. *Technical efficiency versus size of power industry enterprise, measured by its total available output power.*

Year	Enterprises of total available heat & electric output power of	M_CRS	M_VRS	E_S_VRS
2000	below 500 MW	80,90%	92,27%	87,46%
	500 MW÷1500 MW	91,65%	92,51%	99,02%
	over 1500 MW	96,80%	97,49%	99,25%
2001	below 500 MW	83,34%	92,06%	90,50%
	500 MW÷1500 MW	87,27%	88,33%	98,76%
	over 1500 MW	95,25%	97,52%	97,65%
2002	below 500 MW	83,64%	91,27%	91,75%
	500 MW÷1500 MW	87,65%	88,21%	99,31%
	over 1500 MW	94,55%	97,15%	97,28%
2003	below 500 MW	88,92%	92,16%	96,52%
	500 MW÷1500 MW	85,29%	85,82%	99,35%
	over 1500 MW	91,73%	94,04%	97,54%
2004	below 500 MW	90,13%	92,62%	97,37%
	500 MW÷1500 MW	86,82%	87,44%	99,24%
	over 1500 MW	92,40%	94,63%	97,63%

Tab. 3. *Productivity versus size of power industry enterprise, measured by its total available output power.*

Year	Enterprises of total available heat & electric output power of	Malmquist index M_0G	Relative efficiency (zm. T^E)	Technological Progress (zm. T^G)
2001/2000	below 500 MW	107,19%	103,83%	103,31%
	500 MW ÷1500 MW	101,68%	95,43%	106,77%
	over 1500 MW	103,37%	98,40%	105,20%
2002/2001	below 500 MW	99,71%	101,67%	98,12%
	500 MW ÷1500 MW	101,07%	98,13%	103,10%
	over 1500 MW	101,42%	99,27%	102,27%
2003/2002	below 500 MW	100,60%	107,15%	94,47%
	500 MW ÷1500 MW	101,76%	96,81%	105,65%
	over 1500 MW	99,89%	96,78%	103,31%
2004/2003	below 500 MW	103,52%	101,52%	102,07%
	500 MW ÷1500 MW	102,41%	102,38%	100,31%
	over 1500 MW	101,78%	100,77%	100,99%

Tab. 4. *Technical efficiency versus form of ownership of power generation enterprise*

Year	Category of enterprise	M_CRS	M_VRS	E_S_VRS
2000	Polish private enterprises	92,01%	100,00%	92,01%
	Polish state enterprises	87,49%	93,20%	93,65%
	Foreign enterprises	100,00%	100,00%	100,00%
2001	Polish private enterprises	88,61%	92,84%	95,20%
	Polish state enterprises	86,90%	92,37%	94,09%
	Foreign enterprises	98,05%	98,25%	99,78%
2002	Polish private enterprises	88,76%	91,70%	96,53%
	Polish state enterprises	87,43%	92,52%	94,55%
	Foreign enterprises	92,00%	93,42%	98,51%
2003	Polish private enterprises	92,70%	92,75%	99,93%
	Polish state enterprises	87,95%	90,95%	96,76%
	Foreign enterprises	90,90%	91,83%	98,99%
2004	Polish private enterprises	92,28%	92,58%	99,57%
	Polish state enterprises	88,95%	91,63%	97,14%
	Foreign enterprises	92,07%	92,96%	99,08%

Tab. 5. *Productivity versus form of ownership of power generation enterprise*

Year	Category of enterprise	Malmquist index M_0G	Relative efficiency (zm. T^E)	Technological Progress (zm. T^G)
2000	Polish private enterprises	107,94%	104,41%	103,30%
	Polish state enterprises	104,81%	100,06%	104,95%
	Foreign enterprises	100,59%	97,40%	103,29%
2001	Polish private enterprises	102,25%	103,86%	98,42%
	Polish state enterprises	97,06%	96,62%	97,31%
	Foreign enterprises	101,54%	98,70%	103,10%
2002	Polish private enterprises	103,09%	105,32%	97,99%
	Polish state enterprises	100,13%	101,50%	99,48%
	Foreign enterprises	101,18%	97,42%	103,91%
2003	Polish private enterprises	98,35%	96,16%	102,41%
	Polish state enterprises	103,66%	101,95%	101,76%
	Foreign enterprises	101,22%	101,84%	99,53%
2004	Polish private enterprises	92,28%	92,58%	99,57%
	Polish state enterprises	88,95%	91,63%	97,14%
	Foreign enterprises	92,07%	92,96%	99,08%

for the years 2000÷2002. And, almost in the whole investigation period, i.e. in the years 2001÷2004, their technical efficiency, in the case of assuming changeable scale effects, is higher than that of the enterprises of the output between 500 and 1500 MW, and lower than that of the enterprises of over 1500 MW output. The enterprises of the total available power between 500 and 1500 MW are characterised, almost during the whole investigation period, by the lowest technical efficiency measures in the case of assuming changeable scale effects, however they achieve the highest scale efficiency measures. The enterprises of the total available power of over 1500 MW are the most efficient group as their technical efficiency at scale effects assumed constant, as well as its main component, i.e. technical efficiency at scale effects assumed changeable, have achieved the highest values in the whole investigation period. As results from the analysis of Malmquist indices, the improvement of productivity has resulted from activity rationalization by means of increasing the relative efficiency of electric power and heat & electric power stations of the total available power below 500 MW, as well as due to significant technological progress obtained by the entities of the power output greater than 500 MW. To compare efficiency and time-dependent productivity changes in function of ownership forms the enterprises were divided into relevant groups. To this end Polish private enterprises, state enterprises and foreign ones were distinguished. On the basis of the results presented in Tab. 4 it can be stated that in the years 2000÷2004 Polish private enetrprises as well as foreign ones achieved on average higher measures of technical and scale efficiency. Generally the state-owned entities obtained lower estimates in particular categories of efficiency. However disproportions between the state and foreign enterprises were decreasing in the investigated period. As results from the analysis of productivity indices (see Tab. 5) the productivity of Polish private enterprises was increasing a little faster, and that of the state-owned and foreign ones – a little slower. The higher technical efficiency measures achieved by

Tab. 6. *Technical efficiency versus type of activity carried out by enterpriseenterprise*

Year	Category of enterprise	M_CRS	M_VRS	E_S_VRS
2000	Heat & electric power stations and their complexes	86,36%	93,81%	91,79%
	Electric power stations and their complexes	95,16%	95,71%	99,39%
	Complexes of electric power stations and heat & electric power stations	90,13%	91,47%	98,49%
2001	Heat & electric power stations and their complexes	86,94%	92,76%	93,65%
	Electric power stations and their complexes	93,02%	95,25%	97,68%
	Complexes of electric power stations and heat & electric power stations	85,32%	88,74%	96,35%
2002	Heat & electric power stations and their complexes	87,10%	91,98%	94,71%
	Electric power stations and their complexes	93,06%	95,02%	97,96%
	Complexes of electric power stations and heat & electric power stations	84,76%	90,19%	94,14%
2003	Heat & electric power stations and their complexes	89,53%	91,57%	97,81%
	Electric power stations and their complexes	90,50%	91,68%	98,68%
	Complexes of electric power stations and heat & electric power stations	80,16%	87,82%	91,79%
2004	Heat & electric power stations and their complexes	90,69%	92,26%	98,34%
	Electric power stations and their complexes	91,49%	92,67%	98,70%
	Complexes of electric power stations and heat & electric power stations	81,08%	88,79%	91,71%

Tab. 7. *Productivity versus type of activity carried out by enterprise*

Year	Group of enterprises	Malmquist index M_0G	Relative efficiency (zm. T^E)	Technological Progress (zm. T^G)
2001/2000	Heat & electric power stations and their complexes	105,01%	101,47%	103,64%
	Electric power stations and their complexes	103,48%	97,63%	106,09%
	Complexes of electric power stations and heat & electric power stations	104,85%	94,93%	110,54%
2002/2001	Heat & electric power stations and their complexes	99,72%	100,12%	99,73%
	Electric power stations and their complexes	102,59%	99,95%	102,69%
	Complexes of electric power stations and heat & electric power stations	102,46%	99,25%	103,36%
2003/2002	Heat & electric power stations and their complexes	100,80%	103,35%	98,31%
	Electric power stations and their complexes	100,57%	97,08%	103,66%
	Complexes of electric power stations and heat & electric power stations	99,34%	94,31%	105,51%
2004/2003	Heat & electric power stations and their complexes	102,89%	101,65%	101,38%
	Electric power stations and their complexes	101,93%	101,09%	100,81%
	Complexes of electric power stations and heat & electric power stations	102,91%	101,01%	101,86%

Polish private and foreign entities could result from the fact that privatization was mainly focused on the enterprises of good or average financial situation hence they had better production potential right from the beginning. The below presented conclusions were drawn as a result of the performed comparison of the efficiency and changes in productvity of the electric power stations and their complexes and those of the heat & electric power stations and their complexes, i.e. impact analysis of type of carried-out activity on effects (see Tab. 6 and Tab. 7): In the investigation period of 2000÷2004 the mean measures of technical efficiency as well as scale efficiency for the group „electric power stations and their complexes" were higher than those for the group „ heat & electric power stations and their complexes". However the superiority was decreasing along with time in the period in question. The superiority of the electric power stations could result from an advantage they take from large-scale production. The decreasing disproportions could result from growing importance of co-generation.

Summary

The occurring economy transformations, energy marketisation as well as ownership transformations of power industry enterprises have resulted in that power producers more and more attention have focused on the category of efficiency and its measurement. The improving of efficiency of the entities is very important for their functioning in conditions of power market consolidation and liberalization. Technical efficiency, an important element of economic efficiency, is decisive to the future of domestic professional thermal electric power stations. The performed verification of impact of various factors on the effects obtained by power producers provides us with interesting conclusions as to influence of privatization, scale of activity, type of carried-out activity on chvanges occurring in the sector. This work verifies to some extent common opinions dealing with influence of selling-up power generation enterprises to domestic private and foreign entities.

Bibliography

1. Barburski J. : Performance efficiency of financial institutions in the light of micro-economic theory of enterprises (in Polish). Bank i Kredyt, Feb. 2005.
2. Charnes A. W., Cooper W. W., Rhodes E.: Measuring the efficiency of decision making units. European Journal of Operational Research, 2, 1978; (acc. to: Sun S., Lu W.-M.: A cross-efficiency profiling for increasing discrimination in Data Envelopment Analysis, INFOR Journal, vol. 43, no. 1, Feb. 2005)
3. Coelli T.: Total factor productivity growth in Australian coal-fired electricity generation: A Malmquist index approach; presented to the international conference on public sector efficiency, UNSW, Sydney, 27÷28 November 1997; (acc.to: P.-L. Lam, A. Shiu: A data envelopment analysis of the efficiency of China's thermal power generation. Utilities Policy, no. 10 , 2001)
4. Farrell M. J.: The measurement of productive efficiency. Journal of the Royal Statistical Society, series A, vol. 120, 1957 (acc. to: Forsund F. R., Hjalmarsson L.: Generalised Farrell Measures of Efficiency: an application to milk processing in Swedish dairy plants. The Economic Journal, no. 89, June 1979)
5. Färe R., Grifell-Tatjé E., Grosskopf S., Lovell C. A. K.: Biased technical and the Malmquist productivity index, p. 8, (taken on 22.11.2005 from the page: http://econwpa.wustl.edu:8089/eps/mic/papers/9508/950802.pdf)
6. Greene W.: LIMDEP (Version 7): User's Manual and Reference Guide. Econometric Software Inc., New York, 1995 (acc. to: Herrero I., Pascoe S.: Estimation of technical efficiency: a review of some of the stochastic frontier and DEA software. Computer in Higher Education Economics Review, vol. 15, 2002)
7. Herrero I., Pascoe S.: Estimation of technical efficiency: a review of some of the stochastic frontier and DEA software, Computer in Higher Education Economics Review, vol. 15, 2002
8. Koopmans T. C.: An Analysis of Production as an Efficient Combination of Activities, in: Koopmans T. C. (Ed.): Activity Analysis of Production and Allocation, Cowles Commission for Research in Economics, Monograph no. 13, John Wiley and Sons, Inc., 1951; (acc. to: Piyu Yue: Data Envelopment Analysis and Commercial Bank Performance: A Primer With Applications to Missouri Banks, The Federal Reserve Bank of St. Louis Review,, vol. 74, no. 1, Jan/Feb 1992)
9. Kopczewski T.: Technological and cost efficiency of commercial banks in Poland in the years 1997÷2000. Part I (in Polish). Materiały i Studia, Narodowy Bank Polski (Materials and Studies of National Bank of Poland), Bulletin no. 113, Warszawa, 2000
10. Lam P.-L., Shiu A.: A data envelopment analysis of the efficiency of China's thermal power generation. Utilities Policy, no. 10, 2001
11. Sowlati T.: Efficiency studies in forestry using data envelopment analysis. Forest Products Journal, no. 55 (1), 2005.
12. Steering Committee for the Review of Commonwealth/State Service Provision: Data Envelopment Analysis: A technique for measuring the efficiency of government service delivery, AGPS, Canberra, 1997

POLISH MARITIME RESEARCH, Special issue 2009/S1; pp. 45-51
10.2478/v10012-008-0043-3

Optimization of steam cycles with respect to supercritical parameters

Marian Piwowarski.

Abstract

This paper contains an analysis of supercritical power stations have been presently built worldwide. The analysis concerns cycles with single and double interstage superheating and, additionally, with regenerative feed water preheating system equipped with six, seven, eight, nine and ten regenerative heat exchangers, respectively. Relevant calculations were performed for various values of fresh steam temperature and pressure, various pressure values of secondary superheating, as well as with value of condenser internal pressure maintained constant. The calculations show that to increase efficiency of steam cycle with double interstage superheating and extended regeneration even to a value greater than 51%, is possible. In the age of greater and greater demand for electric power and stronger and stronger limitations imposed on emission of noxious compounds to the atmosphere, the developing of power production technologies based on supercritical parameters seems inevitable.

Keywords*: analysis of supercritical power stations, optimization of steam cycles, supercritical parameters, concerns cycles.*

Description of supercritical power stations

Investigations on the increasing of efficiency of steam turbine cycle have been carried out by many research centres of universities and turbine production concerns already for a few dozen of years. In the case of thermodynamic cycles with applied steam turbines the investigations have dealt with steam pressure and temperature values greater than: the 22.12MPa critical pressure and 647.28K critical temperature, respectively. Over the critical point the difference between liquid phase and gas phase disapears [20], [25], [43]. Already in the 1950s the first attempts to developing the turbine power units based on supercritical parameters have been made. In 1957 the first in the world turbine power unit of supercritical parameters was put in motion in the electric power station, Philo, USA. The unit of 314bar/621ºC steam parameters developed 125MW output power. Two years later 325MW power unit of even higher steam parameters (345bar/649ºC/566ºC/566ºC) was built in the Eddystone I electric power station. For the high values of steam parameters special materials suitable to work in high temperatures were required. High investment cost, inadequate quality of materials, faults in assembling and operational problems forced the producers to resign from building the units for so high steam parameters. As late as in 1969 the unit designed for the supercritical parameters with double secondary superheating of 241bar/538ºC/552ºC/566ºC, was set working. The application of such solution to the steam cycle has improved operation of the unit. Therefore in the 1970s, apart from the units with single superheating of 241bar/538/538ºC steam parameters, were built the units with double superheating, which developed output power reaching from 350 do 1100 MW. Progress in material technology, started in the 1980s, has made it possible to apply higher steam parameters (310bar/593ºC/593ºC/593ºC) to steam cycle. The application of better and better materials suitable for very high operational temperatures makes it possible to build the units for the supercritical parameters as well as ultrasupercritical ones (400bar/760ºC). Modern 3-D calculation programs used in designing fluid flow systems as well as highly efficient devices included into equipment of such units have guaranteed to achieve their high reliability and efficiency. In the 1960÷1990s in USA 159 units of the power range of 300÷1400MW, pressure range of 230÷260bar and temperature of 540÷590ºC, including 14 units of double secondary superheating, were set working. In the years 1990÷1998 in Japan and China total output power installed in coal electric power stations has increased threefold. The growth was achieved mainly by applying the units of output power in the range of 400÷700MW, working with the supercritical steam parameters of 255bar/570÷590ºC and the secondary superheating of 570÷595ºC temperature range. In the years 2000÷2003 three 700MW units based on the 246bar/593ºC/593ºC steam parameters, two 900MW units based on the 241bar/593ºC/593ºC steam parameters, two 900MW units based on the 241bar/600ºC/610ºC steam parameters, three 1000MW units based on the 245bar/600ºC/600ºC steam parameters and two 1050MW units based on the 250bar/600ºC/610ºC steam parameters, were put in operation. In Europe significant achievements in building the power units with supercritical parameters can be noted in Denmark and Germany. In 1984 in Denmark the first unit with supercritical parameters was set working in the Studstrupvaerket electric power station. At the beginning of the 21st century two 411MW units with the 290bar/582ºC/580ºC/580ºC steam parameters, including one coal-fired and the other gas-fired, as well as 530MW unit with the 300bar/580ºC/600ºC steam parameters, working on combusted biomass, were put in operation in Avedore electric power station. Germans, basing on the achievements and operational experience of Danes in the area of building coal electric power plants with high steam parameters, have built mainly 800÷900MW power units fitted with brown coal-fired boilers. In 2002, 1012MW power unit based on the 274bar/580ºC/600ºC steam parameters was built in the Niederaussem electric power station. A list of selected power units (presently installed or planned ones) intended for the operating with supercritical parameters is presented in Tab. 1. Pątnów II electric power station is the first Polish electric power plant based on supercritical

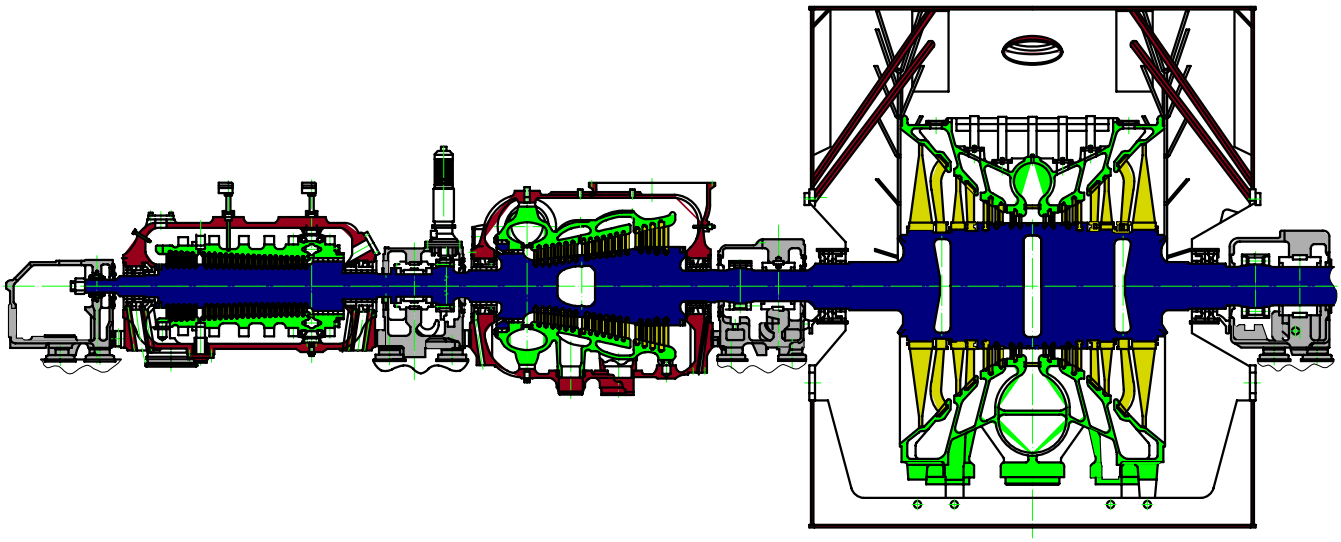

Fig. 2 *Cross-section of 28K460 turbine installed in Łagisza electric power station*

parameters. Its high energy conversion efficiency is associated with lower fuel consumption and limited emission of contaminations to the environment. And, the power unit built in Łagisza is fitted with the biggest in the world monotube boiler of circulation fluid-bed, operating with supercritical parameters. The modern ecological power unit would reach very high efficiency equal to about 45%. Its turbine-set parameters are as follows: electric output power of 460MW, fresh steam pressure of 275bar, fresh steam temperature of 560ºC, secondary steam temperature of 580ºC, secondary steam pressure of 54.6bar. The steam cycle schematic diagram as well as the turbine-set cross-section are presented in Fig. 1 and 2, respectively.

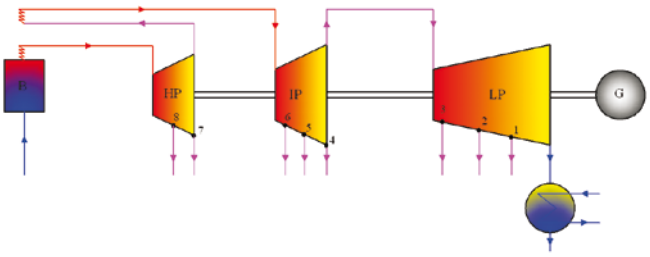

Fig. 1 *Simplified steam cycle diagram of Łagisza electric power plant*

And, in the electric power station of Bełchatów S.A., the largest conventional one in Poland and Europe, working on brown coal and being the biggest electric power producer in Poland, the building of a 833MW power unit based on supercritical parameters has been started. The unit with the 266bar/554/582ºC steam parameters is intended for the fundamental mode of operation of 7500 h/year usage time of its rated power and the total working time of 8100 h yearly. By applying supercritical steam parameters it is already possible to obtain thermal efficiency of over 45% as compared with that of 41÷42% achievable today by conventional thermal electric power plants. Contemporary pulverized-fuel supercritical boilers deliver the steam of 25MPa pressure and 600°C temperature and abt. 610°C superheating temperature, to steam turbine cycle. It is expected that further development of the technology would be focused on the mastering of ultrasupercritical parameters as well as the increasing of efficiency of power units. This mainly depends on progress to be done in the area of material engineering [1], [2], [3], [5], [7], [9], [13], [15], [16], [17], [22], [28], [29], [30], [31], [32], [34], [39], [40], [48], [49], [50]. Investigations are also carried out in the frame of large international projects such as e.g. THERMIE 700 Advanced Power Plant project financially supported by EU, whose simplified scheme is given in Fig. 3, aimed at the obtaining of fresh steam temperature of the order of 700°C and 37.5 MPa pressure. The setting in motion of the power unit is scheduled on 2015 [16].

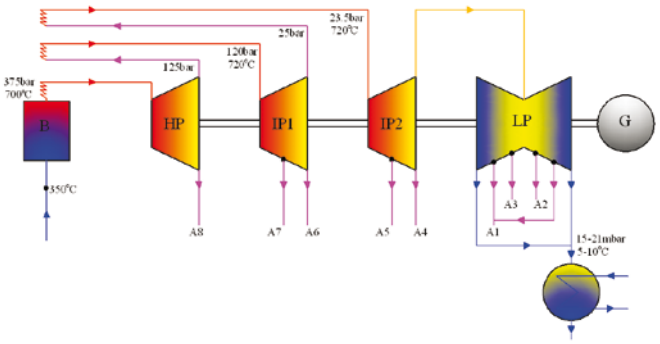

Fig. 3 *Simplified schematic diagram of THERMIE 700 steam cycle*

In the subject-matter literature can be found power plants fitted with turbines operating with supercritical parameters, in which fresh steam (of 26MPa and 570ºC) is produced by cooling nuclear reactors. Efficiency of such systems exceeds 45%, as compared with that of the order of 33% in the case of the power plants co-working with light–water–cooled reactors [4], [38].

High steam temperatures in steam turbine cycles require the first and second stage of turbine placed behind the secondary superheating, to be cooled. The simplified

Tab. 1. *List of selected power units with supercritical parameters, installed in electric power stations worldwide [1], [2], [7], [9], [13], [21], [25], [29], [36], [37], [44], [45] * -planned units or those under construction*

No.	Electric power station	Country	Power [MW]	Steam parameters [bar/ºC/ºC]	Efficiency [%]	Year of building
1	Schwarze Pumpe	Germany	2x800	250/544/562	41	1992
2	Staudinger Unit	Germany	500	250/540/560	43	1993
3	Rostock	Germany	550	285/545/582	-	1994
4	Schwarze Pumpe A/B	Germany	800, 900	250/580/600	33.8	1997
5	Hässler	Germany	720	272/578/600	47.6	1997
6	Schkopau	Germany	2x480	285/545/582	-	1997
7	Lübeck	Germany	400	275/580/600	43.6	1998
8	Lippendofr	Germany	2x800	268/554/554	42.4	2000
9	Boxberg	Germany	1000	266/545/581	43	2000
10	Bexbach II	Germany	750	259/575/595	44.2	2002
11	Niederaussem	Germany	1000	275/580/600	45.2	2002
12	Hemweg-8	Holland	700	250/535/563	44	1994
13	Studstrupvaerket	Denmark	400	270/540/540	42	1985
14	Fynsvaeket-7	Denmark	420	250/540/540	43.5	1991
15	Esbjerg 3	Denmark	415	250/560/560	45.3	1992
16	Skaerbaek-3	Denmark	410	290/582/580/580	49	1997
17	Nordjyllaend-3	Denmark	410	290/582/580/580	47	1998
18	Avedore-2	Denmark	450	300/580/600	45	2001
19	USC 2005	Denmark	-	330/610/630/630	51	2005
20	Meri Pori	Finland	550	244/540/560	45	-
21	Kawagoe-1&2	Japan	700	319/571/569/569	-	1989-90
22	Hekinan-3	Japan	700	255/543/593	-	1993
23	Nanao-ohta	Japan	500	246/566/593	-	1994
24	Noshiro-3	Japan	600	246/566/593	-	1994
25	Haranomaschi	Japan	1000	246/566/593	-	1997
26	Matsuura-2	Japan	1000	255/598/593	41	1997
27	Haramashi	Japan	1050	259/604/602	-	1998
28	Nanaoota-2	Japan	700	255/597/595	-	1998
29	Tachibana-Wan	Japan	1050	285/605/613	-	2001
30	Tachibana-Wan-2	Japan	3x700	250/600/610	42/44	2000
31	Tsuruga-2	Japan	700	255/597/595	-	2000
32	Misumi-1	Japan	600	250/605/600	46	2001
33	Isogo-1	Japan	1x600	251/600/610	46	2002
34	Tomoto Atsuma-4	Japan	700	250/600/600	-	2002
35	Hitachinaka	Japan	1000	245/600/600	43.1	2003
36	Waigaoqiao-1&2	China	2x900	250/538/566	42.7	2004
37	Yuhuan	China	4x1000	262.5/600/600	-	2008
38	Changshu	China	600	259/569/569	42	-
39	Wangqu	China	600	247/571/569	43	-
40	Waigaoqiao-1&2	China	1x1000	270/600/600	-	2009
41	Yonghungdo	Korea Płd.	2x800	246/566/566	43,5	2004
42	Torrevaldaliga	Italy	6x600	250/600/600	45	2006
43	Millmerran	Australia	2x430	249/568/595	37.4	2001
44	Callide	Australia	420	251/566/565	39.4	2001
45	Tarong Nth	Australia	443	250/566/565	39.2	2002
46	Kogan Creek	Australia	750	250/540/560	37.1	2007
47	Tanners Creek	USA	580	241/538/552	39.8/42	-
48	Duke Power	USA	1120	241/538/538	-	-
49	Pątnów II	Poland	464	266/544/566	44.3	2007
50	Genesee at Sunset	Canada	495	241/566/566	-	2005
51	Lagisza *	Poland	460	275/560/580	45	-
52	Belchatów *	Poland	833	266/554/582	-	2010
53	Neurath *	Germany	2x1100	270/600/610	-	2010
54	Boxberg R *	Germany	670	286/600/610	-	2010
55	Dateln *	Germany	1100	286/600/610	-	2011
57	Moorburg *	Germany	2x820	276/600/610	-	2010
58	Walsum *	Germany	790	274/603/621	-	2010
59	Karsruhe *	Germany	820	250/600/620	-	2011
60	Hamm *	Germany	800	286/600/620	-	2012
61	AD700EU Project *	Germany	-	375/700/720/720	50-55	2020

schematic diagram of the external cooling is shown in Fig. 4. The cooling steam taken before the first superheating is directed to the high-pressure (HP) part, to be mixed with the superheated steam. The cooling steam for the first stages of the intermediate-pressure (IP) turbine is taken from the third or fourth stage of HP turbine.

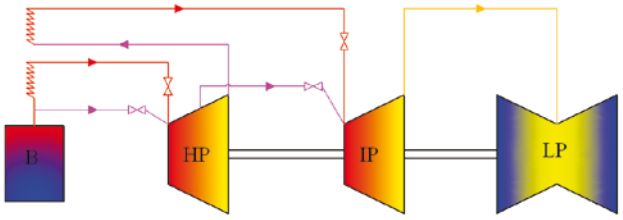

Fig. 4 *Schematic diagram of external cooling*

Application of the high parameters is associated with necessity of using special materials. Elements of HP and IP turbines, which are in direct contact with superheated steam, are made of a high–alloy steel (of high percentage content of such elements as Cr, Mo and V). The first stages of HP and IP turbine are made of Ni-alloy steel which is resistant to thermal loads resulting from the difference between temperature of superheated steam and that of steam after expansion. The low-pressure (LP) turbine module is made of NiCrMoV-high-alloy steel. The material is brittle-crack resistant due to lowered content of such elements as P, Sn, Mn and Si and increased Ni content. For the LP part it is very important to appropriately design the last stages exposed to high loads and erosion.

In present for steam temperatures up to 600ºC ferritic steels, e.g. SAVE12 steel, are used; for temperatures over 650ºC – austenitic steels, e.g. SUPER304H steel and HR6W steel; and for temperatures in the range of 620÷720ºC – various alloys, e.g. Inconel 617, Haynes 230, Inconel 740 etc. Tab. 2 shows chemical element composition of selected kinds of materials used for the units of supercritical parameters.

To produce the steam of suprecritical parameters, monotube boilers with elements made of special steels (e.g. high-temperature creep resisting, austenitic or ferritic-martensitic ones), are used. For its flow system a turbine-driven water-feed pump of high elevation head is necessary to overcome high flow drag resulting from higher density of medium and smaller internal diameters of pipes in the boiler. Another kinds of steam generators with supercritical parameters are atmospheric fluid-bed boilers as well as those of circulation fluid-bed. Boilers of pressurized fluid-beds make it possible to reach higher power concentration and higher efficiency values. Circulation fluid-bed technology in association with supercritical steam parameters constitutes a safe solution, more technologically and economically effective than the option of pulverized-fuel boiler. Advantages of the technology are: fuel flexibility, possible co-combustion of coal, sludge and biomass, compliance with WE80/2001/EU directive in the area of pollution emission, limitation of hazard to occurrence of high-temperature corrosion and erosion, increasing power unit's cycle effciency due to heat recovery and lowering exhaust gas temperature, uniform distribution of heat flow in combustion chamber as well as improved dynamics of load changes [2], [3], [7], [8], [10], [11], [12], [14], [22], [23], [24], [27], [33], [41], [42], [46], [47].

Results of calculations of steam cycles

The increasing of fresh steam pressure and temperature at steam pressure in condenser kept constant, is the first step to the achieving of a higher cycle efficiency [6], [18], [19], [26], [32]. Successive figures present respectively: Fig. 5 – relation of ideal efficiency, Fig. 6 – real efficiency, and Fig. 7 – cycle efficiency -with wetness loss taken into account -of Clausius-Rankine cycle, all in function of fresh steam pressure (5÷55MPa) and temperature (500÷760ºC) at condenser internal pressure kept constant (4kPa); and, in each of the figures the dryness degree limit line (xgr=0.85) is depicted. The figures illustrate the possibly obtainable increase of efficiency in function of values of fresh steam parameters at inlet to turbine, at condenser internal pressure kept constant. In the diagrams can be distinctly observed the limitation of upper value of steam initial pressure, resulting from the limit wetness. The C-R cycle ideal efficiency obtainable due to application of high fresh steam parameters exceeds 52% (see Fig. 5), whereas the real efficiency of the cycle does not exceed 43% (see Fig. 6). It should be also noted that the real efficiency of the cycle in which steam wetness degree has been taken into account does not exceed 39%, and that C-R cycle optimum pressure values amount to about 100 bar (see Fig. 7). The applied here notion of the taking into account of wetness degree means that work is done only by steam and that water does not provide any work [26].

Application of the interstage superheating is the next way to increase efficiency of the cycle with steam turbine. Its efficiency depends, apart from fresh steam parameters and condenser internal pressure, on superheating pressure

Tab. 2*. List of chemical element composition of materials used for the power units of supercritical parameters [14]*

Name/ Composition	C	Si	Mn	Ni	Cr	W	Co	V	Nb	N	Ta	Nd	Cu	Ti	B	Al	Mo	Fe	La
SAVE12	0.01	0.3	0.20	-	11.0	3.0	3.0	0.20	0.07	0.04	0.07	0.04	-	-	-	-	-	-	-
SUPER304H	0.1	0.2	0.8	9.0	18.0	-	-	-	0.4	0.1	-	-	3.0	-	-	-	-	-	-
HR6W	0.08	0.4	1.2	43.0	23.0	6.0	-	-	0.08	-	-	-	-	0.08	0.003	-	-	-	-
Haynes 230	0.07	-	-	-	22.0	14.0	12.5	-	-	-	-	-	-	-	-	1.0	9.0	-	-
Inconel 617	0.1	-	-	55.0	22.0	-	5.0	-	-	-	-	-	-	-	0.015	0.35	2.0	3.0	0.02
Inconel 740	0.03	0.5	0.03	48.3	25.0	-	20.0	-	2.0	-	-	-	-	1.8		0.9	0.5	0.7	

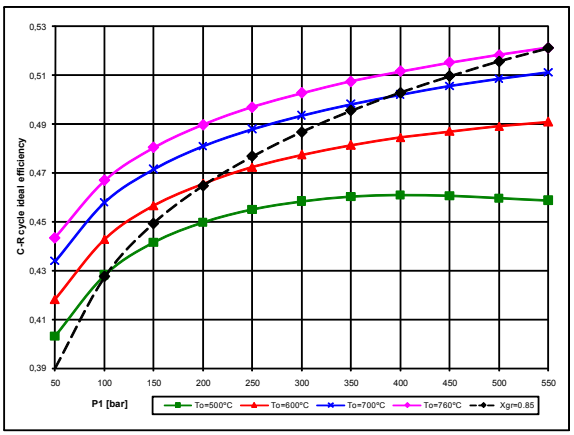

Fig. 5 Relation of ideal efficiency of Clausius-Rankine cycle in function of fresh steam pressure and temperature at condenser internal pressure kept constant (4kPa), and the wetness degree limit curve xgr=0.85

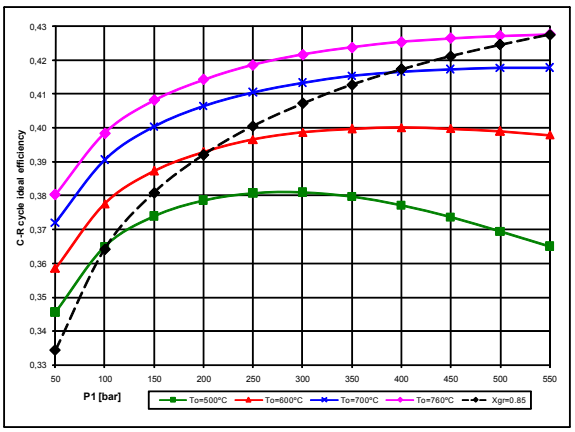

Fig. 6 Relation of real efficiency of Clausius-Rankine cycle in function of fresh steam pressure and temperature at condenser internal pressure kept constant (4kPa), and the wetness degree limit curve xgr=0.85

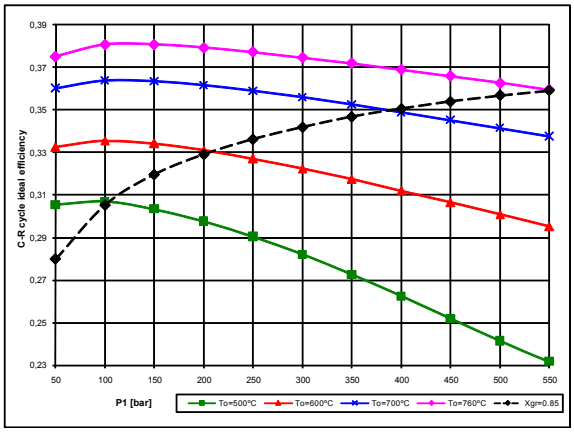

Fig. 7 Relation of Clausius-Rankine cycle efficiency (with steam wetness degree taken into account according to Bauman formula) in function of fresh steam pressure and temperature at condenser internal pressure kept constant (4kPa), and the wetness degree limit curve xgr=0.85

value too. There is one optimum pressure value for which the cycle efficiency reaches its maximum. In steam power units various configurations of the system with single interstage superheating applied in the boiler are possible. The solution in which HP part and IP part are placed in a common casing, is often applied. The integrated HP/IP module is connected with LP part which can be of single or double jet. Such system is characteristic of compact structure and lower investment and operational costs. The units which operate with supercritical parameters and have that kind of structure can reach output power of over 600 MW. The system in which HP and IP turbine parts are placed is seperate casings is only sporadically applied. In the units of a greater power the solution in which single-jet HP part and double-jet IP part are placed in separate casings and connected with double-jet LP part, is applied. The LP module is consisted of one, two or three casings, depending on the output power the unit has to develop. In practice, finds also application the system in which the first casing contains HP part and single-jet IP part of countercurrent flow, and in the other casing double-jet IP part connected with LP module consisted of two casings, is placed. Its alternative is to place HP and IP parts in separate casings [2], [6], [9], [15], [18], [19], [26], [32], [33], [35], [36].

The profits resulting from the application of double superheating became obvious as early as in 1960s. In optimizing the cycle with double secondary superheating attention should be paid to appropriate choice of the pressure for the first and second superheating.

In practice the 1st superheating pressure is selected depending on thermodynamic optimum, the 2nd superheating pressure is usually chosen depending on an assumed steam temperature at inlet to LP turbine. Maximum temperature of inlet steam to LP part is limited with respect to thermal strength of materials. Classical turbine-set consists of three separate modules designed for definite steam parameters, i.e.: HP, IP, and LP parts. Electric generator is directly connected with the last part, i.e. LP. The arrangement of steam turbine for supercritical parameters depends first of all on choice of a kind of secondary superheating, unit's operation range as well as special requirements as to regenerative preheating. To the arrangement with double superheating the solution in which HP part is placed in a separate casing and connected with casing of double-jet IP part after 2nd superheating, is often applied. LP part is consisted of one or two casings. In order to obtain higher power values the solution in which HP parts and IP1 part after 1st superheating are placed in common casing, is used. The second casing is intended for IP2 double-jet part after 2nd superheating, connected with LP module consisted of one, two or three double-jet parts [2], [6], [9], [15], [18], [19], [26], [32], [33], [35], [36].

Increase of cycle efficiency to a large extent depends on an appropriate choice of number and kind of preheaters. Regenerative preheating is a very important element of the power unit and it influences the unit's main elements, i.e. boiler, turbine, condenser and feed pump. The increased jet of steam produced in boiler, resulting from regeneration, is associated with the necessity of fitting the unit with feed pumps of greater capacity. High feed water temperature makes it difficult to maintain low exhaust gas temperature on which to a large extent depends boiler efficiency. It should be also remembered that along with increasing number of exchangers degree of complexity of the entire system also increases, that consequently leads to increasing investment cost. The first step in optimizing the system is to select an appropriate number of regenartion stages. To high power units 6÷10 stages of superheating are usually applied. When considering profits due to

application of regenerative superheating attention should be first of all paid to possible achieving higher efficiency of turbine stages. Drop of steam jet in LP part makes blade system forming easier and, on the other hand, absorption of steam from interstage space of the turbine makes its design more complex and results in generating flow losses within the turbine [6], [18], [19], [26].

In this work the analysis is performed of the cycles with single and double interstage superheating and, additionally, with the regenerative feed water preheating system fitted with six, seven, eight, nine and ten regenerative heat exchangers. Respective calculations were performed for various values of fresh steam temperature (500ºC, 600ºC, 700ºC) and pressure (5÷65MPa), various pressure values of secondary superheating: $p_2=(0.24\div0.36)*p_0$, and $p_2=(0.06\div0.12)*p_0$, as well as with internal pressure value in condenser maintained constant (4kPa). The performed calculations indicate that the increase of efficiency of the steam cycle with double interstage superheating and extended regeneration, up to 51%, is possible.

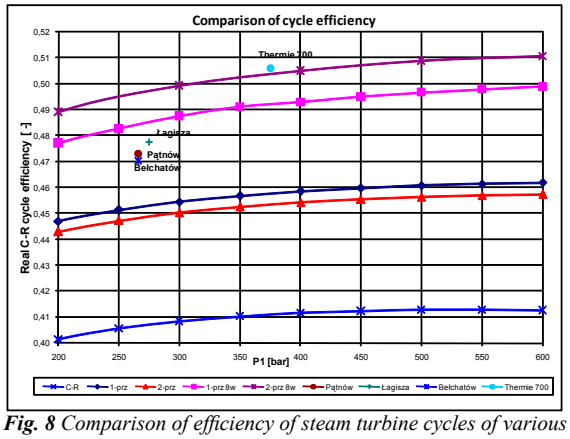

Fig. 8 *Comparison of efficiency of steam turbine cycles of various configurations, including values for Polish electric power stations operating with supercritical parameters*

Fig. 8 presents comparison of efficiency of the following cycles:

- Clausius-Rankine cycle (marked C-R);
- The steam cycle with single interstage superheating without regeneration (marked 1-prz);
- The steam cycle with single interstage superheating and 8 regenerative heat exchangers (marked 1-prz 8w);
- The steam cycle with double interstage superheating without regeneration (marked 2-prz);
- The steam cycle with double interstage superheating without regeneration and 8 regenerative heat exchangers (marked 2-prz 8w);
- The steam cycle with supercritical parameters operating in Pątnów electric power station (marked Pątnów);
- The steam cycle with supercritical parameters operating in Łagisza electric power station (marked Łagisza);
- The steam cycle with supercritical parameters operating in Bełchatów electric power station (marked Bełchatów);
- The demonstrative cycle for supercritical parameters (marked Thermie 700).

Fig. 8 was prepared for optimum values of interstage superheating pressure, fresh steam temperature (of 700ºC) and constant value of condenser internal pressure (of 4kPa) in function of fresh steam pressure (in the range of 20÷60MPa). From the diagram it can be concluded that the application of double interstage superheating increases the cycle efficiency by about 1.5 % as compared with that of the cycle with single single superheating and by about 9 % as compared with the simple C-R cycle.

Summary

In Poland coal plays the most important role in the process of electric power production. With a view of it resources, gained experience and reliability of the coal-based technology of electric power production that fuel will be dominating for electric power generation in the years to come. Ecological and energy policy, both in Poland and EU, compels to apply low-emission technologies, e.g. clean coal-based technology. In Poland, because of its coal resources and its role for the state's energy balance, investments in clean coal technologies should be a natural phase of power industry development in this country. Other probable development directions of Polish power industry are a.o. the following: coal gasification integrated with high-temperature fuel cells, power systems with fuel cells combined with coal hydro-gasification, cola gasification and liquefaction, coal-nuclear synergy systems, pressurized coal combustion in fluid-bed boilers, combined production systems of electric power and hydrogen, or polygeneration. In the age of greater and greater electric power demand and stronger and stronger limitations imposed on emission of noxious compounds to the atmosphere, development of power production technologies based on supercritical and ultrasupercritical parameters, seems inevitable. The turbine power units fed with steam of supercritical parameters, which have been built so far, are characteristic of a higher efficiency and lower carbon dioxide emission, resulting from it.

Bibliography

1. Avrutskii G. D., Savenkova I. A., Lazarev M. V., Akulenko V. V., Shvarts A. L., Ivanov S. A.: Development of Engineering Solutions for Creation of Turbine Plant for Power Unit With Supercritical Steam Parameters. Power Technology and Engineering Vol. 39, No. 6, 2005;
2. Baumgartner R.: Advanced Coal Technology to Power the World. World Bank Energy Week, Siemens Power Generation, Germany, 2006;
3. Beer J. M.: High efficiency electric power generation: The environmental role. Progress in Energy and Combustion Science 33, 2007;
4. Boehm C., Starflinger J., Schulenberg T., Oeynhausen H.: Supercritical Steam Cycle for Lead Cooled Nuclear Systems. Paper No. 035, Proceedings of GLOBAL 2005, Tsukuba, Japan, Oct 9-13, 2005;
5. Bugge J., Kjaer S.: High-Efficiency Coal-Fired Power Plants Development and Perspectives. Elsam Engineering A/S, 2004;
6. Chmielniak T.: Power technologies (in Polish). Publishing House of Silesian University of Technology (Wydawnictwo Pol. Śląskiej), Gliwice, 2004;
7. Chmielniak T.: Development state and prospects of power units for electric power stations based on pulver technique (in Polish). Silesian Cluster for Clean Coal Technologies (Śląski Klaster Czystych

Technologii Węglowych), Gliwice, 2007;
8. Coleman K., Viswanathan R., Shingledecker J., Sarver J., Stanko G., Mohn W., Borden M., Goodstine S.: Boiler Materials for Ultrasupercritical Coal Power Plants. USC Materials, Quarterly Report October, December 2003 -January 23, 2004;
9. DTI Brochure: Advanced Power Plant Using High Efficiency Boiler/ Turbine. Best Practice Brochure No. BPB010, Carbon Abatement, Technologies Programme, 2006;
10. Goidich S. J., Wu S., Fan Z., Bose A. C.: Design Aspects of the Ultra-Supercritical CFB Boiler. International Pittsburgh Coal Conference, Pittsburgh, PA, Sept. 12-15, 2005;
11. Goidich S. J., Fan Z., Sippu O., Bose A. C.: Integration of Ultra-Supercritical OTU and CFB Boiler Technologies. International Pittsburgh Coal Conference, Pittsburgh, PA, Sept. 12-15, 2005;
12. Golec T. et al.: Scenarios of technological development of power production based on hard and brown coal versus energy supply safety of the state (in Polish). Instytut Energetyki, Zakład Procesów Cieplnych (CPC), Katowice, 2006;
13. Golec T., Rakowski J., Świrski J.: Prospects of technical progress in electric power production based on hard coal, brown coal as well natural gas with taking into account effects to the environment (in Polish). Elektroenergetyka, Nr 1/2004 (48), 2004;
14. Holcomb G. R., Alman D. E., Bullard S. B., Covino Jr. B. S., Cramer S. D., Ziomek-Moroz M.: Ultra-Supercritical Steam Corrosion. U. S. Department of Energy, Albany Research Center, 1450 Queen Avenue SW, Albany, OR 97321, 2003;
15. Hurd P., Truckenmueller F., Thamm N., Pollak H., Neef M., Deckers M.: Modern Reaction HP/IP Turbine Technology Advances & Experiences. Proceedings of PWR2005-50085, ASME POWER, Chicago, Illinois, April 5-7, 2005;
16. Kjaer S., Bugge J., Stolzenberger C.: Europeans still aiming for 700ºC steam. MPS Review Supercritical PF Technology, Modern Power Systems - November 2004;
17. Kolev N., Schaber K., Kolev D.: A new type of a gas-steam turbine cycle with increased efficiency. Applied Thermal Engineering 21, 2001;
18. Kosowski K.: Ship Turbine Power Plants Fundamentals of Thermodynamical Cycles. Publishing House of Gdańsk University of Technology (Wydawnictwo Politechniki Gdańskiej), Gdańsk; 2005;
19. Kosowski K. et al.: Steam and gas turbines with examples of Alstom technology. Alstom, France, Switzerland, United Kingdom, Poland, 2nd Edition – three parts in one volume, ISBN 978-83-925959-3-9, 2007;
20. Kretzschmar H.-J., Cooper J. R., Dittmann A., Friend D. G., Gallagher J. S., Harvey A. H., Knobloch K., Mareš R., Miyagawa K., Okita N., Stöcker I., Wagner W., Weber I.: Supplementary Backward Equations T,p,h…, v,,p,h…, and T,,p,s…, v,,p,s… for the Critical and Supercritical Regions. Region 3… of the Industrial Formulation IAPWS-IF97 for Water and Steam. Journal of Engineering for Gas Turbines and Power, Vol. 129, January 2007;
21. Leizerovich A. S.: Steam Turbines for Modern Fossil-fuel Power Plants. ISBN:0881735485, Inc NetLibrary, 2007;
22. Masuyama F.: History of Power Plants and Progress in Heat Resistant Steels. ISIJ International, Vol. 41, No. 6, 2001;
23. Nowak W.: Development state and prospects of power units of electric power stations based on fluid technique (in Polish). Silesian Cluster for Clean Coal Technologies (Śląski Klaster Czystych Technologii Węglowych), Gliwice, 2007;
24. Oakey J. E., Pinder L. W., Vanstone R., Henderson M., Osgerby S.: Review of Status of Advanced Materials for Power Generation. Report No. COAL R224, DTI/Pub URN 02/1509, 2003;
25. Paul I.: Supercritical coal fired power plants. A Technology Successfully Deployed in Developing Countries. Siemens Power Generation, 2002;
26. Perycz S.: Steam and gas turbines (in Polish). Publishing House of Gdańsk University of Technology (Wydawnictwo Politechniki Gdańskiej), Gdańsk; 1988;
27. Pitsinki J.: An example of novel energy technologies for power production – OTSC CFB boiler. International Conference on Early Stage Energy Technologies and Tool Training Seminar for Assessment of their Market Potential, 31th May, 2005;
28. Radcenco V., Vasilescu E. E., Popescu G., Apostol V.: New approach to thermal power plants operation regimes: maximum power versus maximum efficiency. International Journal of Thermal Sciences 46, 2007;
29. Rakowski J., Pinko L., Świrski J.: Ecological aspects of electric power production by domestic thermal electric power stations (in Polish). Int. Conf. on Ecological Aspects of Electric Power Production (Międzynarodowa Konferencja Ekologiczne Aspekty Wytwarzania Energii Elektrycznej), Warsaw, 14-16 November 2001;
30. Rao A. D., Samuelsen G. S., Robson F. L., Geisbrecht R. A.: Coal-Based Power Plant System Configurations for the 21st century. GT2003-38942, Proceedings of ASME Turbo Expo 2003, Atlanta, Georgia, USA, June 16–19, 2003;
31. Rao A. D., Samuelsen G. S., Robson F. L., Geisbrecht R. A.: Coal-Based Power Plant System Configurations for the 21st century. GT2004-53105, Proceedings of ASME Turbo Expo 2004, Vienna, Austria, June 14-17, 2004;
32. Retzlaff K. M., Ruegger W. A.: Steam Turbines for Ultra-Supercritical Power Plants. GER-3945A, GE Power Generation, 1996;
33. Riordan T: New Generation Strategy of Ultra-Supercritical Technology. New Generation Design & Eng., APP Site, 2006;
34. Romanosky R. R., Rawls P. A., Purgert R. M., Viswanathan V. R.: Steam Turbine Materials for Ultra Supercritical Coal Power Plants. Advanced Research, National Energy Technology Laboratory, 08/2007;
35. Rosenkranz J., Wichtmann A.: Balancing economics and environmental friendliness -the challenge for supercritical coal-fired power plants with highest steam parameters in the future. Siemens Power Generation, Germany, 2005;
36. Susta M. R., Peter P.: Supercritical Steam Power Plants -an Attractive Option for Malaysia. Kuala Lumpur 28-29 April 2003, Malaysia Power 2003;
37. Susta M. R., Seong K. B.: Supercritical and Ultra-Supercritical Power Plants – SEA's Vision or Reality?. POWERGEN ASIA 2004;
38. Tulkki V.: Supercritical Water Reactors. A Survey on International State of Research in 2006, Otaniemi, November 6, 2006;
39. Turek M.: Scenarios of technological development of coal-based power industry (in Polish). Instytut Energetyki, Zakład Procesów Cieplnych (CPC), Katowice, 2006;
40. Venäläinen I., Psik R.: 460 MWe Supercritical CFB Boiler Design for Łagisza Power Plant. PowerGen, Barcelona, Spain, 2004;
41. Viswanathan R., Henry J.F., Tanzosh J., Stanko G., Shingledecker J., Vitalis B., Purgert R.: U.S. Program on Materials Technology for Ultra-Supercritical Coal Power Plants. Journal of Materials Engineering and Performance, Volume 14 (3), June 2005;
42. Viswanathan R., Coleman K., Rao U.: Materials for ultra-supercritical coal-fired power plant boilers. International Journal of Pressure Vessels and Piping, 83, 2006;
43. Wagner W.,·Kretzschmar H.-J.: International Steam Tables Properties of Water and Steam Based on the Industrial Formulation IAPWS-IF97 Tables, Algorithms, Diagrams, and CD-ROM Electronic Steam Tables. Springer-Verlag, Berlin, Heidelberg, 2008;
44. Watanabe S., Tani T., Takahashi M., Fujii H.: 495-MW Capacity Genesee Power Generating Station Phase 3: First Supercritical Pressure Coal-fired Power Plant in Canada., Hitachi, Ltd. and Babcock-Hitachi, 2001;
45. Wibberley L., Cottrell A., Palfreyman D., Scaife P., Brown P.: Techno-Economic Assessment of Power Generation Options for Australia. Technology Assessment Report 52, 2006;
46. Wright I.G., Maziasz P.J., Ellis F.V., Gibbons T.B., Woodford D.A.: Materials Issues For Turbines For Operation In Ultra-Supercritical Steam. Research sponsored by the U.S. Department of Energy, Office of Fossil Energy, Advanced Research Materials Program, under Contract DE-AC05-00OR22725 with UT-Battelle, LLC., 2004;
47. Yi Y-S., Watanabe Y., Kondo T., Kimura H., Sato M.: Oxidation Rate of Advanced Heat-Resistant Steels for Ultra-Supercritical Boilers in Pressurized Superheated Steam. Journal of Pressure Vessel Technology, Vol. 123, 2001;
48. Zaporowski B.: Economic effectiveness analysis of electric power production by the system's electric power stations and combined thermal-electric power production by small thermal-electric power plants (in Polish). Proceedings of 3rd Scientific Technical Conference on Electric Power Plants and Thermal-Electric Power Gas and Steam-Gas Fed Plants (Materiały III Konferencji Naukowo-Technicznej: Elektrownie i elektrociepłownie gazowe i gazowo-parowe), Poznań-Kiekrz, 2005;
49. Zaporowski B.: Economic effectiveness analysis of gas-fired thermal-electric power plants after introduction of origin certificates of highly efficent co-generation (in Polish). Rynek Energii nr 6 (73), 2007;
50. Ziębik A.:Future EU Energy MIX -Will Coal Play an Important Role?. Silesian Cluster for Clean Coal Technologies (Śląski Klaster Czystych Technologii Węglowych), Gliwice, 2007.

POLISH MARITIME RESEARCH, Special issue 2009/S1; pp. 52-57
10.2478/v10012-008-0045-1

A method for analysing ram pressure characteristics of impeller pump rotor

R. Puzyrewski,
K. Żochowski,
P. Flaszyński.

Abstract

This paper presents a method in which typical tests of centrifugal pump are used to obtain information on real value of discharge angle of flow leaving the rotor. The method can be applied to properly choose inlet angle to blade palisade of centrifugal guide vanes in the case when to perform measurements of velocity fields behind the rotor more precisely is not possible.

***Keywords**: impeller pumps, characteristics, tests*

Introduction

Characteristics of impeller machines such as efficiency or ram pressure of experimental stages, are determined on the basis of certain definitions and measurements of relevant quantities, performed on a tested machine. This work deals with the following characteristics: ram pressure of radial pump rotor, as well as liquid flow torque generated by pump rotor, determined on an experimental test stand. The characteristics were determined either at constant rotational speed or at constant volumetric flow rate and varying rotational speed. The problem has been formulated as follows: if and in which way the rotor channel characteristics in the form of triangle of velocity vectors at outlet from the rotor can be determined on the basis of experimentally obtained ram pressure and torque characteristics. An important parameter belonging to the rotor characteristics is the outlet angle of flow leaving the rotor, which is usually much different from the rotor blade outlet geometrical angle. For this reason the erroneous mating of rotor to blades of guide vanes channels often occurs. The correct mating is conditioned by information on the outlet angle from rotor and inlet angle to guide vanes channel behind the rotor. This paper presents a method to obtain such information by measuring the rotor characteristics on the tested pump. The problem is in opposition to the method commonly used for determining the pump rotor characteristics on the basis of the characteristics of rotor channels.

Basic relations

Fig. 1 presents schematic diagram of a test stand on which tests of a model pump were performed. The stand has made it possible to measure basic quantities necessary for determination of the characteristics and to perform their subsequent analysis.

The basic relation intended to be used in analysing measured quantities is the energy conservation equation

$$\frac{c_1^2}{2}+\frac{p_1}{\rho}+e_1+a=\frac{c_2^2}{2}+\frac{p_2}{\rho}+e_2 \qquad (1)$$

in the absolute coordinate system:

where:

a	-energy delivered to rotor,
$\frac{c^2}{\rho}+\frac{p}{2}+e$	-kinetic, pressure and internal energy at inlet (index '1') and at outlet (index '2'), respectively.

For single rotor the potential energy differences $gz_1 \cong gz_2$ are usually very small or can be taken into account by introducing the piezometric pressure $p+\rho gz$ to Eq. (1). The applied notation complies with that used in classical technical literature on pumps [1], [2].

If to introduce the total pressure increase measured on the model machine (marked 'm'):

$$\Delta p_m=\left(p_2+\rho\frac{c_2^2}{2}\right)-\left(p_1+\rho\frac{c_1^2}{2}\right) \qquad (2)$$

then Eq. (1) can be expressed as follows

$$a=\frac{\Delta p_m}{\rho}+\Delta e \qquad (3)$$

In Eq. (3) energy dissipation (losses) is determined by the increase of internal energy:

$$\Delta e=e_2-e_1>0$$

Eq. (3) states that the energy delivered by the rotor is transformed to the total pressure increase and energy losses inside the rotor.

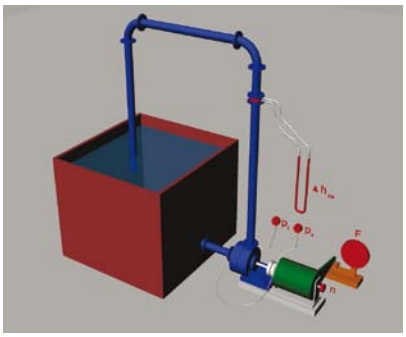

***Fig. 1.** Schematic diagram of model pump test stand (throttle valve not shown).*

Notation: pt – forcing pressure, ps – suction pressure, hzw – pressure difference on measuring orifice plate, F – force of action of driving motor pivotely fixed stator, n – rotational speed.

According to Euler formula, for axial inflow direction to rotor the delivered energy is expressed by the relation:

$$a = u\, c_u \tag{4}$$

determined by the rotor discharge parameters (index '2' assigned to the circumferential velocity u_2 and its projection to circumferential direction, c_{u2}, has been here omitted).

The energy conservation equation:

$$u\, c_u = \frac{\Delta p_m}{\rho} + \Delta e \tag{5}$$

is expressed in the form in which appear two measured quantities:

$$\Delta p_m \quad \text{and} \quad u = \frac{\pi D_2 n_m}{60}$$

where the rotational speed n_m is measured. In Eq. (5) the quantities c_u and Δe are unknown. For the torque M_m measured at the pivotely fixed stator of the electric driving motor of the pump, the following relation can be written:

$$M_m = \rho \frac{D_2}{2} \cdot c_u \cdot Q_m + M_t \tag{6}$$

where:

Q_m -measured volumetric flow rate;

M_t -moment of friction of rotor disk and cover against liquid.

In Eq. (6) the quantities c_u and M_t are unknown.

By analysing the following characteristics:

$$\Delta p = p(Q), \quad \text{where } n = \text{const} \tag{7}$$

$$M_m = M(Q_m), \quad \text{where } n_m = \text{const} \tag{8}$$

and

$$\Delta p_m = \Delta p(n_m), \quad \text{where } Q_m = \text{const} \tag{9}$$

$$M_m = M(n_m), \quad \text{where } Q_m = \text{const} \tag{10}$$

it is possible to determine parameters of the velocity triangle, under additional assumptions as to the velocity triangle at outlet from the rotor. Like in the above mentioned case, with exception of the characteristics (10), changes of M_t values proportional to n_m^2 with an unknown proportionality coefficient, will be equivalent to changes of the rotational speed n_m. For n_m = const and varying Q_m the velocity triangle shown in Fig. 2.

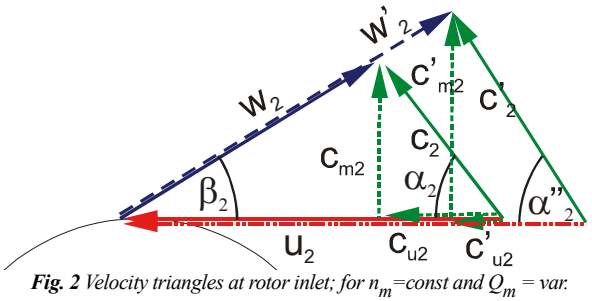

Fig. 2 Velocity triangles at rotor inlet; for n_m=const and Q_m = var.

The meridional velocity c_m in the rotor outlet cross-section of the breadth h_2 at the diameter D_2, is determined by the formula:

$$c_m = \frac{Q_m}{\pi D_2 h_2} \tag{11}$$

If to assume that change of Q_m does not cause any significant change of the angle β then the differentiation of the relation:

$$\operatorname{tg}\beta = \frac{Q_m}{\pi D_2 h_2 (u - c_u)} = \text{const} \tag{12}$$

with respect to Q_m yields:

$$\frac{dc_u}{dQ_m} = \frac{c_u - u}{Q_m} \tag{13}$$

For Q_m=const (c_m=const) and varying u (n_m=var) the velocity triangles are such as shown in Fig. 3.

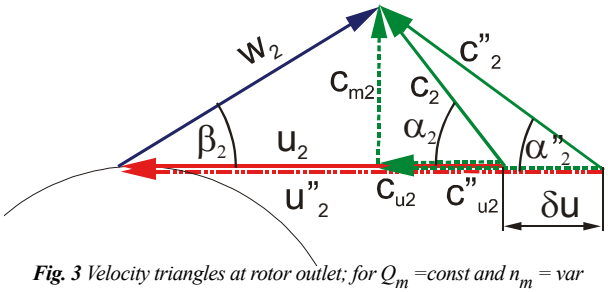

Fig. 3 Velocity triangles at rotor outlet; for Q_m =const and n_m = var

It is easy to observe that in this case the following yields from Eq. (12):

$$\frac{dc_u}{du} = 1 \tag{14}$$

Eqs. (13) and (14) will be further used for analysis of the characteristics.

Analysis of the ram pressure characteristics $\Delta p_m = \Delta p(Q_m)$.

In Fig. 4 is presented the pump rotor characteristics $\Delta p = f(Q)$ where: Δp [Pa] -ram pressure rise in function the volumetric flow rate Q [m^3/h] at the rotational speed n=const, obtained by means of the measurements carried out on the model test stand. In Fig. 4 the indices 'm' appearing in the notation of coordinates, are omitted.

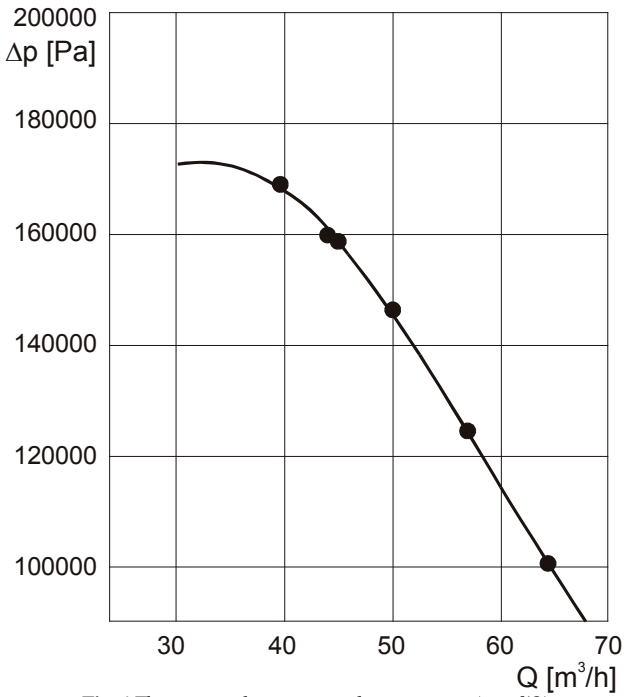

Fig. 4 *The measured pump rotor characteristics Δp = f(Q)*

The measurement points were interpolated by using a 3rd order curve which yielded a satisfactory approximation within the range of flow rate of 40÷70 [m^3/h].

Eq. (5) in the form:

$$\rho \cdot u \cdot c_u = \Delta p + \rho \cdot \Delta e \tag{15}$$

after differentiation with respect to Q, yields:

$$\rho\, u\, \frac{dc_u}{dQ} = \frac{d\Delta p}{dQ} + \rho \frac{d\Delta e}{dQ} \tag{16}$$

By making use of Eq. (13) the following equation is obtained:

$$\rho\, u\, c_u = \rho\, u^2 + Q\frac{d\Delta p}{dQ} + \rho\, Q\, \frac{d\Delta e}{dQ} \tag{17}$$

which, after dividing by $\rho u c_u$, makes it possible to estimate the following parameter crucial for the velocity triangle:

$$\frac{c_u}{u} = \frac{1}{1 - \frac{Q}{\rho u c_u}\frac{d\Delta p}{dQ} - \frac{\rho Q}{\rho u c_u}\frac{d\Delta e}{dQ}} \tag{18}$$

By introducing the approximations:

$$\rho\, u\, c_u \cong \Delta p \tag{19}$$

and:

$$\frac{d\Delta e}{dQ} \approx 0 \tag{20}$$

the following formula is achieved:

$$\frac{c_u}{u} \cong \frac{1}{1 - \frac{Q}{\Delta p}\frac{d\Delta p}{dQ}} \tag{21}$$

Eq. (21) makes use of information taken from the characteristics, inclusive of derivative in a selected point of it.

After determination of the quantities:

$$u = \frac{\pi D_2 n}{60} \text{ and } c_m = \frac{Q}{\pi D_2 h_2} \tag{22}$$

for known values of: the flow rate Q, rotational speed n, rotor outlet diameter D_2, and breadth h_2, the following angles appearing in the velocity triangle, can be determined:

$$\alpha = \mathrm{ArcTan}\frac{c_m}{c_u} \text{ and } \beta = \mathrm{ArcTan}\frac{c_m}{u - c_u} \tag{23}$$

Analysis of the rotor torque characteristics $M_m = M(Q)$

As the pump motor stator is pivotely fixed there is possible to measure the rotor - generated torque. Example results of the torque measurements are depicted in Fig. 5 where the experimental points has been interpolated by using a 2nd order curve. For their analysis the relation (6) will serve as the basis. Let's observe that at the constant rotational speed n and only the flow rate Q variable the following approximation seems to be good:

$$\frac{dM_t}{dQ} \approx 0 \tag{24}$$

Hence by differentiating the relation (6) the following expression is obtained:

$$\frac{dM}{dQ} = \rho\, \frac{D_2}{2}\, \left(c_u + Q\, \frac{dc_u}{dQ} \right) \tag{25}$$

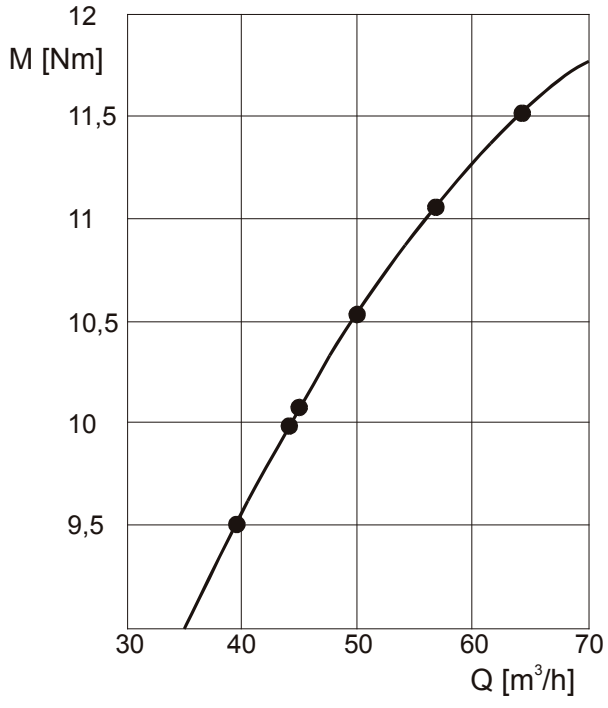

Fig. 5 *The measured pump rotor characteristics M = f(Q)*

From Eq. (25), by making use of Eq. (13), the following formula can be obtained:

$$\frac{dM}{dQ}=\rho\,\frac{D_2}{2}\,(2\,c_u-u) \tag{26}$$

from which it yields:

$$\frac{c_u}{u}=\frac{1}{2}+\frac{1}{\rho D_2 u}\frac{dM}{dQ} \tag{27}$$

The right hand side of the relation is determined on the basis of the experimental characteristics M(Q) and measured values of the rotational speed n_m. The angles are determined from the expressions (23).

Analysis of the ram pressure characteristics $\Delta p_m=\Delta p(u)$.

A similar analysis can be performed for the pump rotor characteristics $\Delta p=f(u)$ at Q=const. The characteristics are shown in Fig. 6 where the experimental points were interpolated by using a 2nd order curve which provides a good approximation.

$$c_u+u\frac{dc_u}{du}=\frac{1}{\rho}\frac{d\Delta p}{du}+\frac{d\Delta e}{du} \tag{28}$$

Differentiation of the relation (5) with respect to *u* gives:

$$1+\frac{u}{c_u}=\frac{u}{\rho c_u u}\frac{d\Delta p}{du}+\frac{\rho u}{\rho c_u u}\frac{d\Delta e}{du} \tag{29}$$

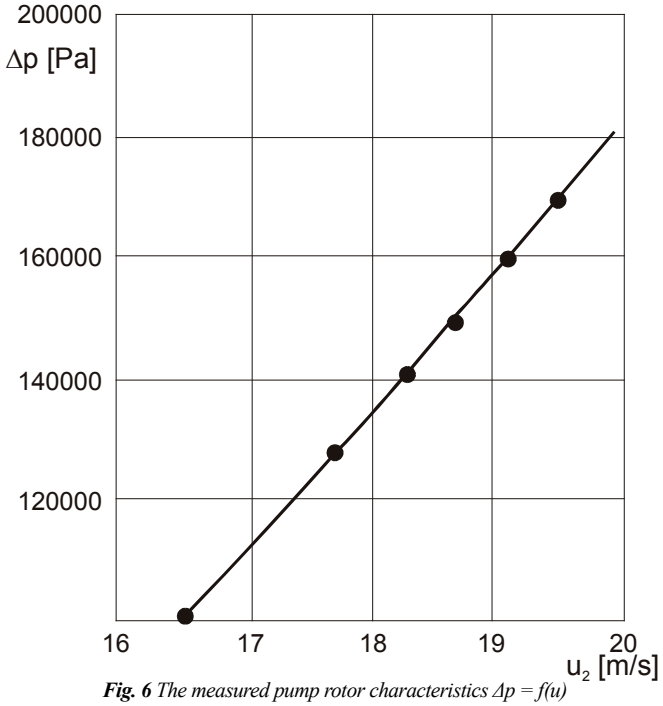

Fig. 6 *The measured pump rotor characteristics Δp = f(u)*

By making use of Eq. (14) the above given relation can be transformed into the following:

$$\frac{c_u}{u}\cong\frac{1}{\frac{u}{\Delta p}\frac{d\Delta p}{du}-1} \tag{30}$$

Finally the approximation (19) and the assumption on a small change of losses resulting from u (see Eq.(20) yields the formula:

whose right-hand-side values can be determined from the characteristics such as given in Fig. 6. Next from the expressions (23) the angles can be determined.

Discussion of results of analysis of experimental characteristics

The calculation results of the outlet angles α and β for particular characteristics, are presented in Figs. 8 through 10. The values obtained from the calculations according to Eqs. (21), (27), (30) are burdened both by measurement systematic errors and simplifying assumptions.

The characteristics $\Delta p=\Delta p(Q)$ are „ contaminated" by backflow drag behind the rotor and guide vanes drag in the centripetal channel behind the rotor. In the conditions of the performed experiment it was not possible to obtain seperate characteristics for the rotor only. Drag rise behind the rotor at greater values of Q leads to lower values of measured ram pressures, that - in consequence - gives greater values of the angle α. If behind-the -rotor drags were reduced and

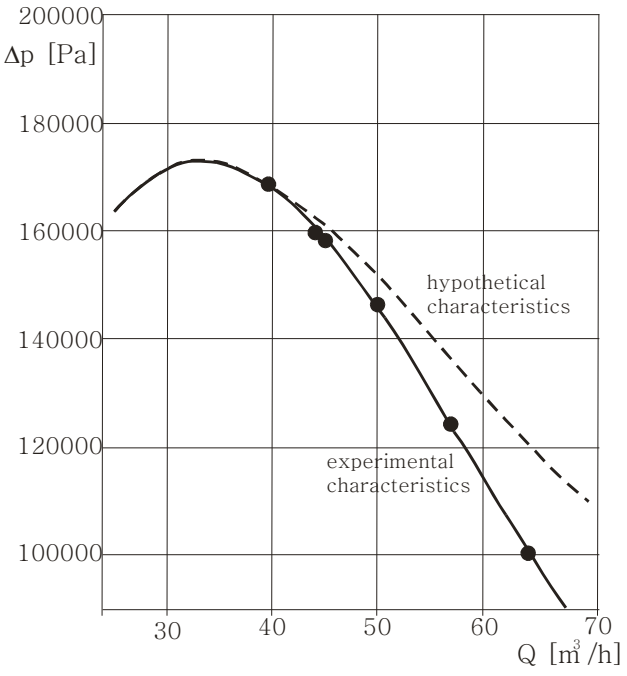

Fig. 7 *Comparison of the experimental and hypothetical pump rotor characteristics*

a greater ram pressure rise were this way obtained as it indicate the hypothetical characteristics shown in Fig. 7, then good comformity between the angles α calculated from Eqs. (21) and those obtained from torque measurements, acc. Eq. (27), would be achieved. The comparison of the values calculated according to the formula (21) for the experimental and hypothetical characteristics demonstrates influence of the error residing in the characteristics on the determined values characterizing the velocity triangle. In Fig. 8 the point determined on the basis of the calculations performed by using a 3D code, is presented. This is the value of the angle α, calculated as the surface average. The value relatively well fits those determined from the characteristics.

The determined angle α makes it possible to calculate value of the rotor outlet angle β which constitutes an important feature of rotor blades palisade. Fig. 9 presents the calculation results. The change of the angle β, observed in the diagram, demonstrates an approximate character of the assumption on its invariance. Only variability ranges for Q – values, within which the changes would be sufficiently small, can be indicated.

Analysis results of the characteristics Δp=Δp(u) are given in Fig. 10 and11. The experimental point shown in Fig. 10 is situated relatively close to the point obtained from the analysis of experimental characteristics. The small changes of the angle β, seen in Fig. 11, seem to satisfy the assumption on its invariance, better. However, by comparing

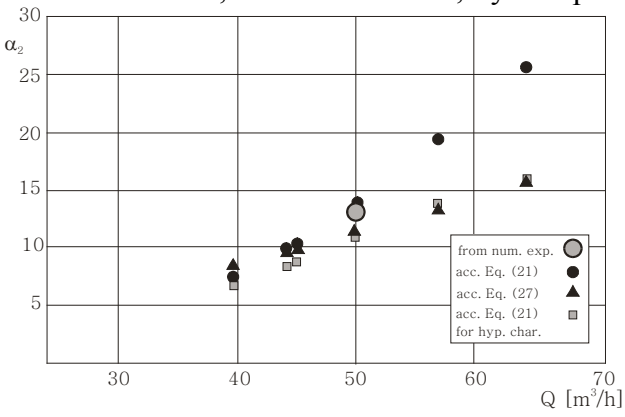

Fig. 8 *Comparison of calculation results of the discharge angle α_2, obtained from experiment with those obtained from 3D-calculations*

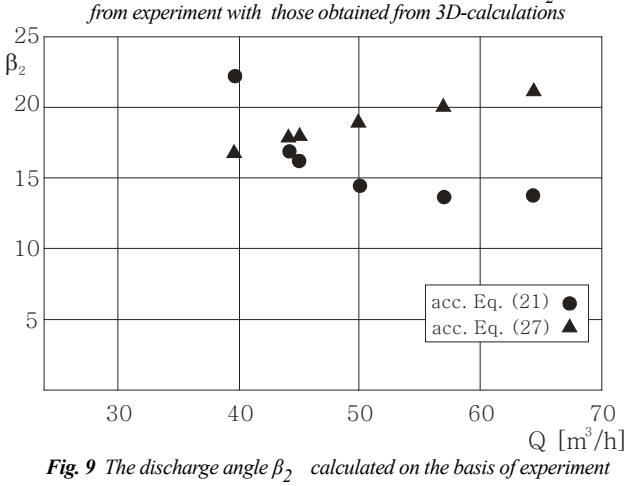

Fig. 9 *The discharge angle β_2 calculated on the basis of experiment*

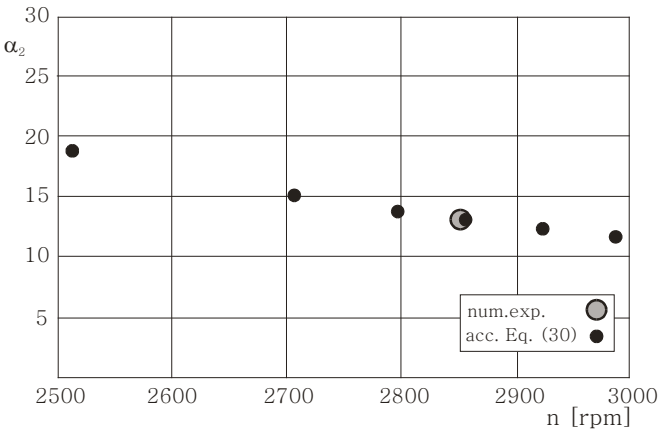

Fig. 10 *Comparison of calculation results of the discharge angle α_2 acc. Eq.(30) with those obtained from numerical experiment*

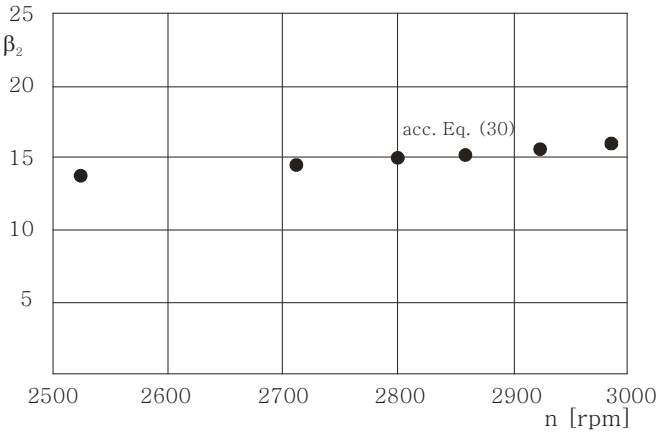

Fig. 11 *Values of the discharge angle β_2 calculated acc. Eq. (30)*

Fig. 9 with Fig. 11, the discrepancy in the angle β values of the range from 14° to 20°, was revealed. The value of the geometrical angle of the rotor outlet edge amounted to about 30°.

The angle α determined from the analysis makes it possible to more properly design the inlet to guide vanes channel behind the rotor for a given nominal value of Q.

Final remarks

The presented method for determining the velocity triangle parameters on the basis of the pump rotor characteristics can be used in the case if other possibilities to measure flow parameters are lacking. Information on the angle of flow discharge from the rotor is especially important. It much differs from the rotor blade geometrical outlet angle. This is an important parameter for correct forming the inlet to guide vanes ring behind the rotor. In this paper attention has been also drawn to the necessity of exact determination of discharge pressure from the rotor. In the described experiment the pressure was „contaminated" by flow drag occurring in the space between the rotor outlet and the forcing pressure measurement point. For this reason the experiment was not sufficiently „pure" for the presented method. Nevertheless its relatively good conformity with the experiment was achieved at some scatter of values of the determined angles.

The analysis demonstrates in which sense the rotor characteristics constitute „carriers" of information on flow parameters.

Bibliography

1. Pfleiderer C.: *Strőmungsmaschinen* (in German). Springer Verlag, Berlin 1957
2. Troskolański A. T., Łazarkiewicz S.: *Rotary pumps* (in Polish). Wydawnictwa Naukowo Techniczne (Scientific Technical Publishing House), Warszawa 1973.

Nomenclature

a – work determined by Euler equation;

c – absolute velocity;

e – internal energy;

h – rotor breadth;

n – rotational speed;

p – pressure;

u – circumferential velocity;

z – location height;

D – rotor diameter;

M – torque;

Q – volumetric flow rate (volumetric flow capacity);

α – angle between directions of the absolute velocity (c) and the circumferential velocity (u);

β – blade angle;

Δ – rise of a quantity;

ρ – liquid density;

Indices

1 – (stands for) parameters at intlet edge of rotor blade;

2 – parameters at outlet edge of rotor blade;

m – parameters of model machine;

u – projection towards direction of circumferential velocity;

t – quantities associated with friction.

POLISH MARITIME RESEARCH, Special issue 2009/S1; pp. 58-63
10.2478/v10012-008-0046-0

Remarks on aerodynamic forces in seals of turbine stages

Robert Stępień,
Krzysztof Kosowski

Abstract

This paper presents results of numerical examination of flow through over-shroud seals of turbine stages. Various labyrinth seals of different configurations and number of sealing teeth were considered. It was demonstrated that results of investigations of isolated seals cannot be directly used for analyzing turbine stage operation. Such approach may lead to relatively large errors in determining value of aerodynamic force and direction of its action.

***Keywords**: rotor dynamics, self-excited vibrations, aerodynamic forces, blade seals, turbine shrouds*

Introduction

Turbine rotor often moves along a complex trajectory during operation, usually it is displaced by the eccentricity **e** relative to turbine cylinder centre, it changes its logitudinal position **a**, and its axis can be situated aslant relative to cylinder axis, forming with it the angle φ (Fig.1). This results in circumferential and axial change of clearance in turbine stage seals (over-shroud ones as well as external glands), that in turn causes that distribution of flow both in seals and grids of blades becomes no longer circularly symmetrical. Unbalanced aerodynamic forces appear (called blade-ring forces if occur in passages of grid of blades, and pressure forces if in seals). The forces can lead to self-excited vibrations of turbine rotors and -in some cases -prevent turbine form developing its rated power.

For more than fifty years the phenomenon has been investigated in many research centres worldwide. Many results of experimental, theoretical and numerical investigations have been so far published. In the beginning, analyses based on the so called „bulk-flow theory" have been developed ([11]-[13], [15]). In the method, simplifications are implemented in solving three-dimensional, non-stationary equations of flow through the clearance, consisting in linear association of shear stresses on the walls with average flow velocity (that is only possible at rather small rotor displacements against casing). This way flow behaviour equations were simplified to 2nd order ones as well as it was made possible to consider the flow to be axially symmetrical and stationary and that in which only small disturbances described by linear relations occur. As a result of solving such set of equations distributions of velocity and pressure fields in the clearance are achieved; they are then used for determining forces and moments generated in the clearance. The end of the 1980s and the 1990s brought development of computer calculation techniques used also in the modelling of flows through the clearance between rotor and casing, as well as in the determining of dynamic coefficients for such systems. The simulations are based on three-dimensional Navier-Stockes equations with Reynolds averaging (RANS), closed by means of the k-ε turbulence model. For calculations algorithms based on the methods of finite elements [7], finite differences [9], [14], [17], [18] and finite volumes [1]÷[6], [8], [10], are used. Analysis of forces generated in isolated seals is only of a limited usefulness for design practice. Flows through seal are also influenced by phenomena which occur both in passages of vane blades and rotor blades grids. Therefore results obtained from investigations of isolated seals cannot be directly applied to analysis of operation of a complete turbine stage.

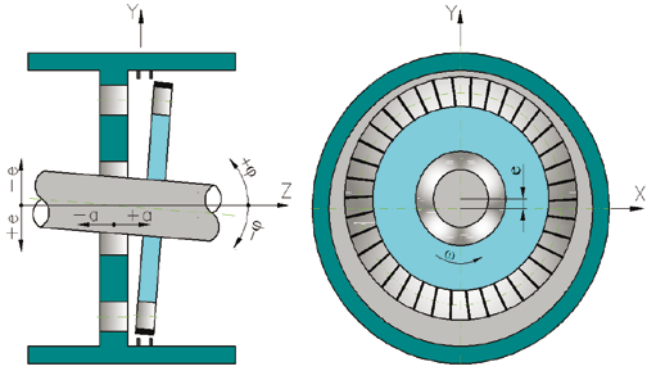

***Fig. 1** Changes in position of rotor against casing, **a** – change of axial clearance, **e** - eccentricity, **φ** - angle of aslant displacement of rotor axis against casing axis*

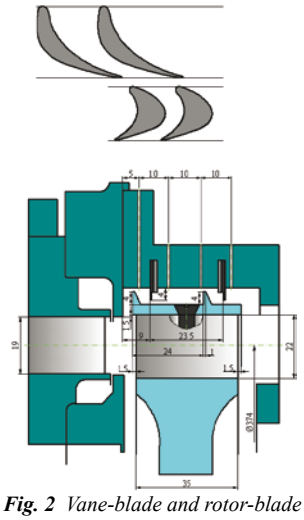

Vane blades grid

Effective diameter	374 mm
Blade height	19 mm
Chord of airfoil section	74 mm
Pitch of grid	41,9 mm
Number of blades	28
Blade-angle setting	39°42'
Outlet angle	9°42'

Rotor blades grid

Effective diameter	374 mm
Blade height	22 mm
Chord of airfoil section	37,2 mm
Pitch of grid	30,9 mm
Number of blades	34
Blade-angle setting	74°30'
Outlet angle	14°50'

***Fig. 2** Vane-blade and rotor-blade profiles as well as scheme of turbine stage flow part*

Object of the investigations – a turbine stage

The schematic diagram of the flow part of the investigated turbine stage is shown in Fig. 2. Three-dimensional flow analysis of the invstigated turbine stage was performed by means of the CFD Fluent code in which the method of finite volumes is used for solving the set of Navier-Stokes equations. The calculations were performed for compressive, viscous (with constant viscosity coefficient) and turbulent flow without any heat exchange with environment. Geometry of the turbine flow part (Fig.2) was modeled by means of a computational mesh split into four blocks: inlet to the stage together with guide vanes, rotor, over-shroud seal, and outlet diffuser, which are so connected to each other as to form one computational entity (the applied kind of computational mesh and interfaces between particular blocks are described in detail in [16]).

All the flow calculations were performed for the nominal clearance L = 0.5 mm and the eccentricity ew = 60% (vertical).

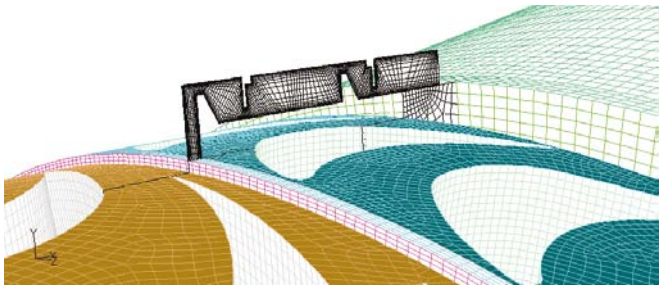

Fig. 3 *Example of computational mesh of turbine stage flow part*

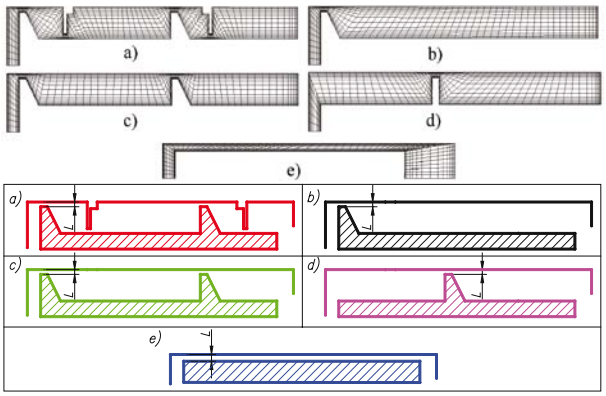

Fig. 4 *Schemes and meshes of the investigated seals as follows:* ***a)*** *with 4 teeth (marked U4),* ***b)*** *with single tooth at inlet (marked U1),* ***c)*** *with 2 teeth (marked U2),* ***d)*** *with single tooth in the middle of shroud (marked U1s),* ***e)*** *smooth one – without teeth (marked U0)*

In Fig. 3 an example of the applied computational mesh is presented, and in Fig. 4 are shown schemes, notations and computational meshes of the considered over-shroud seals, namely:

- the seal with 4 teeth (marked U4),
- the seal with single tooth at inlet (marked U1),
- the seal with 2 teeth (marked U2),
- the seal with single tooth in the middle of shroud (marked U1s),
- the smooth seal, i.e. without teeth (marked U0)

Influence of type of seal on pressure forces

To investigate influence of geometry of an isolated seal on forces generated in it, a simplified computational model was elaborated; in the model guide vanes were replaced with a smooth pipe and rotor blades grid was omitted. Fig. 5 shows cross-section through the upper part of the computational system geometry. The calculations were carried out for the constant value of working medium overpressure of at inlet to the pipe, equal to 5kPa. This value is equivalent (roughly) to the pressure at inlet to the seal (after expansion in guide vane), which occurs in the case of analysis of flow through the real turbine stage operating with the rotor angular frequency of 566 rad/s and the inlet overpressure of 20kPa.

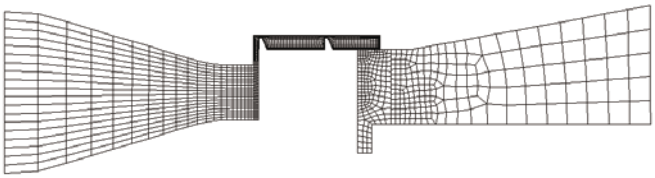

Fig. 5 *Cross-section through geometrical model of 'isolated' seal*

The run of pressure in the investigated seals along shroud breadth is shown in Fig. 6, and the pressure fields in the lower cross-section of seal, (D), and the upper one (G) – in Fig. 7. All the presented characteristics are in compliance with the Lomakin effect [5] according to which at inlet to unsymmetrical clearance the maximum pressure value occurs in the place where the lowest clearance value

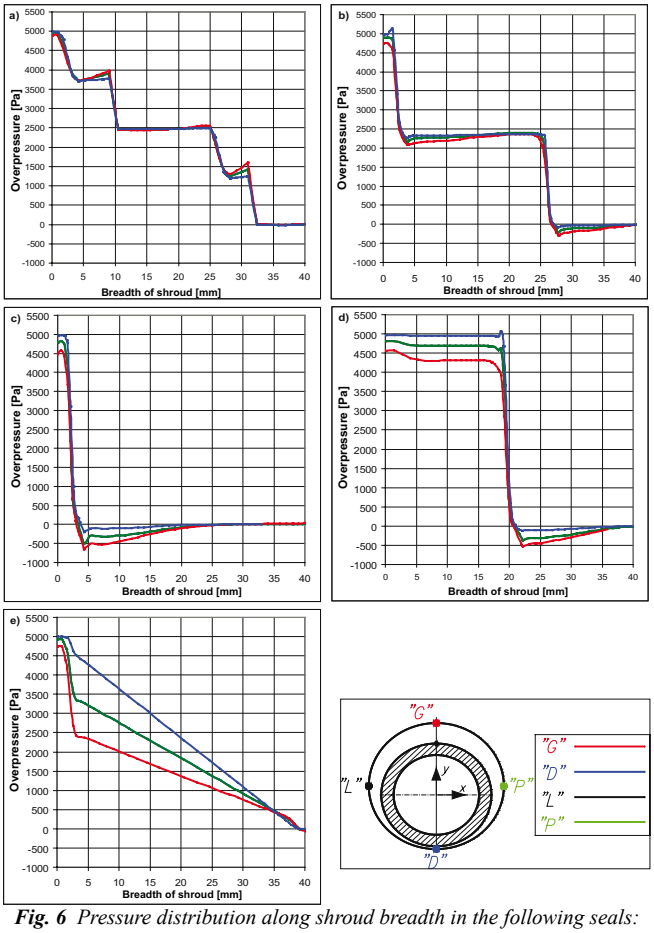

Fig. 6 *Pressure distribution along shroud breadth in the following seals:* ***a)*** *U4,* ***b)*** *U2,* ***c)*** *U1,* ***d)*** *U1s,* ***e)*** *U0,*
(f – arrangement of the cross-sections along seal circumference)

appears (cross-section D), and the minimum pressure value – in the place where the maximum clearance value appears (cross-section G). The resulting pressure difference causes the force acting in opposite direction to eccentricity, called also righting force, to appear. In the plane perpendicular to that direction the pressure distributions on both sides of the examined seal (cross-sections: L and P in Fig. 6f) are symmetrical, therefore no horizontal component of the resultant force appears.

Also, velocity fields in the analyzed cross-sections of the seal appear to be different respectively. Velocity of working medium flowing through the seal reaches its maximum value in the place where the maximum clearance occurs (cross-section G), and its minimum value where the minimum clearance occurs (cross-section D). Direction of the flow is axial. The pathlines of the working medium flow through the seal U0 are presented in Fig. 8. Red colour of the presented lines, which appears in the upper part of the seal, stands for the maximum flow velocity of working medium. For the sake of clarity, the flow through inlet pipe as well as pathlines in outlet diffuser have been omitted in the figure.

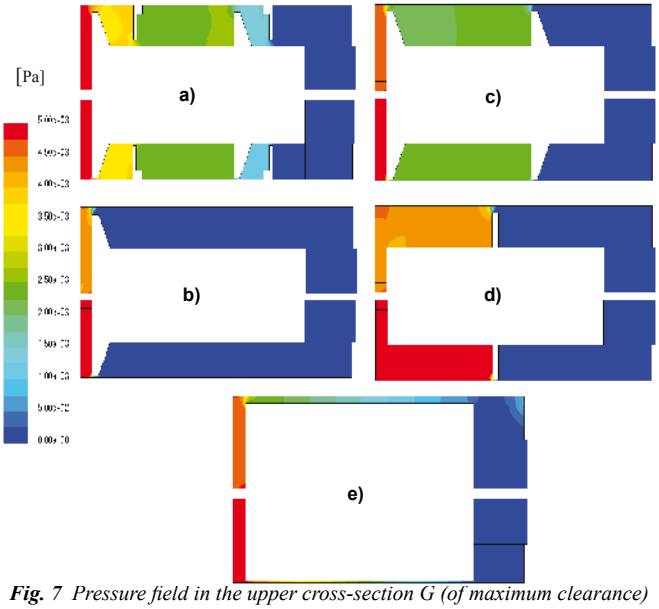

Fig. 7 *Pressure field in the upper cross-section G (of maximum clearance) and lower cross-section D (of minimum clearance) of the following seals:* ***a)*** *U4,* ***b)*** *U2,* ***c)*** *U1,* ***d)*** *U1s,* ***e)*** *U0*

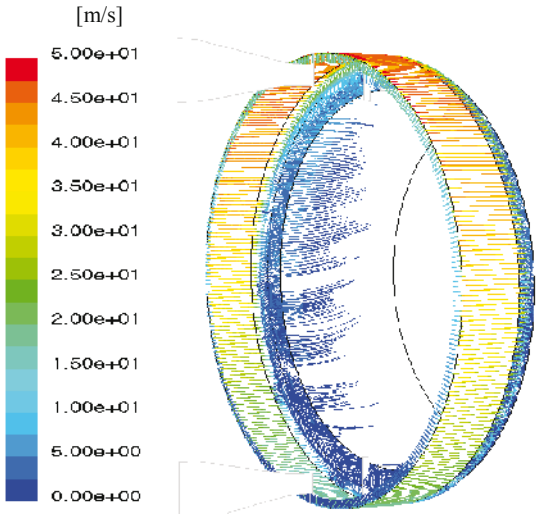

Fig. 8 *Pathlines of the working medium flowing through the seal U0*

Analyzing the obtained results one can concluded that type of applied seal decisively influences distribution of pressure field occurring in its clearance, consequently also pressure forces generated in it. In the same boundary conditions, values of the forces in particular seals differ several times or even a dozen or so times, to each other (Fig. 9).

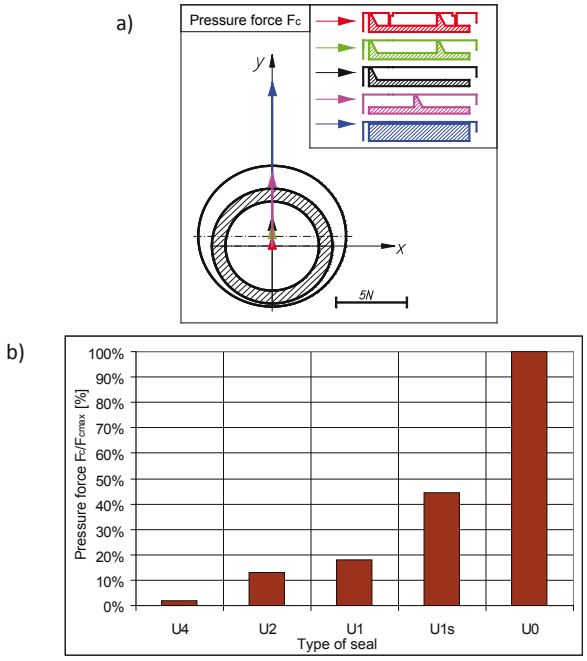

Fig. 9 *Vectors,* ***(a)****, and values,* ***(b)****, of the pressure force* F_C *occurring in the investigated seals (the force values are related to that which occurs in the seal U0) (red colour stands for the seal U4, green colour– the seal U2, black colour– the seal U1, violet colour– the seal U1s, blue colour– the seal U0)*

The Lomakin effect is observed in the cases in which shroud is motionless or working medium non-viscous. For viscous working medium and rotating shroud viscosity forces make pressure field in the seal clearance and location of its extremes, changing. Pressure distributions in the plane perpendicular to eccentric displacement, on both sides of the seal (cross-sections: L and P), become no longer symmetrical, and, as a result, a force vector deviation from direction of eccentric displacement of rotor occurs. The pressure field distribution in the considered seals, for the case of viscous working medium and shroud rotating with the frequency of 566 rad/s, is presented in Fig. 10, and in Fig. 11 – the vectors and values of the calculated pressure forces.

The greatest deviation of vector of generated forces, resulting from shroud wall rotation, occurs in the seals characterized by greater number of teeth (U2 and U4 type). Moreover, in the seals friction effects due to motion cause a significant increase of generated pressure forces. For instance, in the seal of four teeth, U4, the force is increased almost ten times. In the remaining seals, smooth one, U0, and that of single tooth, U1, values of the forces do not undergo so significant changes as those observed in the motionless seal system. Even a small decrease of the force FC was observed in the seals of U1s and U0 type.

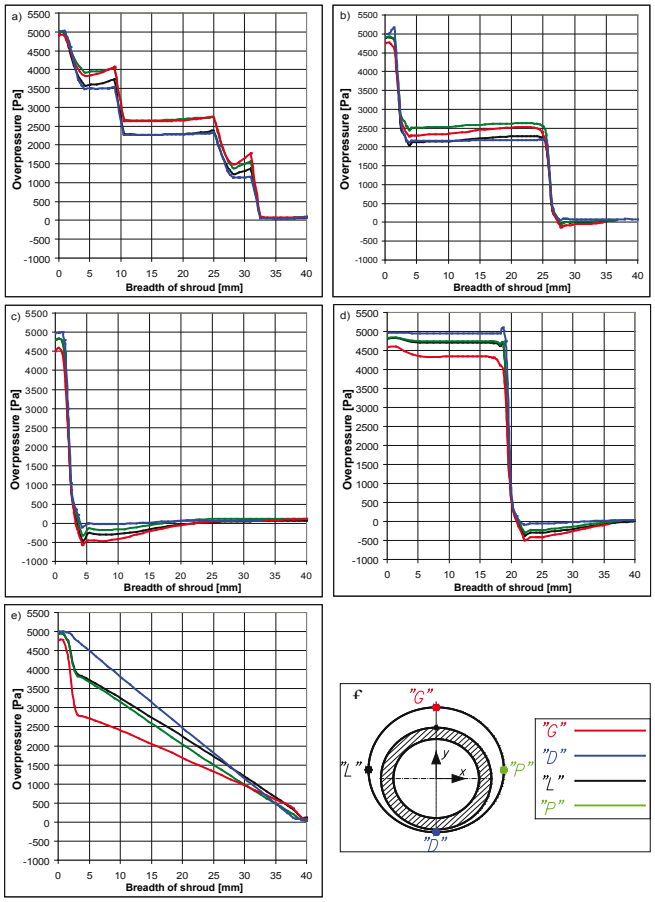

Fig. 10 *Pressure distribution in the seals along shroud breadth for viscous working medium and the shroud angular frequency equal to 566 rad/s:* ***a)*** *U4,* ***b)*** *U2,* ***c)*** *U1,* ***d)*** *U1s,* ***e)*** *U0 (f – arrangement of the cross-sections along seal circumference)*

In Fig. 12 flow through the four-teeth seal U4 is compared for the variants: when the seal shroud is motionless and when it rotates. In the latter case the flow through over-shroud clearance is no longer only axially directed because circumferential velocity components due to viscosity forces, appear.

From additional numerical analyses of non-viscous flow through the examined seals no deviation of the direction of action of pressure forces from the eccentricity direction, resulting from shroud rotatary motion, was stated. Character of pressure field distribution in the seal as well as values of generated forces were in compliance with results of the analyses in the case of motionless shroud wall.

Forces in the turbine stage with seals of various types

Numerical investigations of operation of the turbine of 7.5kW output power at the angular frequency of 566 rad/s (at 20kPa inlet working medium overpressure) were performed in order to make comparative analysis and determine resultant forces acting on the rotor in the real turbine stage fitted with labyrinth over-shroud seals of various types. Fig. 13 presents pressure distributions on the shroud of the examined seals, and Fig. 14 -vectors of the pressure forces FC, blade-ring forces FW and resultant force FP, acting on the rotor. As values of the

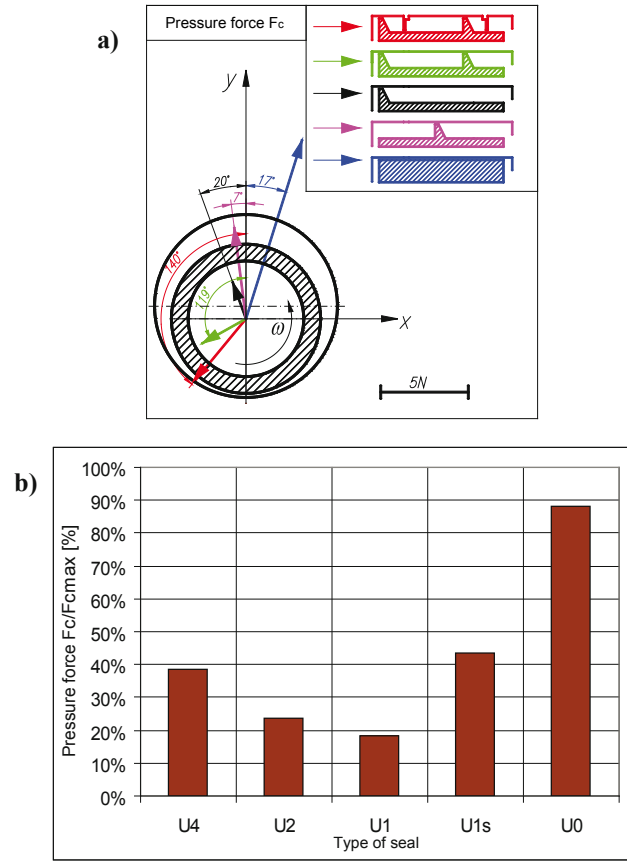

Fig. 11 *Vectors,* ***(a)****, and values,* ***(b)****, of the pressure force FC occurring in the investigated seals for viscous working medium and the shroud wall angular frequency equal to 566 rad/s (the force values are related to that which occurs in the U0 seal of motionless shroud)*

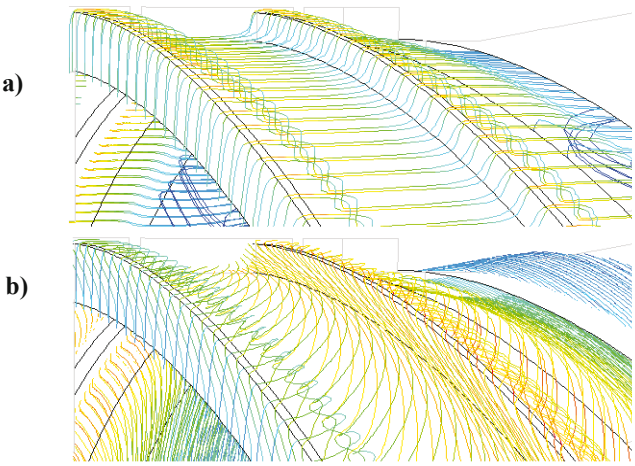

Fig. 12 *Pathlines of viscous working medium flowing through the seal U4:* ***(a)*** *in the case of motionless shroud,* ***(b)*** *in the case of rotating shroud with the angular frequency equal to 566 rad/s*

blade-ring forces are small they are shown in five times greater scale than the remaining – pressure and resultant ones.

In Fig.15 are presented the values of the forces calculated for the investigated seals, related to the value of the resultant force FP occurring in the two-teeth seal U2. Blade-ring forces are marked blue, pressure forces – brown, and resultant force acting on turbine rotor – yellow.

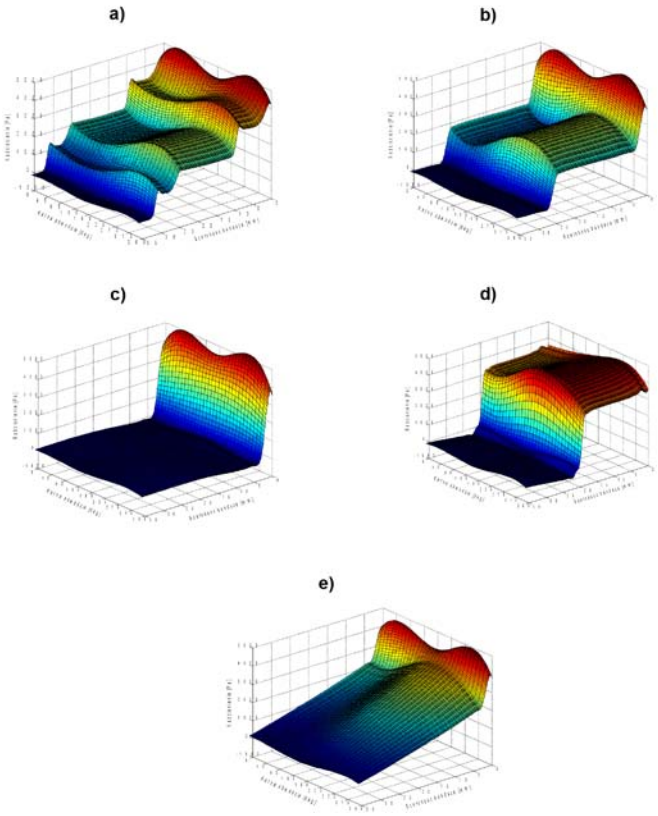

Fig. 13 *Pressure distribution in the seals:* ***a)*** *U4,* ***b)*** *U2,* ***c)*** *U1,* ***d)*** *U1s,* ***e)*** *U0 -for 20kPa working medium overpressure at inlet to turbine stage, and the rotor angular frequency equal to 566 rad/s*

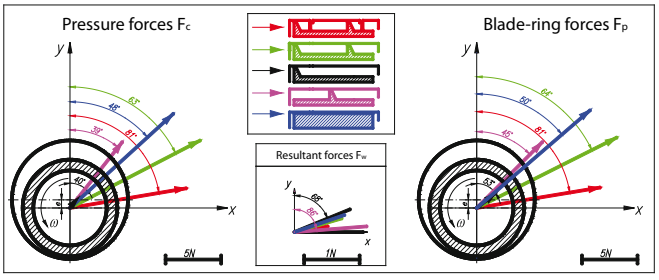

Fig. 14 *Vectors of: the pressure force FC (on the left), blade-ring force FW (in the middle) and resultant force FP (on the right), acting on the rotor, for the model IV at 20kPa inlet overpressure and the rotor angular frequency of 566 rad/s (red colour stands for the seal U4, green – the seal U2, black– the seal U1, violet– the seal U1s, blue– the seal U0)*

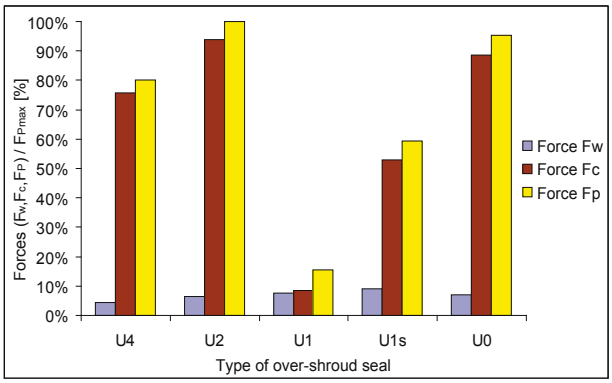

Fig. 15 *Values of the blade-ring forces FW (blue), pressure forces FC (brown), resultant force FP (yellow), at 20kPa inlet overpressure and 566 rad/ s rotor angular frequency*

Analyzing the obtained results one can state that influence of seal design on blade-ring forces generated in rotor passages is small (comp. Fig.14 and Fig.15). For all the examined systems generated blade-ring forces are of comparably small values regardless of type of applied seal.

Type of over-shroud seal decisively influences pressure forces generated in it. As results from analysis of the diagrams shown in Fig. 13, working medium pressure at inlet to and outlet from the seal is almost of the same value for all the compared systems, and it has been determined by values of the turbine stage operational parameters and eccentricity value. However type of over-shroud seal decisively influences pressure field distribution in its clearance (between inlet and outlet), and consequently pressure forces generated in it.

As it turned out, the smallest pressure forces (Fig.15) occurred in the seal of single tooth placed at inlet to the seal U1 and were nine times smaller than those in the seal U2 of two teeth, and over seven times smaller than those in the seal U4 of four teeth. This results from a favourable pressure distribution occurring in the clearance, determined by the conditions prevailing behind the rotor blade ring, and which is levelled out to a constant value over whole breadth of the shroud. Therefore no large circumferential differences in pressure appear (in contrast to the seals of a few teeth), and the generated forces are relatively small.

In should be also observed that the pressure forces obtained in the real turbine stage differ from those generated in the isolated seals, i.e. without taking into account other elements of turbine stage. In the case of isolated seals the largest forces occurred in the smooth seal, U0, as well as that of single tooth placed in the middle, U1s. In the real turbine stage the largest forces are generated in the seal of two teeth, U2, the seal of smooth shroud, U0, as well as the seal of four teeth, U4. In all the performed analyses the seal of single tooth at inlet to the clearance, U1, appeared to be characterized by the smallest pressure forces.

However it should be taken into consideration that the lowering of number of teeth in over-shroud

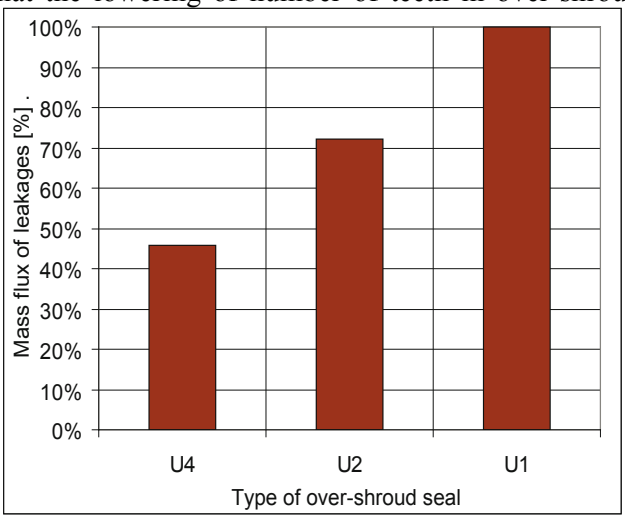

Fig. 16 *Mass flux of leakages flowing through the seal U4, U2 and U1 at the rotor angular frequency of 566 rad/s and 20kPa overpressure of working medium at inlet (the values are related to the mass of leakage from the single-tooth seal U1)*

seal, favourable due to smaller values of generated aerodynamic forces, leads to the increasing of leak flux of medium flowing through seal clearance and in consequence to the lowering of total turbine stage efficiency, in the clearance. The working medium mass fluxes in the seal related to the largest leakage occurring in the single-tooth seal U1, are shown in Fig. 16. From the efficiency point of view the most favourable appears the four-teeth seal U4 which simultaneously - as results from the performed investigations - is, apart from that of two teeth, U2, the least favourable from the point of view of generation of pressure forces in it, which are able to trigger self-excited vibrations of rotor. Direction of action of generated pressure forces depends - as results from the previously performed investigations - a.o. on type of seal and number of teeth applied in it. For single-tooth seals (of U1 and U1s type) directions of action of pressure forces amount to about 38°, counting from eccentricity direction (Fig.14). However for the two-teeth seal U2 such deviation from eccentrity direction amounts to 63°, and for the four-teeth seal U4 – as much as 80°. The smaller number of teeth in the seal the less deviated direction of action of pressure force from eccentricity, however the conclusion does not concern the smooth-shroud seal U0 because of another mode of expansion of working medium in a long and narrow clearance.

Summary

From analysis of the obtained results the following conclusions can be drawn:

- The making use of force coefficients for isolated seals without taking into account the remaining elements of turbine stage can lead to very large errors in determining aerodynamic forces occurring in a real device. Therefore the coefficients determined for isolated seals should not be used in analyzing operation of a turbine stage.
- For all the considered seals, direction of action of pressure force in the systems in which influence of working medium expansion in rotor blades grid or guide vanes has been not taken into account, is significantly different (even by 180°) from direction of action of pressure force in a real turbine stage.
- For all the analyzed systems, pressure distributions in the planes perpendicular to turbine axis, at inlet to and outlet from seal clearance, are similar and determined a.o. by assumed boundary conditions, nominal clearance and eccentricity of the system. To a much lower extent they depend on design type of applied seal which decisively influences distribution of pressure field in its interior.

The results presented in this paper are obtained from numerical calculations, however they have been confirmed by results of the investigations carried out on experimental stand.

Bibliography

1. Arghir M., Frěne J.: Rotordynamic Coefficients of Circumferentially-Grooved Liquid Seals Using the Averaged Navier-Stockes Equations.Transactions of the ASME Journal of Tribology, Vol 119, July 1997
2. Arghir M., Frěne J.: Analysis of a Test Case for Annular Seal Flows. Transactions of the ASME Journal of Tribology, Vol 119, July 1997
3. Arghir M., Frěne J.: Forces and Moments Due to Misalignment Vibrations in Annular Liquid Seals Using the Averaged Navier-Stockes Equations. Transactions of the ASME Journal of Tribology, Vol 119, April 1997
4. Arghir M., Frêne J.: A Quasi-Two-Dimensional Method for the Rotordynamic Analysis of Centered Labyrinth Liquid Seals. Transactions of the ASME Journal of Engineering for Gas Turbines and Power, January 1999
5. Arghir M., Defaye C., Frêne J.: The Lomakin Effect in Annular Gas Seals under Choked Flow Conditions. ASME paper GT2006-91151, Proceedings of ASME Turbo Expo, Barcelona, Spain, May 8-11 2006
6. Arghir Mihai, Mathieu Hélène, Jean Frene: Analysis of Tangential-Against-Rotation Injection Lomakin Bearings. Transactions of the ASME Journal of Engineering for Gas Turbines and Power, Vol. 127, p. 781-790, October 2005
7. Baskharone E. A., Hensel S. J.: Interrelated Rotordynamic Effects of Cylindrical and Conical Whirl of Annular Seal Rotors. Transactions of the ASME Journal of Tribology, Vol 113, July 1992
8. Chew J.W., Guardino C.: Simulation of flow and heat transfer in the tip region of a brush seal. International Journal of Heat and Fluid Flow 25, p.649–658, 2004
9. Dietzen F. J., Nordmann R.: Calculating Rotordynamic Coefficients of Seals by Finite Difference Techniques. Transactions of the ASME Journal of Turbomachinery, Vol 109, July 1987
10. Guo Z., Rhode D. L., Davis F. M.: Computed Eccentricity Effects on Turbine Rim Seals at Engine Conditions with a Mainstream. Transactions of the ASME Journal of Turbomachinery, Vol 118, January 1996
11. Hsu Y., Brennen C.: Fluid Flow Equations for Rotordynamic Flows in Seals and Leakage Paths. Transactions of the ASME Journal of Turbomachinery, Vol. 124, March 2002;
12. Lindsey Todd W., Childs D. W.: The Effect on Converging and Diverging Axial Taper on the Rotordynamic Coefficients of Liquid Annular Pressure Seals: Theory Versus Experiment. Transactions of the ASME Journal of Vibrations and Acoustics, April 2000
13. Marquette O. R., Childs D. W., San Andres L.: Eccentricity Effects on the Rotordynamic Coefficients of Plain Annular Seals: Theory Versus Experiment. Transactions of the ASME Journal of Tribology, Vol 119, July 1997
14. Rhode D. L., Hensel S. J., Guidry M. J.: Labyrinth Seal Rotordynamic Forces Using a Three-Dimensional Navier-Stockes Code. Transactions of the ASME Journal of Turbomachinery, Vol 114,
15. San Andrés L., Soulas T.: A Bulk-Flow Model Of Angles Injection Lomakin Bearings. Proceeding of ASME Turbo Expo, GT-2002-30287, June 2002
16. Stępień R., Kosowski K.., Piwowarski M., Badur J.: Numerical and Experimental Investigations into Pressure Field in Blade Shroud Clearance, Part II: Numerical Analysis.Task Quarterly, 2003
17. Tam L. T., Przekwas A. J., Muszynska A., Hendricks R. C., Braun M. J., Mullen R. L.: Numerical and Analytical Study of Fluid Dynamic Forces in Seals and Bearings. Transactions of the ASME Journal of Vibration, Acoustic, Stress, and Reliability in Design, Vol 110, July 1988
18. Williams M., Chen W. C., Baché G., Eastland A.: An Analysis Methodology for Internal Flow Swirling Flow Systems with a Rotating Wall.Transactions of the ASME Journal of Turbomachinery, Vol 113, January 1991

POLISH MARITIME RESEARCH, Special issue 2009/S1; pp. 64-70

10.2478/v10012-008-0047-z

Analysis of application of feed-water injector heaters to steam power plants

Marian Trela,
Roman Kwidziński,
Jerzy Głuch,
Dariusz Butrymowicz

Abstract

Steam-water injectors are devices in which exchange of mass, momentum and energy between two fluids being in direct contact, occurs. They can operate as pumps, mixers or direct contact heat exchangers. In the last aspect their use as feed-water heaters in Rankine thermal cycle of steam power plants both in land and sea applications (to merchant and naval ships) is very interesting. This paper presents selected results of heat-and-flow investigations of a supercritical steam-water injector, obtained in Institute of Fluid Flow Machinery, Polish Academy of Sciences (IMP PAN). On their basis value of average heat transfer coefficient for mixing chamber was determined; the obtained values were even a few dozens greater than those for classical shell-and-tube heaters. In the theoretical part of this work is presented an original injector model based on balances of mass, momentum and energy, written for control volumes containing separately particular elements of injector. On the basis of the model flow parameters in characteristic cross-sections of injector were determined. The calulations were performed for two different injectors tested in IMP PAN (Gdańsk) and SIET (Piacenza, Italy), and their good compliance with experimental data was achieved.

Keywords*: power plants, feed-water heaters, supercritical steam-water injector, injector model based on balances of mass.*

Introduction

Steam-water injectors are devices in which exchange of mass, momentum and energy occurs due to direct contact between two fluids. In 1901 an injector was used by Charles Parsons to air extraction from condensers, and in 1910 Maurice Leblanc applied an injector to a cooling device. Generally, injectors can operate efficiently as pumps, mixers or direct contact heat exchagers. In engineering a special role is given to double phase steam-water injectors. In recent years interest to such injectors has increased because of new proposals of their application to Rankine cycle of thermal power plants both land-based and marine ones (on merchant and naval ships). The most important advantages of such injectors consist in their possible operation without electric supply, rather small gabarites and lack of movable parts, resulting in their high operational reliability.

Two-phase steam-water injectors can be generally split into two kinds: (a) -subcritical ones (Fig. 1a) and (b) -supercritical ones (Fig. 1b). In both the cases water steam is their driving medium. In subcritical injector steam expands in the tapered steam nozzle SN and its discharge velocity w_{V1} is smaller than or at most equal to the sonic velocity a, ($w_{V1} \leq a$), hence Mach number reaches value: $M \leq 1$. In the second case (Fig. 1b) water steam expands down to the pressure smaller than critical one, as a result the discharge velocity from the nozzle is greater than the sonic one, hence Mach number reaches value: $M \geq 1$. Discharge steam from the nozzle flows into the mixing chamber MC and contacts there with cold water. Due to difference of temperatures and velocities between both the phases heat exchange (steam condensation) and momentum exchange takes place. The processes terminate in vicinity of mixing chamber throat, that is manifested by a sudden rise of pressure, characteristic for shock wave. Behind the wave, only the liquid flows through the diffuser. From the cognitive point of view the steam-water injector exemplifies a device which, though of simple design, is characteristic of a variety of flow phenomena. In the two-phase flow zone (covering the mixing chamber and condensation shock wave) drastic change in flow structure takes place – from stratified (annular) flow to homogeneous (bubbly one). Also flow velocity undergoes large changes – from a high subcritical value (smaller than about 450 m/s for the version a) or supercritical one (of the order of 500÷1000 m/s for the version b) at inlet to the mixing chamber, down to the value of the order of 20 m/s in the diffuser.

In this paper the results are presented of the authors' experimental investigations which covered measurements of pressure and temperature distribution along injector at different flow parameters, between inlet to and outlet from the injector. The investigations were carried out for the supercritical injector, (Fig. 1b), [1], i.e. the case considered more general. The critical injector ($M = 1$) is finally obtained by shortening the divergent part of the steam nozzle at maintaining the same inlet steam parameters. If steam pressure at inlet to the nozzle SN is now decreased then subcritical flows in the nozzle are obtained, and at the inlet: $M < 1$.

On the basis of the investigations were determined the maximum values of the injector discharge pressure (p_{4max}) at which the device can operate stably. Also, value of the average heat transfer coefficient for mixing chamber as well as injector efficiency, were determined. The injector's theoretical model based on balances of mass, momentum and energy, written for control volumes containing flow through particular elements of the injector, i.e. steam nozzle, water nozzle, mixing chamber, condensation shock wave zone and diffuser, shown in Fig. 1, has been also presented. By solving the model's equations for given parameters of driving steam and sucked-in water, flow parameters were determined in the injector characteristic cross-sections located on the boundaries of the above mentioned control volumes.

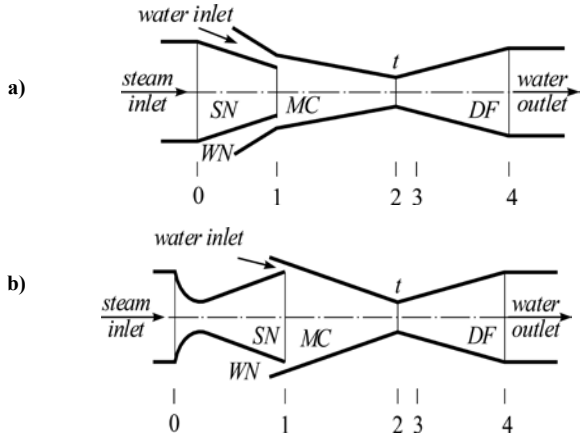

***Fig. 1**. Schematic diagram of steam – water injector: a) subcritical injector, b) supercritical injector. Main parts of injector : SN – steam nozzle, WN – water nozzle, MC – mixing chamber, DF – diffuser, t – throat*

Experimental investigations of steam-water injector

In the Institute of Fluid Flow Machinery of Polish Academy of Sciences, Gdańsk, experimental investigations of the supercritical two-phase steam – water injector driven by water steam (Fig. 1), were performed with the use of the laboratory model [1]. They were carried out by using the so called „short" injector of the mixing chamber pressure $p_{MC} \cong 20\,\text{kPa}$, with the aim to determine two quantities characteristic for injectors, namely: the maximum pressure p_{4max} and value of the average heat transfer coefficient $\overline{\alpha}$ for the mixing chamber MC. The tests were a continuation of the work carried out previously with the use of the so called „long" injector (of the pressure $p_{MC} \cong 8\,\text{kPa}$) [2, 3] with the aim to investigate their applicability to feeding nuclear reactor in failure states. Inlet parameters of the tested laboratory injector could be controlled within the following ranges: steam flow rate between 85÷130 kg/h, inlet steam pressure down from 0.5 MPa, steam superheating temperature between 0÷40 ºC, water flow rate between 1÷6 m^3/h, water temperature between 15÷20 ºC. It was also possible to change conditions of two-phase flow through mixing chamber by controlling the water nozzle gap size within the range of 0.5÷1.5 mm.

During the steam-water injector investigations, apart from the above mentioned inlet parameters, also temperature and pressure distributions along mixing chamber and diffuser, were recorded. Moreover, value of counterpressure at outlet from the injector, possible to be set by means of control valve, was measured. In Fig. 2 typical distributions of pressure and temperature along mixing chamber and diffuser, measured at different values of discharge pressure (Fig. 2a) and water flow rate (Fig. 2b), are presented. During investigations of injector performance characteristics the maximum discharge pressure at different values of the injection coefficient $U = m_{L0}/m_{V0}$ for three selected values of water nozzle gap, was determined. Results of the measurements are presented in Fig. 3. On the basis of the obtained characteristics it can be concluded that an increase of injector discharge pressure can be achieved both by increasing the coefficient U and mass flow of steam and or water at inlet to mixing chamber.

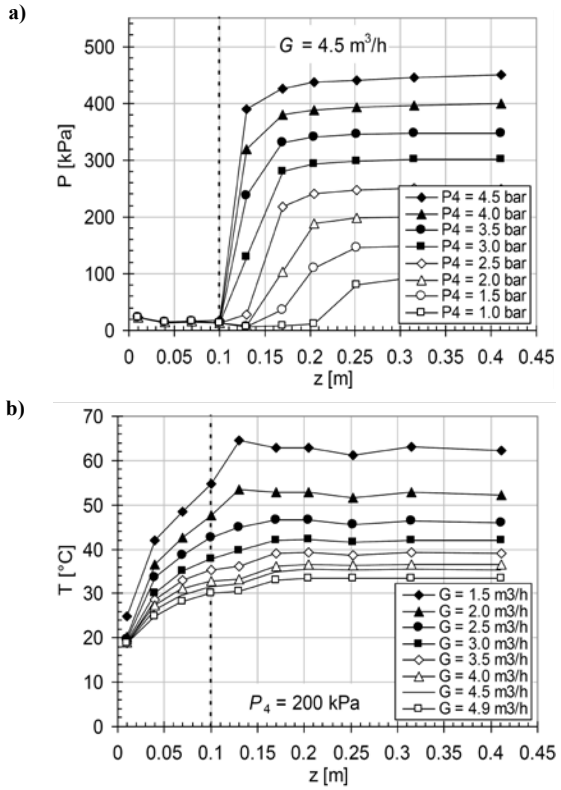

***Fig. 2**. Example profiles of pressure, (a), and temperature, (b), measured in mixing chamber and diffuser of a steam-water injector operating with selected values of the outlet pressure p4 and water flow rate G. The inlet steam mass flux.*

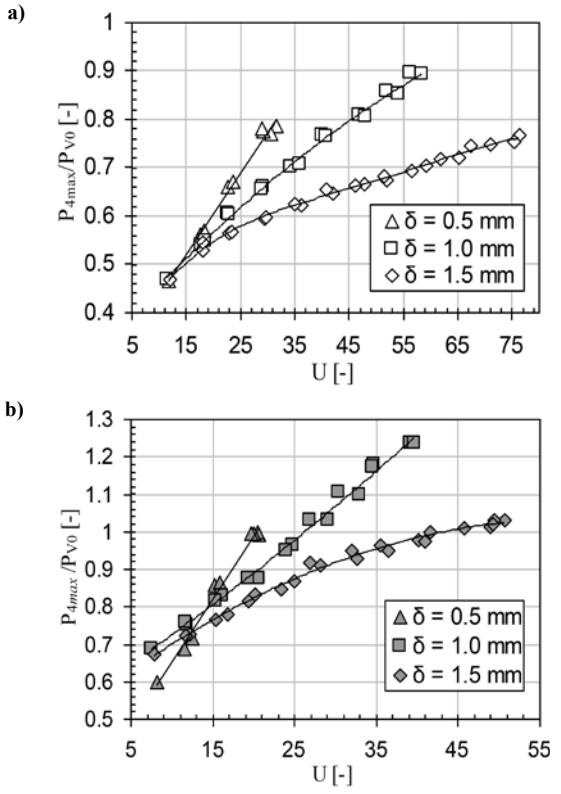

***Fig. 3**. Values of the dimensionless maximum outlet pressure p_{4max}/p_{V0} in function of the injection coefficient U, measured for three selected values of the water nozzle gap δ at the inlet steam flux equal to: a) 85 kg/h, b) 125 kg/h.*

Heat exchange in mixing chamber

The average heat transfer coefficient for the injector mixing chamber was determined on the basis of experimental data by using the method proposed in [3, 4]. By assuming that the flow of both phases through injector mixing chamber is one-dimensional and balanced it is sufficient, in order to determine thermodynamical parameters of water, to measure temperature only as steam parameters are depending only on pressure. Taking the above into account one can write the following energy balance equation for the mixing chamber:

$$m_{V1}h_{V1} + m_{L1}h_{L1} = (m_{L1} + m_c)h_L(T_3) + (m_{V1} - m_c)h_V(p_3) \quad (1)$$

from which it results that the condensed steam mass flow is equal to:

$$m_c = \frac{m_{V1}[h_{V1} - h_V(p_3)] + m_{L1}[h_{L1} - h_L(T_3)]}{h_L(T_3) - h_V(p_3)} \quad (2)$$

Now the average heat transfer coefficient for mixing chamber of the investigated steam–water injector can be calculated as follows:

$$\overline{\alpha} = \frac{m_c h_{fg}}{A_{MC}\Delta\overline{T}_{MC}} \quad (3)$$

The so determined $\overline{\alpha}$ values were generalized and presented in dimensionless form with the use of similarity numbers resulting from dimensional analysis of the equations of mass, momentum and energy conservation, written for flow through injector [1,6]. The dimensional analysis resulted in a correlation function expressed in the form of Nusselt number dependent on dimensionless similarity parameters, for the average heat transfer coefficient.

With the use of the authors' experimental data for the two injectors which have been so far examined in IMP PAN [1,2,3] (comprising altogether 2051 measurement points from testing the „short" injector as well as the „long" one) the following correlation function was obtained for the average Nusselt number:

$$Nu = 0.00284\ \mathrm{Re}_v^{0.974}\ S^{0.186}\ U^{0.112}\ \xi^{0.605} \quad (4)$$

where:

$$\mathrm{Nu} = \frac{\overline{\alpha}\, D_{SN}}{\lambda_{L1}}$$

$$Re_V = \frac{\rho_V\, w_V\, D_{SN}}{\mu_V}$$

$$U = \frac{m_{L1}}{m_{V1}}$$

The correlation (4) is valid for values of the dimensionless parameters contained within the following intervals, respectively:

$88240 \le \mathrm{Re}^v \le 234950$, $24 \le S^i \le 211$, $11 \le U \le 76$, $50 \le \xi \le 111$

together with the correlation coefficient R = 0.91. Physical parameters of water and steam as well as flow velocities in both the phases are calculated at the inlet cross-section of mixing chamber.

In order to make use of the correlation (4) to know geometry of steam and water nozzles is necessary because pressure and velocities at inlet to mixing chamber are associated with it. In Fig. 4 are presented example calculation results of heat transfer coefficient in compliance with the correlation (4), for two values of steam mass flow rate and one value of water flow rate, which correspond with the conditions of the experiments carried out in IMP PAN. The points representing two values of the mixing chamber pressure p_{MC}, equal to 8 and 20 kPa, are depicted on the diagram. The steam flow velocities w_{V1} as well as the steam nozzle outlet diameters D_{SN} corresponding with the pressures were determined on the basis of thermodynamical calculations of expansion in steam nozzle (from the initial pressure p_{V0} to the final pressure p_{MC}). As the water nozzle outlet area was known, the water flow velocity w_{L1} and the slip ratio S could be determined. The term expressing the physical properties ξ was determined for the given pressure p_{MC} from the water vapour tables. From the calculations two important observations result:

- In mixing chamber the heat transfer coefficient $\overline{\alpha}$ obtains very large values.
- Values of the coefficient $\overline{\alpha}$ are increasing along with pressure increasing in mixing chamber. For the pressure p_{MC} = 8 kPa its average value amounted to 350 kW/m^{2}K, and for the pressure p_{MC} = 20 kPa - as much as 725 kW/m^{2}K.

Such influence of the pressure on intensity of steam condensation on water film was confirmed by results of the injector investigations performed in Japan [12].

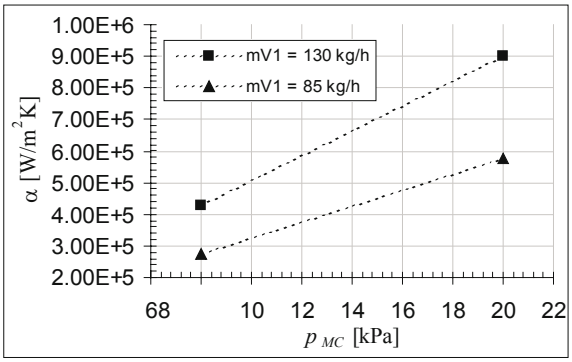

Fig. 4. Run of mean values of mean heat transfer coefficient, $\overline{\alpha}$, for mixing chamber, calculated acc. (4) in function of the pressure p_{MC} for two selected values of the steam mass flux $\dot{m}_{V1}$, at a set value of the outlet nozzle diamater D_{SN}, and the water mass flux $\dot{m}_{L1}$= 3000 kg/h..

Calculation of maximum discharge pressure

Modeling the flow through steam-water injector faces great difficulties especially in the zone of two-phase

flow in mixing chamber and condensation wave zone. The difficulties result first of all from the complexity of flow structures occurring successively in various parts of mixing chamber (annular, drop-like and bubble-like), presence of phase transformations (condensation on water film and in shock wave) and large changes in flow velocity (interphase slip at inlet to mixing chamber, transition from supercritical to subcritical shock wave). However it is possible to determine the maximum injector discharge pressure by using a simple model based on balances of mass, momentum and energy, written for control volumes containing mixing chamber and condensation shock wave zone, separately.

In the proposed model equations which describe flow through steam nozzle, and water nozzle as well, can be solved for parameters given at inlet to injector, and consequently yield the flow parameters at inlet to mixing chamber (marked '1'). Next, the solution of the balance equations of mass, momentum and energy for two-phase mixture in mixing chamber provides data to solve the set of equations for the successive control volume (between the cross-sections '2' and '3'), i.e. the shock wave zone. Now, on the basis of Bernoulli equation for liquid (water) flow through diffuser the pressure and temperature at outlet from injector, (marked '4'), can be determined.

The equations which describe driving steam expansion in steam nozzle were obtained under the assumption that the flow is adiabatic and irreversible. The steam parameters at outlet from the nozzle (cros-section '1') result from the following mass and energy balances:

where s -index stands for isentropic expansion value (i.e. when $s_{V1} = s_{V0}$). In real flow irreversibility losses contribute to lowering the discharge velocity w_{V1}, that can be taken into account by applying the velocity coefficient

$$A_{V0}\rho_{V0}w_{V0} = A_{V1}\rho_{V1}w_{V1} \tag{5}$$

$$h_{V0} + \frac{w_{V0}^2}{2} = h_{V1s} + \frac{w_{V1s}^2}{2} = h_{V1} + \frac{w_{V1}^2}{2} \tag{6}$$

c_v defined as follows:

$$c_v = \frac{w_{V1}}{w_{V1s}} \tag{7}$$

The coefficient takes into account not only losses resulting from friction but also due to condensation (when expanding steam parameters exceed Wilson's line) and formation of shock wave in the vicinity of the steam nozzle outlet (which takes place when at inlet to the mixing chamber a difference between steam and water pressure appears). As results from the investigations presented in [2], the above mentioned irreversible phenomena cause that value of the coefficient c_v for injector steam nozzle is relatively low, i.e. equal to about 0.9.

Under the relation (7) the double equation (6) can be transformed to the following form:

$$h_{V1} = h_{V1s} + \left(1 - c_v^2\right)\frac{w_{V1s}^2}{2} = c_v^2 h_{V1s} + \left(1 - c_v^2\right)\left(h_{V0} + \frac{w_{V0}^2}{2}\right) \tag{6a}$$

In the typical steam-water injector the driving steam is superheated at inlet to the nozzle but during expansion it enters wet-steam zone, hence the balance equations make the below given constitutive relationships to be complete:

$$\rho_{V0} = \rho\left(p_{V0}, h_{V0}\right) \ , \ s_{V0} = s\left(p_{V0}, h_{V0}\right) \tag{8a}$$

$$h_{V1s} = x_{1s}h_{V,sat}\left(p_{V1}\right) + \left(1 - x_{1s}\right)h_{L,sat}\left(p_{V1}\right) \tag{8b}$$

$$x_{1s} = \frac{s_{V0} - s_{L,sat}\left(p_{V1}\right)}{s_{V,sat}\left(p_{V1}\right) - s_{L,sat}\left(p_{V1}\right)} \tag{8c}$$

$$\rho_{V1} = \frac{x_1}{\rho_{V,sat}\left(p_{V1}\right)} + \frac{1 - x_1}{\rho_{L,sat}\left(p_{V1}\right)} \tag{8d}$$

$$x_1 = \frac{h_{V1} - h_{L,sat}\left(p_{V1}\right)}{h_{V,sat}\left(p_{V1}\right) - h_{L,sat}\left(p_{V1}\right)} \tag{8e}$$

where x stands for steam quality and the index sat concerns parameters in state of saturation.

Water nozzle discharge parameters can be determined under the assumption that pressure of water is the same as that of steam: $p_{V1} = p_{L1} = p_1$, and its temperature is the same as that at inlet to injector. Then $\rho_{L1} = \rho(p_{V1}, T_{L0})$ and the mass conservation equation:

$$\dot{m}_{L0} = A_{L1}\rho_{L1}w_{L1} \tag{9}$$

is sufficient to determine the water nozzle discharge velocity w_{L1}.

Flow parameters on the mixing chamber boundaries satisfy the balances of mass, momentum and energy, counted between the inlet cross-section 1 and the throat 2 (see Fig. 1), which are expressed by the following equations:

$$A_2\rho_2 w_2 = A_{V1}\rho_{V1}w_{V1} + A_{L1}\rho_{L1}w_{L1} \quad \text{or} \quad m_2 = m_{V1} + m_{L1}, \tag{10}$$

$$m_2 w_2 + A_2 p_2 + (A_1 - A_2)p_{MC} = m_{V1}w_{V1} + m_{L1}w_{L1} + A_1 p_1 \tag{11}$$

$$m_2\left(h_2 + \frac{w_2^2}{2}\right) = m_{V1}\left(h_{V1} + \frac{w_{V1}^2}{2}\right) + m_{L1}\left(h_{L1} + \frac{w_{L1}^2}{2}\right) \tag{12}$$

It was assumed here that steam phase is always in state of saturation and in the cross-section 2 both the phases (steam and water) move with the same velocity w_2. Therefore to determine the enthalpy h_2 the relationship valid for homogeneous mixture can be used:

$$h_2 = h\left(p_2, \rho_2, T_{L2}\right) = x_2 h_{V2}(p_2) + (1 - x_2)h_{L2}(\rho_{L2}, T_{L2}) \tag{13}$$

Moreover, it was assumed that the average pressure which acts on the mixing chamber conical surface and appears in the momentum balance equation (11), is equal to $p_{MC} = (p_1 + p_2)/2$.

When the mixing chamber inlet parameters (cross-section 1) are known to solve the set of balance equations (10)÷(12) is still necessary in order to know the liquid

phase temperature in the throat, T_{L2}, which is lower than the steam temperature T_{V2}. The temperature T_{L2} can be determine on the basis of heat flow which rises water temperature during condensation of driving steam in mixing chamber. The heat flow is connected with the average heat transfer coefficient $\overline{\alpha}$ by the relation (4).

The balance equations for the shock wave zone (between the cross-sections 2 and 3) are similar to those for mixing chamber and take the following form:

$$A_3 \rho_3 w_3 = A_2 \rho_2 w_2 \quad \text{or} \quad m_3 = m_2 \tag{14}$$

$$m_3 w_3 + A_3 p_3 + (A_2 - A_3) p_{SW} = m_2 w_2 + A_2 p_2 \tag{15}$$

$$m_3 \left(h_3 + \frac{w_3^2}{2} \right) = m_2 \left(h_2 + \frac{w_2^2}{2} \right) \tag{16}$$

In the shock wave zone complete steam phase condensation takes place, hence in the cross-section 3 only liquid (water) appears, whose enthalpy amounts to

$$h_3 = h(p_3, \rho_3).$$

The average pressure which acts, within the shock wave zone, on the diffuser conical surface, was determined from the approximate relation: $p_{SW} = (p_2 + p_3)/2$. Shock wave width and location of the cross-section 3, resulting from it, was determined on the basis of pressure profile measurements.

On the basis of the balance equations (14)÷(16) e.g. water pressure in the cross-section 3 can be determined. By taking into account the pressure increase determined form the Bernoulli equation:

$$p_4 + \frac{\rho_4 w_4^2}{2} = p_3 + (1 - \zeta) \frac{\rho_3 w_3^2}{2}$$

$$\text{where} \quad \rho_4 = \rho_3, \; w_4 = \frac{A_3}{A_4} w_3 \tag{17}$$

value of the injector discharge pressure p_4 can be achieved. Value of the pressure loss coeficient ζ in (17) can be determined acc. [5]. As in the equations (14)÷(16) it was assumed that shock wave is located in direct vicinity of mixing chamber throat the determined pressure p_4 obtains its maximum value to keep injector's operation stable.

The presented model was used to determine the maximum discharge pressure for the flow conditions complying with the measurements performed in IMP PAN, [1], and presented in Fig. 3b, as well as with the investigations carried out in SIET (Piacenza, Italy), [7,8]. Relatively good calculation conformity was obtained between the above mentioned experiments (Fig. 5 and 6), namely with the error of about 15%.

Injector efficiency

In the subject-matter literature different definitions of injector efficiency can be met [9,10]. It is usually the ratio of compression work done within injector and steam energy delivered to the injector. As steam-liquid injector

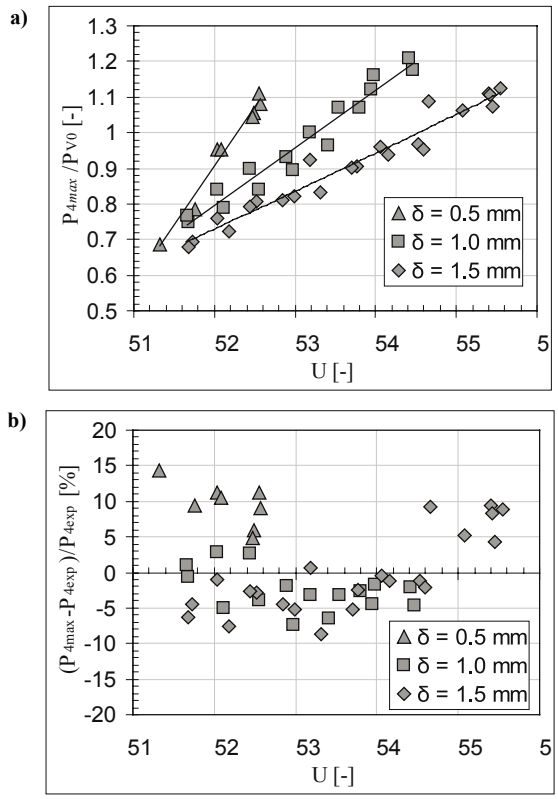

Fig. 5. Results of calculations of the maximum outlet pressure p_{4max} for the flow conditions given in Fig. 3b: a) calculated dimensionless maximum outlet pressure, b) relative difference between the calculated value, p_{4max}, and measured one, p_{4exp}.

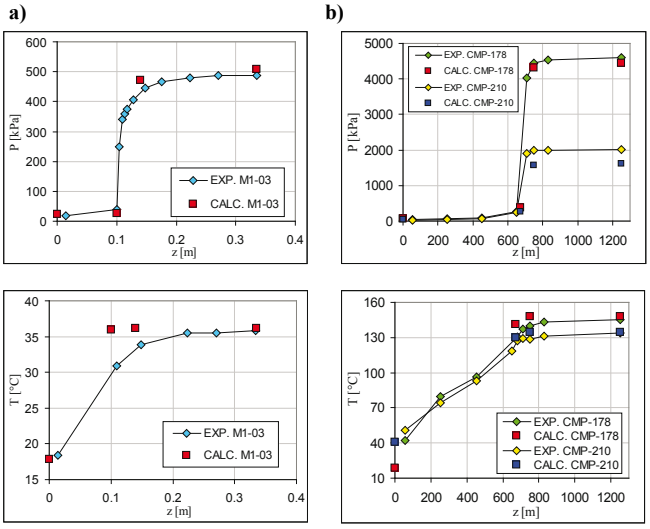

Fig. 6. Measured and calculated values of the pressure p and water temperature T on wall of mixing chamber and diffuser : the left column (a) concerns IMP- PAN conditions, the right one (b) concerns SIET conditions (Piacenza, Italy) [7,8].

can operate as a heat exchanger or jet pump therefore acceptance of two definitions of injector efficiency is justified.

In the case of injector operation as a heat exchanger it is proposed to use the notion of the exergetic efficiency η_b defined as the ratio of exergy of working fluid discharged from injector and exergy delivered to it:

$$\eta_b = \frac{(\dot{m}_{v0} + \dot{m}_{L0}) b_4}{\dot{m}_{v0} b_{v0} + \dot{m}_{L0} b_{L0}} = (1 + U) \frac{b_4}{b_{v0} + U b_{Lo}} \tag{18}$$

Calculation results of the efficiency for two versions („long" and „short") of the injectors examined in IMP PAN are presented in Fig. 7a.

In the case of injector operation as a jet pump, water exergy after compression is not so much important as its pressure part [11]. Hence the jet pump efficiency ηp can be defined as the ratio of compression mechanical work and delivered exergy:

$$\eta_p = \frac{(\dot{m}_{v0} + \dot{m}_{L0})}{\rho_L} \frac{p_4 - p_{MC}}{\dot{m}_{v0} b_{v0} + \dot{m}_{L0} b_{L0}} = \frac{1+U}{\rho_L} \frac{p_4 - p_{MC}}{b_{v0} + U b_{L0}} \quad (19)$$

Calculation results of the jet pump efficiency η_p are presented in Fig. 7b. From comparison of the efficiency η_b with the ηp it can be observed that the first is much greater.

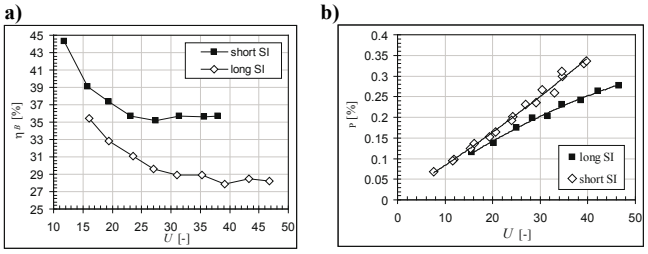

Fig. 7. *Efficiency calculated for two versions of the injector experimentally tested at IMP PAN: a) exergetic efficiency, b) injector pump efficiency.*

Final remarks

In this paper the comprehensive results have been presented of model tests of two-phase steam-water injector, aimed at its application to steam power plants operating in compliance with Rankine cycle. In such cycle the so called regeneration heating of water feeding the boiler takes place within shell-and-tube heater. It is planned to use steam-water injectors instead of shell-and-tube heaters, that could significantly lower investment cost of power plant.

The model tests of two-phase steam-water injector performed in IMP PAN were aimed at determination of the coefficient of heat transfer between steam and water in mixing chamber as well as the maximum pressure of water discharged from the injector.

In the theoretical part of the work the injector's model based on the balance equations of mass, momentum and energy, written for particular injector elements, was elaborated. In the model correlation of heat exchange within mixing chamber was used to determine temperature difference between steam and water in the mixing chamber's throat. The model makes it possible to determine, apart from flow parameters in characteristic control cross-sections, also the maximum pressure p_{4max} at outlet from the injector. Correctness of the model, in the aspect of the pressure, was examined with taking into account the authors' experiments as well as those performed in SIET (Piacenza, Italy). Good comformity between results of the calculations and experiments was achieved as the error amounted to about 15% within a wide range of flow paramters at inlet to injector.

The experimental test results of heat exchange in injector mixing chamber confirmed that to achieve very high values of the heat transfer coefficient $\overline{\alpha}$, reaching even 700 kW/m² K, is possible. They are over 100 times greater than the heat transfer coefficient k in shell-and-tube heaters (which reaches the value of about 3 kW/m² K). The so large values of $\overline{\alpha}$ could make it possible to decrease, by about a hundred times, surface area of steam-water contact in mixing chamber (at the same value of transferred heat flow rate), that could potentially result in the decreasing of gabarites of an alternative heat exchanger in the form of injector, by about 10-times. Hence, such application of the injector could significantly lower investment cost of steam power plant.

The lowering of gabarites of steam power plant devices is especially important in case of merchant and naval ships where shortage of space takes place. By applying injector water heaters their number could be increased, that could result in increasing Rankine cycle efficiency and -in consequence -lowering operational costs. Another factor which leads to improving operational parameters of the cycle fitted with feed-water injectors is lack of thermal degeneration. In injectors, in contrast to shell-and-tube heaters, heat transfer occurs by direct contact of vapour phase with liquid one, hence in such devices heat transfer effectiveness is not worsened due to accumulation of contaminations on heat transfer surface during their long-lasting operation. Preliminary estimations indicate that the increase of Rankine cycle thermal efficiency by about 0.2 %, resulting from the above, can be expected. Another gain can be achieved due to injector pump effect which makes it possible to decrease feed-water pump power by a few dozen percent.

This scientific research project (the ordered project No. PBZ-MEiN-4/2/2006) has been financed from science budget resources for the years 2007÷2009.

Bibliography

1. Trela M., Kwidziński R., Butrymowicz D.: Experimental investigation of steam injector in respect to heat and momentum transfer (in Polish). IFFM Internal Report No 7732/07, Gdańsk 2007.
2. Trela M., Kwidziński R.: Exergy analysis of steam-water injector performance. Archives of Thermodynamics, Vol. 29, No 1, 2008.
3. Trela M., Butrymowicz D., Dumaz P.: Experimental investigations of heat transfer in steam-water injector. 5th Int. Conference on Multiphase Flow (ICMF'04), Yokohama, Japan, 2004, CD-ROM, Paper No. 544.
4. Dumaz P., Duc B.: The DIVA program: Some experimental results and first CATHARE calculations. Proc. of 9th Topical Meeting on Nuclear Thermal Hydraulics (NUTRETH-9), San Francisco, October 3-8, 1999.
5. Idelchik I.E.: Handbook of Hydraulic Resistance, 3rd Edition. Begell House, New York, 1996.
6. Trela M., Kwidziński R.: Modeling of physical phenomena in supercritical two-phase steam injector. Archives of Thermodynamics, Vol. 25, No 4, 2003.
7. Ferri R., Achilli A., Gandolf S.: DEEPSSI Project: IETI Component Test, Experimental Data Report. Societa Informazioni Esperienze Termoidrauliche (SIET), Document 00 966 RP 02, 2002.
8. Ferri R., Achilli A., Gandolf S.: DEEPSSI Project: IETI

Additional Component Test, Experimental Data Report. Societa Informazioni Esperienze Termoidrauliche (SIET), Document 00 987 RP 02, 2002.
9. Cattadori G., Galbiatti L., Mazzocchi L., Vanini P.: A single – stage high pressure steam injector for next generation reactors: test results and analysis. Int. Journal of Multiphase Flow, Vol. 21, No. 4, 1995.
10. Sokolow E. Y., Singer N. M.: Jet apparatus (in Russian). Ed. Energoizdat, Moscow, 1989.
11. Szargut J.: Exergy (in Polish). Publ. Technical University of Gliwice, Poland, 2007.
12. Abe Y., Kawamoto Y., Iwaki Ch., Narabayashi T., Mori M., Ohmori S.: Development of technologies on innovative-simplified nuclear power plant using high-efficiency steam injectors (Operation characteristic evaluation using visualization test of the supersonic steam injector) [in Japanese]. Progress in Multiphase Flow Research, Vol. 1, 2006 [http://www.jstage.jst.go.jp/article/pmfr/1/0/223/_pdf].

Nomenclature

A – cross-section area, m^2 ;
a – sonic velocity, $a = (dp/d\rho)^{1/2}_{s=const}$;
A_{MC} – surface area of mixing chamber wall, m^2 ;
b – specific exergy, kJ/kg;
D, d – diameters, m;
G – volumetric water flow rate, m^3/h;
$\dot{m}$ – mass flow rate, kg/s;
M – Mach number, M = w/a;
Nu – Nusselt number, $Nu = \overline{\alpha}\, d_e / \lambda_L$;
h – specific enthalpy, kJ/kg;
h_{fg} – heat of condensation, kJ/kg;
p – pressure, Pa;
Re – Reynolds number, $\mathrm{Re} = w \rho\, d_e / \mu$;
s – thermal capacitance, kJ/kg K;
S – slip coefficient, $S = w_{V1} / w_{L1}$;
T – temperature, K;
$\Delta\overline{T}_{MC}$ – logarithmic mean temperature in mixing chamber, K;
U – injection coefficient, $U = m_{L0}/m_{V0}$, ;
w – flow velocity, m/s;
x – steam quality, $x = \dot{m}_V / (\dot{m}_V + \dot{m}_L)$;
$\overline{\alpha}$ – mean heat transfer coefficient for mixing chamber, W/m^2 K;
δ – water nozzle gap, mm;
λ – thermal conductivity coefficient, W/(m*K);
η – injector efficiency;
μ – dynamic viscosity, kg/(m*s);
ξ – parameter of physical properties,
$\xi = (\rho_{L1} / \rho_{V1})^{0.5} (\mu_{V1} / \mu_{L1})^{0.1}$
ρ – density, m^3/kg.

lower indices:

0 – at injector inlet;
1 – at inlet to mixing chamber;
2 – at mixing chamber throat;
3 – behind shock wave;
4 – at outlet from injector;
b – (stands for) exergy;
e – equivalent;
max – maximum;
L – (stands for) liquid (water);
p – (stands for) pump;
SN – (stands for) steam nozzle;
V – (stands for) vapour (of water).

POLISH MARITIME RESEARCH, Special issue 2009/S1; pp. 71-74

10.2478/v10012-008-0048-y

On the modelling of aerodynamic force coefficients for over-shroud seals of turbine stages

Wojciech Włodarski,
Krzysztof Kosowski.

Abstract

This paper presents experimental investigations which made it possible to determine dynamic coefficients of labyrinth over-shroud seal of a model air turbine. The coefficients associate pressure forces with turbine rotor displacement, velocity and acceleration respective to turbine casing (linear model) and play important role in analyzing turbine-set dynamics. The obtained results indicated that involving serious errors can be expected in the case of application of the simplification consisting in neglecting inertia coefficients, proposed in the literature. It was simultaneously demonstrated that seals can be also met of weak damping qualities, for which to neglect damping coeffcients is allowable.

Keywords: *rotor dynamics, self-excited vibrations, aerodynamic forces, blade seals, turbine shrouds*

Introduction

In engineering many cases are known of occurrence of aerodynamically generated vibrations of turbine rotors. Such phenomena can lead to dangerous vibrations which make correct operation of turbine set impossible. Self-excited aerodynamic forces occur as a result of phenomena associated with non-stationary flow of working medium through a turbine stage in the case of eccentric position of turbine's rotor respective to its casing. During operation of a rotary machine whose rotor axis is deviated from casing axis, local flows through particular passages between rotor blades are changed as well as working medium leakages along circumference of radial gap of over-shroud seal are also changed. As a result, a circularly unsymmetrical distribution of forces acting on rotor blades and shroud surface occurs. Hence in publications devoted to the problem two main components of aerodynamic forces resulting from different character of their occurrence, are distinguished:

- resultant force due to non-uniform distribution of circumferential forces in rotor blade ring, called blade-ring force,
- resultant force due to non-uniform distribution of pressure in radial gap over rotor blades, called pressure force.

In most cases of design solutions of turbine stages the pressure forces are of decisive influence on occurrence of self-excited rotor vibrations of aerodynamic origin. For this reason to know dynamic features of over-shroud seals in designing process of a new turbine set is very important. The features are tried to be determined in a theoretical way, however results of experimental investigations appear extremely valuable because of a highly complex character of flow through turbine stage.

Pressure forces – linear model

Mutual relationship between pressure force and displacement of rotor against casing is usually described by means of the so called „seal dynamic coeffcients" [1-8, 12-14] which can be incorporated into whole model of turbine set during its designing process. Three kinds of the dynamic coefficients can be distinguished: stiffness, damping nad inertia ones. They are associated with displacement, velocity and acceleration of rotor relative to casing, respectively.

In such system, forces and moments generated in radial gap over turbine rotor blades are described by using the linear model which takes form of the following vectorial equation:

$$[F]=[K]\begin{bmatrix} x \\ y \\ \varepsilon_x \\ \varepsilon_y \end{bmatrix}+[C]\begin{bmatrix} \dot{x} \\ \dot{y} \\ \dot{\varepsilon}_x \\ \dot{\varepsilon}_y \end{bmatrix}+[M]\begin{bmatrix} \ddot{x} \\ \ddot{y} \\ \ddot{\varepsilon}_x \\ \ddot{\varepsilon}_y \end{bmatrix} \tag{1}$$

where:

F – vector of aerodynamic forces and moments generated in seal,
x, y – rotor linear displacements in the assumed frame of coordinates,
εx, εy – angular displacements of rotor axis,
K – matrix of stiffness coefficients,
C – matrix of damping coeffcients,
M – matrix of inertia coefficients,
$\dot{x}, \dot{y}, \dot{\varepsilon}_X, \dot{\varepsilon}_Y$ – the first time-related derivatives of linear and angular displacements,
$\ddot{x}, \ddot{y}, \ddot{\varepsilon}_X, \ddot{\varepsilon}_Y$ – the second time-related derivatives of linear and angular displacements.

In the subject-matter literature a simplification which consists in neglecting the inertia coeffcients in the model, can be found [5,6], [8÷11]. The vectorial equation of the linear model takes then the following form:

$$[F]=[K]\begin{bmatrix} x \\ y \\ \varepsilon_x \\ \varepsilon_y \end{bmatrix}+[C]\begin{bmatrix} \dot{x} \\ \dot{y} \\ \dot{\varepsilon}_x \\ \dot{\varepsilon}_y \end{bmatrix} \tag{2}$$

Research stand

The above mentioned investigations were performed by using a research stand of model turbine installed in the Laboratory of the Ship Automation of Turbine Propulsion Department, Faculty of Ocean Engineering and Ship Technology, Gdańsk University of Technology. Schematic diagram of the stand is presented in Fig. 1. The turbine is fed with compressed air delivered from the compressor through the piping system. The compressor is driven by the electric motor through the reduction gear. Th electric brake absorbs the turbine's output power. The electric energy generated in the electric brake is transformed into heat in the set of resistors.

The examined turbine is a single-stage impulse turbine with labyrinth over-shroud seal having two teeth in the shroud and casing (Fig. 2). Construction of the turbine makes it possible to change mutual position of casing and rotor during operation of the stand.

The measuring system of the stand makes it possible to measure non-stationary distribution of pressure along circumference of the over-shroud seal. The turbine's casing is adjusted to fastening the ENTRAN EPE miniature pressure sensors (Fig. 2). Altogether 88 pressure measurement points are provided for: 4 in each row, circumferentially distributed every 15o, except for the parting plane of the casing.

During the carried-out investigations a displacement of the turbine's casing (precisely, of the vane blade-ring with seal ring) against the turbine' rotor, was forced (during operation of the turbine). The casing displacement was measured by using an induction sensor of linear displacements. The sensor was fastened to the motionless part of the stand and its measuring tip was leaned against outer surface of the movable casing of the turbine.

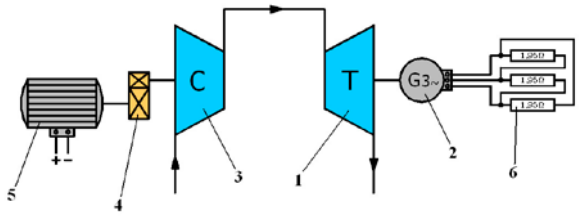

Fig. 1 *Schematic diagram of the model air turbine stand: 1 – turbine, 2 – brake, 3 – compressor, 4 – reduction gear, 5 – electric motor, 6 – set of resistors*

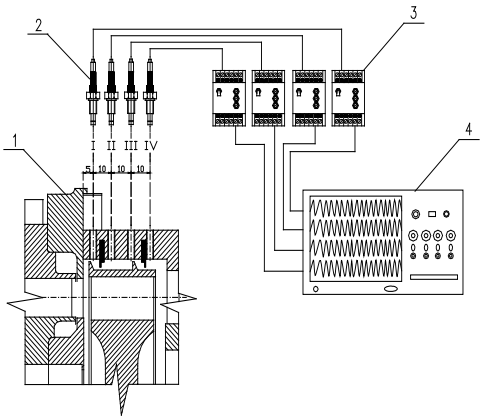

Fig. 2 *Schematic diagram of the measurement system of pressure in over-shroud gap of the model turbine: 1 – axial cross-section of the turbine stage, 2 – pressure sensor, 3 – measurement amplifier, 4 – recording system of measurement data, I, II, III, IV – measurement planes perpendicular to rotor axis*

Experimental investigations

The research was aimed at verifying validity of the simplification of linear model, consisting in neglecting the inertia coefficients (Eq. 2), as proposed in the literature. To this end the dynamic coefficients of the over-shroud seal of the model air turbine were experimentally determined in compliance with the following vectorial equation: where:

$$\begin{bmatrix} F_X(t) \\ F_Y(t) \end{bmatrix} = \begin{bmatrix} K_{XX} & K_{XY} \\ Kyx & Kyy \end{bmatrix} \cdot \begin{bmatrix} x(t) \\ y(t) \end{bmatrix} + \begin{bmatrix} C_{XX} & C_{XY} \\ Cyx & Cyy \end{bmatrix} \cdot \begin{bmatrix} \frac{dx}{dt} \\ \frac{dy}{dt} \end{bmatrix} + \begin{bmatrix} M_{XX} & M_{XY} \\ Myx & Myy \end{bmatrix} \cdot \begin{bmatrix} \frac{d^2x}{dt^2} \\ \frac{d^2y}{dt^2} \end{bmatrix} \quad (2)$$

F_X, F_Y	– components of pressure force vector,
t	– time,
x, y	– rotor displacements in the assumed frame of coordinates,
K_{XX}, K_{YY}, K_{XY}, K_{YX}	– stiffness coefficients,
M_{XX}, M_{YY}, M_{XY}, M_{YX}	– inertia coefficients,
C_{XX}, C_{YY}, C_{XY}, C_{YX}	– damping coefficients.

During the investigations changes of pressure in the sealing, which result from mutual transverse displacement of rotor and casing, were recorded; next on the basis of the experimental data pressure forces

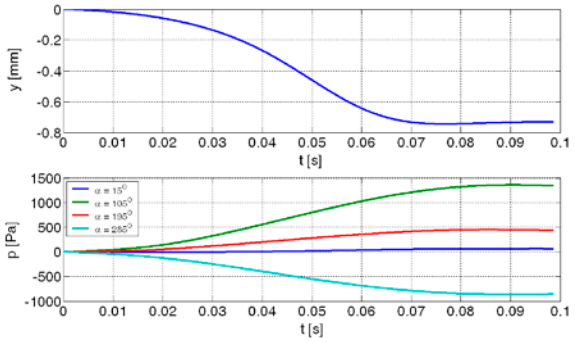

Fig. 3 *Displacement of rotor against casing as well as change of pressure in the over-shroud seal, resulting from it and measured in 4 points distributed every 900 along circumference of the turbine stage; α – angle which determines location of measurement point along circumference of the seal*

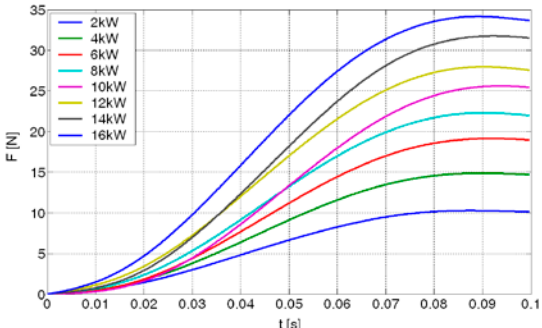

Fig. 4 *Increase of the resultant pressure force at the step change of mutual position of rotor and casing by 0,74 mm and different turbine's loads*

and dynamic coefficients of the sealing were calculated. The investigations were carried out at the constant rotor speed equal to 3600 rpm, and the turbine power values of 2 kW, 4 kW, 6 kW, 8 kW, 10 kW, 12 kW, 14 kW, 16 kW, as well as the values of eccentricity of rotor against casing, changed by 0,16 mm, 0,35 mm, 0,61 mm, and 0,74 mm. The nominal radial gap in the seal was equal to 1 mm (rotor co-axially aligned in casing).

In Fig. 3 is presented the example run of position of rotor against casing as well as that of change of pressure in the over-shroud seal, resulting from it and measured in 4 points located every 90^0 along circumference of the turbine stage, at the turbine's power of 12 kW and its rotor speed of 3600 rpm.

On the basis of the measurements the forces acting on the turbine's shroud were determined; the example of the obtained results is presented in Fig. 4.

As pressure force changes with time and rotor displacements against casing are known, it was possible to determine the stiffness, damping and inertia coefficients appearing in the linear model equations. The coefficients were determined by searching for solution of Eq. 3 with the use of the least squares method. The example results are shown in Fig. 5, 6, and 7. As observed on the basis of the obtained results, the relationship between the dynamic coefficients of the considered over-shroud seal and the turbine's output power, is linear.

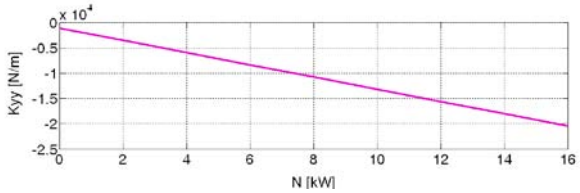

Fig. 5 Stiffness coefficients of the seal in function of output power of the turbine

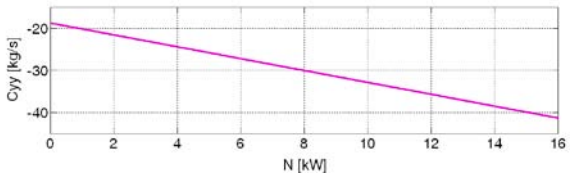

Fig. 6 Damping coefficients of the seal in function of output power of the turbine

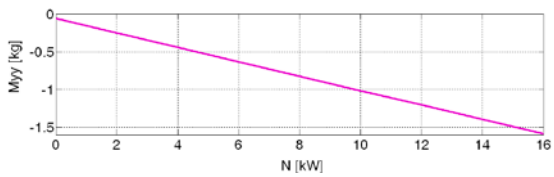

Fig. 7 Inertia coefficients of the seal in function of output power of the turbine

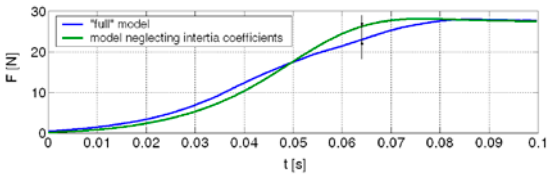

Fig. 8 Pressure force calculated by means of the linear model and that calculated by means of the model neglecting inertia coefficients.

By making use of the determined dynamic coeffcients of the seal it was possible to determine pressure force for a given value of displacement of turbine's rotor against its casing. The example run of the pressure force calculated by means of the linear model with the use of the determined coefficients is presented in Fig. 8. In the same figure is also drawn the similar run but determined with the use of the model neglecting inertia coefficients.

The diagram in Fig. 8 shows that the neglection of inertia coeffcients in the linear model equations can lead to distinct differences in runs of the calculated force. In the presented example the differences reached as far as 15 %.

On the other hand, rather small influence of the inertia coeffcients on the determined forces has been revealed. In

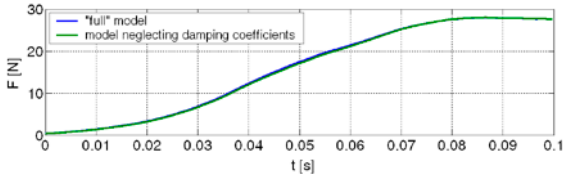

Fig. 9 Pressure force calculated by means of the linear model and that calculated by means of the model which neglects damping coefficients.

Fig. 9 are presented the example runs of the pressure force calculated by means of the complete linear model, i.e that in which all three kinds of the coefficients have been taken into account, and that calculated by using the simplified model neglecting the term associated with damping coefficients -they differ only a little to each other. Such situation repeated within all the range of values of turbine's load and change of rotor displacement against casing, for which measurements have been performed. This suggests that the considered type of seal (i.e. the labyrinth over-shroud seal with two teeth on the shroud and two on the casing) is of very low damping qualities.

Therefore in the case of this kind of seal it was proposed to simplify the model which describes pressure forces, by omitting its part associated with velocity of rotor displacement against casing. In such case the equation which describes generation of pressure forces would take the following form:

Conclusions

$$[F]=[K]\begin{bmatrix} x \\ y \\ \varepsilon_x \\ \varepsilon_y \end{bmatrix}+[M]\begin{bmatrix} \ddot{x} \\ \ddot{y} \\ \ddot{\varepsilon}_x \\ \ddot{\varepsilon}_y \end{bmatrix} \quad (4)$$

- in the case of labyrinth over-shroud seal, values of dynamic coefficients of the seal change proportionally along with turbine's power changing;
- in the case of seals of low damping qualities, omittance of inertia coefficients can lead to noticeable

errors in determining the aerodynamic forces;

- the labyrinth over-shroud seal with two teeth on the shroud and two on the casing has as much low damping qualities that in the case of the seal in question the linear model can be simplified by omitting the term associated with damping coefficients.

Bibliography

1. Baskharone E. A., Hensel S. J.: Interrelated Rotordynamic Effects of Cylindrical and Conical Whirl of Annular Seal Rotors. Transactions of the ASME Journal of Tribology,July 1992, Vol 113
2. Childs D. W., Shin Yoon-Shik: A design to increase the static stiffness of hole pattern stator gas seals. ASME Turbo Expo 2006: Power for Land, Sea and Air, Barcelona, Spain;
3. Childs D. W.: Finite-length Solutions for Rotordynamic Coefficients of Turbulent Annular Seals. Transactions of the ASME Journal of Lubrication Technology, July 1983, Vol 105;
4. D'Souza R. J., Childs D. W.: A comparasion of rotordynamic-coefficient predictions for annular honeycomb gas seals using three different friction-factor models.Transactions of the ASME Journal of Tribology, July 2002
5. Ertas B., Gamal A., Vance J.: Rotordynamic Force Coefficients of Pocket Damper Seal. ASME Turbo Expo 2006: Power for Land, Sea and Air, May 8-11, 2006, Barcelona, Spain;
6. Holt Ch. G., D. W. Childs: Theory versus experiment for the rotordynamic impedances of the two hole-pattern-stator gas annular seals.Transactions of the ASME Journal of Tribology, January 2002
7. Kanemori Y., Iwatsubo T.: Forces and Moments Due to Combined Motion of Conical and Cylindrical Whirls for a Long Seal. Transactions of the ASME Journal of Tribology, July 1994, Vol 116;
8. Lindsey Todd W., Childs D. W.: The Effect on Converging an Diverging Axial Taper on the Rotordynamic Coefficients of Liquid Annular Pressure Seals: Theory Versus Experiment. Transactions of the ASME Journal of Vibrations and Acoustics, April 2000;
9. Nielsen K. K., Childs D. W., Myllerup C. M.: Experimental and Theoretical Comparison of Two Swirl Brake Designs. Transactions of the ASME Journal of Turbomachinery, April 2001, Vol. 123;
10. Picardo A., D. W. Childs:Rotordynamic coefficients for a tooth-on-stator labirynth seal at 70 bar supply pressures: measurements versus theory and comparisons to a hole-pattern stator seal. Transactions of the ASME Journal of Engineering for Gas Turbines and Power, October 2005
11. Schettel J., Deckner M., Kwanka K., Lüneburg B., Nordmann R.: Rotordynamic: Coefficients Of Labseals For Turbines -Comparing CFD Results With Experimental Data On A Comb-Grooved Labyrinth. ASME paper GT-2005-68732, Proceedings of ASME Turbo Expo, June 6 9 2005 -Reno Tahoe, Nevada USA;
12. Simon F., Frěne J.: Static and Dynamic Characteristics of Turbulent Annular Eccentric Seals: Effect of Convergent-Tapered Geometry and Variable Fluid Properties. Transactions of the ASME Journal of Tribology, April 1989, Vol 111
13. Simon F., Frěne J.: Analysis for Incompressible Flow in Pressure Seal. Transactions of the ASME Journal of Tribology, July 1992, Vol 114
14. Staubly T., Bissing M.: Numerical parameter study of rotor side spaces. Proceedings of the Hydraulic Machinery and Systems, 21st IAHR Symposium, Lausanne, 9÷12 September, 2002.